Metal Nanoparticles and Nanocomposites as Antibacterial and Anticancer Agents

A Thesis
Submitted in Partial Fulfillment of the
Requirements for the award of the degree of

DOCTOR OF PHILOSOPHY

By

SHILPA SHARMA

Centre for Nanotechnology
Indian Institute of Technology Guwahati
Assam, India

September 2012

Dedicated to

My Parents

DECLARATION

I, hereby, declare that the matter embodied in this thesis entitled "***Metal Nanoparticles and Nanocomposites as Antibacterial and Anticancer Agents***" is the result of investigations carried out by me under the supervision of Prof. Siddhartha Sankar Ghosh, Department of Biotechnology, Indian Institute of Technology Guwahati, Guwahati, India and Prof. Arun Chattopadhyay, Department of Chemistry, Indian Institute of Technology Guwahati, Guwahati, India for the award of degree of Doctor of Philosophy. This work has not been submitted elsewhere for any degree, diploma, associateship or membership etc. of any institute or university to the best of my knowledge and belief.

IIT Guwahati **Shilpa Sharma**

September, 2012 Roll No. 08615302

INDIAN INSTITUTE OF TECHNOLOGY GUWAHATI
CENTRE FOR NANOTECHNOLOGY

CERTIFICATE

This is to certify that the thesis entitled ***"Metal Nanoparticles and Nanocomposites as Antibacterial and Anticancer agents"*** being submitted to the **Indian Institute of Technology Guwahati** by **SHILPA SHARMA** for the award of the degree of **Doctor of Philosophy** in **Nanotechnology**, is a bonafide record of research work carried out by her. The contents of this thesis have not been submitted to any other University or Institute for the award of any degree or diploma.

Prof. Siddhartha Sankar Ghosh
(Supervisor)

Prof. Arun Chattopadhyay
(Supervisor)

Acknowledgement

It gives me a deep sense of satisfaction to have an opportunity to pay my gratitude to all the people who have helped me directly and indirectly during my IIT Guwahati stay for the degree of Doctor of Philosophy. During this period, they have played a big role in my growth and evolution both on personal as well as professional front. Thank you all.

First of all, I would like to express my deepest gratitude to my reverent thesis supervisors Prof. Siddhartha Sankar Ghosh and Prof. Arun Chattopadhyay for channelizing my potential to the desired end. It was under their constant guidance and motivation at every step of my research endeavour that I could take ventures in the field of nanotechnology and successfully complete them. Throughout this period, they always encouraged me to explore new ideas and gave me ample freedom to work. I shall always remain indebted to them for their unending support, understanding, care and concern. Thank you very much Sirs. I am blessed to have you as my mentors.

Next to them, it was the doctoral committee comprising of Dr. Biplab Bose, Dr. Lingaraj Sahoo and Dr. Bhubaneswar Mandal which evaluated my performance time to time and underscored the gaps where I had to work hard. I sincerely thank them for their critical comments and valuable suggestions which helped me to gain insight in the work I had undertaken. I am also thankful to Department of Science & Technology, Govt. of India for providing me financial assistance to attend an international symposium in Miami that gave me an opportunity to meet many world renowned eminent scientists and experts in my field. I also owe my gratitude to the Centre for Nanotechnology, Department of Biotechnology, Department of Chemistry, Department of Chemical Engineering and Central Instrument Facility, IIT Guwahati for providing me all supports and necessary facilities. Here I would like to thank Mr. Kaustubh Acharyya, Mr. Indrajit Talukdar, Mr. Chandan Borgohain, Dr. Kula Kamal Senapati, Mr. Madhurjya Borah and Mr. Prasun Bhattacharjee for their help with instruments. I am also grateful to other Centre for Nanotechnology staff: Mr. Paran Jyoti Dutta and Ms. Pranjoli Das for their help whenever required.

Next, I take this opportunity to acknowledge Dr. Madhuchanda Banerjee for her help at the initial stage of my research work. I am also grateful to my senior Dr. Pallab Sanpui who helped me to foster attitude required to carry out research work. I feel extremely lucky to share my lab with Amaresh, Amit and Upashi who were not only

wonderful cooperative lab mates to work with, but also very good friends. Time spent with each of them will always remain in my special memories. I am grateful to Chockalingam for teaching me mammalian cell culture techniques, Francis for FTIR, Subhojit for TEM and Ravi for SEM measurements. I am fortunate to have other group members like Sadhu Da, Rumi, Rama, Kohila, Subhamoy, Nidhi, Raihana, Jashmini Di, Palash, Satya, Sunil, Anushree, Archita, Sharmila, who provided me a healthy and enjoyable environment for smooth conductance of my work at Departments of Chemistry and Biotechnology. I also thank Ashish, Jitendra, Santosh, Subbarao, Krishna Bhaiya, Dilip Bhaiya, Rama Bhaiya and Agile Bhaiya at Centre for Nanotechnology. My sincere thanks to Sunil, Saurabh, Ankita, Deepika, Vikas, Nivedita, Sabitoj for their help in providing me the journal publications unavailable here at the earliest. I will always cherish my friendship with Shraddha, Garima, Jyoti, Saloni, Poly Di, Manideepa Di, Atreyi Di, Punit, Savant, Babina, Ruchika, Momina, Mohsen, Perumalla Bhaiya……. and many other friendly faces in IIT.

Last but not the least, my parents, sister and brother during these four years of my career were constantly keeping my spirits high with their deep understanding, concern and support they offered me in difficult moments. I thank them for their endless love, affection and care. I am also grateful to my grandparents for their blessings for my success. Above all, my thanks to Almighty for giving me an opportunity to carry out research in a prestigious institute with His loving manifestations around me.

Shilpa Sharma

CONTENTS

ABSTRACT

In the present era of nanotechnology, advances are being made in the understanding of the physico-chemical and optoelectronic properties of materials at nanoscale in order to develop impressive functional nanomaterials with applications in diverse areas of science and technology. In healthcare too, the potential of nanotechnology to revolutionize the present ways of handling health related issues is being continuously demonstrated by the researchers all over the world. In this context, a better understanding of fundamental molecular basis of interactions between nanomaterials and biological systems has become important in order to develop novel nanomaterials with potential therapeutic implications. The present thesis is focussed on the development of novel nanoscale materials in the form of metal nanoparticles (NPs) or their composites with biofriendly polymers and study of the effect of these nanomaterials on both prokaryotic and eukaryotic systems with the aim of finding promising candidates for therapeutic applications.

The interaction of metal NPs in the form of bimetallic gold silver (Au@Ag) core-shell NPs with bacterial systems was studied. The results demonstrated superior antibacterial potential of ~30 nm Au@Ag core-shell NPs against both Gram positive and Gram negative bacteria at low silver concentrations in contrast to similar sized Ag NPs alone, with more activity against Gram negative bacteria. Green fluorescent protein (GFP) expressing recombinant *Escherichia coli* was used as model bacterium to study the mechanistic aspects of the bactericidal activity by fluorescence microscopy, transmission electron microscopy (TEM) and fluorescence activated cell sorting (FACS) assay of membrane damage. The findings established that the core-shell NPs attached to the bacterial surface causing disruption of membrane integrity eventually leading to cell death. In addition, the Au@Ag core-shell NPs exhibited superior catalytic activity in comparison to similar sized monometallic Au NPs and Ag NPs.

This was followed by investigating antibacterial potential of a polymer-NP composite *viz.* chitosan based nanocarrier (NC) containing Ag NPs (Ag NP-Chi NCs) against both Gram positive and Gram negative bacteria. The composite, due to synergy between Ag NPs and chitosan NCs was found to exhibit higher antibacterial activity than its components at their respective concentrations present in the composite, with more efficacy against Gram negative bacteria. Detailed antibacterial studies carried out with GFP expressing recombinant *Escherichia coli* by TEM and FACS established

attachment of composite with the bacteria and subsequent membrane damage. The advantage of using chitosan NCs over bulk form was that the antibacterial tests could be easily performed in bacterial medium pH (~7.2), unlike chitosan that precipitates at this pH.

In the next part, a new and completely 'green' method of synthesis of Ag NPs using a natural biopolymer sodium alginate as both reducing and stabilizing agent was developed. The alginate stabilized Ag NPs (Alg-Ag NPs) were characterized and demonstrated to possess antibacterial potency against both Gram positive and Gram negative strains. The Alg-Ag NPs composite was blended with chitosan to form polyelectrolyte complex that was cast into stable films for potential practical applications. The films were characterized by field emission scanning electron microscopy (FESEM), optical microscopy, Fourier transform infrared spectroscopy (FTIR) and X-ray diffraction (XRD) and their water uptake and mechanical properties were also studied. The antibacterial tests carried out with both Gram positive and Gram negative bacteria implicated the potential of films for use in various antibacterial applications.

The methodology developed in the above study was subsequently used to decipher the underlying mechanism of cytotoxicity of Ag NP on mammalian cells to pursue it as therapeutic drug in cancer treatment. Using Alg-Ag NPs and chitosan stabilized Ag NPs, a new 'green' method of preparing a novel biodegradable NC for Ag NPs (Alg-Chi-Ag NP NC) was developed. The Ag NPs in the blended NC induced apoptosis in human glioblastoma U87MG cancer cells at very low concentration; the concentration of Ag NPs to reduce the viability of U87MG cells by 50% was 2.4 μg mL^{-1} which is much less than previously reported data. The fluorescence and scanning electron microscopy (SEM) studies of treated cells revealed nuclear and morphological changes characteristic of apoptosis. TUNEL assay further confirmed apoptotic cell death. The cells underwent oxidative stress marked by elevation in reactive oxygen species (ROS) level. Mitochondrial dysfunction was evident from the depolarization of mitochondrial membrane potential ($\Delta\Psi_m$) suggesting possible involvement of mitochondria in cell death. The cell cycle data implicated DNA damage resulting in apoptosis.

Finally, reversible aggregation and disaggregation behaviour of Alg-Ag NPs was demonstrated via alginate gel formation and breakage. Alg-Ag NPs were aggregated by inducing gelation in alginate by strontium ions (Sr^{2+}). On addition of ethylenediaminetetraaceticacid (EDTA), which is a well known chelating agent, Sr^{2+}

were sequestered causing breakage of gel, leading to reversibility of aggregation of NPs. The aggregation behaviour and its reversibility were studied by UV-Vis spectroscopy, TEM and changes in hydrodynamic diameter and zeta potential values.

In summary, the present thesis focussed on the effect of metal NPs and their nanocomposites on biological systems with the aim of pursuing their therapeutic implications. The potential of bimetallic gold silver core-shell NPs, chitosan nanocarrier containing Ag NPs and alginate stabilized Ag NPs as antibacterial agents, has been established. The three-component composite film containing alginate, chitosan and Ag NPs developed in the present case can be used for various antibacterial applications. Furthermore, alginate-chitosan based blended NC of Ag NPs could serve as alternative therapeutic agent in cancer therapy, after appropriate *in vivo* experiments. Finally, reversible aggregation and disaggregation behaviour of Ag NPs was achieved in a simple and green approach.

Keywords: gold nanoparticle, silver nanoparticle, bimetallic nanoparticle, core-shell, antibacterial, chitosan, nanocarrier, alginate, nanocomposite, glioblastoma, apoptosis, gelation, reversible aggregation of nanoparticles.

LIST OF TABLES

LIST OF FIGURES

FIGURE **PAGE**

|Chapter 1|

Introduction and Literature Review

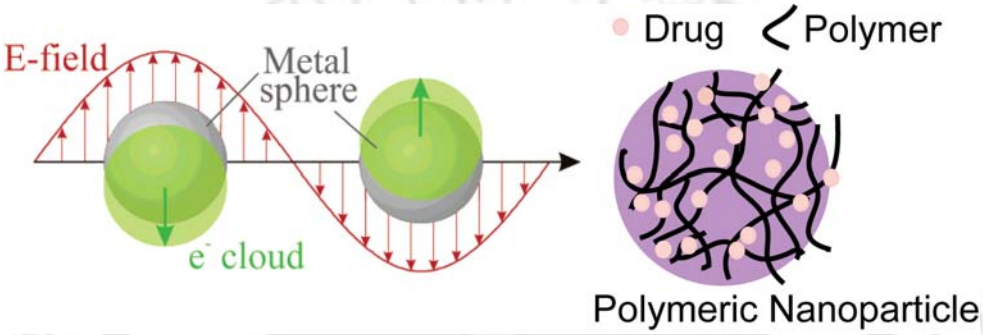

Chapter 1

INTRODUCTION AND LITERATURE REVIEW

1.1. Introduction

The broad field of nanotechnology has sparked immense interest and enthusiasm for its ample potential to develop newer useful materials and devices with applications in diverse areas of science and technology. The modern idea of nanotechnology was principally introduced in 1959 when the great physicist and Nobel laureate Richard Feynman, in his visionary talk 'There's Plenty of Room at the Bottom' suggested the possibility to precisely manipulate matter at atomic level to obtain novel materials with highly desirable properties.

Nanotechnology deals with all those materials which have at least one dimension in the nanometer scale (≤100 nm) range. As the material approaches nanoscale dimensions, it shows new behaviour and properties that are different from its bulk counterparts and these properties are size- and shape- dependent. The small size of the nanomaterial leads to an increased surface area to volume ratio, which ensures increase in the number of atoms at the surface in comparison to those in interior. Recent advancements in understanding the properties of nanomaterials have enabled researchers to create new materials showing novel behavior for various applications. The nanomaterials can be fabricated using either of two approaches:

Top-Down approach: It utilizes traditional workshop and microfabrication methods to subdivide bulk precursors into nanoparticles. This is usually achieved by employing lithographic techniques (e.g. UV, electron or ion beam, scanning probe, optical near field), laser-beam processing, and mechanical techniques (e.g., machining, grinding, and polishing).

Bottom-Up approach: It exploits chemical properties of atoms and molecules causing them to self-assemble in a controlled manner to give some useful conformation. The bottom-up approaches include chemical synthesis, chemical vapor deposition, laser-induced assembly, self-assembly and colloidal aggregation. This approach produces

much smaller sized particles and is more cost effective for mass-production of metal nanoparticles.

1.2. Nanomaterials in Biology

The interdisciplinary field of nanotechnology holds great promise in the field of healthcare too. The application of nanotechnology in healthcare for treatment, diagnosis, monitoring and control of biological systems is referred to as 'nanomedicine' by the National Institutes of Health, Bethesda, USA (Moghimi et al., 2005). Recent advances made in this field include developing nanotechnology based-newer drugs and drug delivery systems for therapeutics and nanomaterials for bioimaging, biosensing and biodiagnostic applications. An important goal in this regard is to understand interaction between nanomaterials and biological systems. In addition, the researchers also aim to construct functional nanostructures out of biological or biologically inspired components such as oligonucleotides, proteins, viruses, and cells (Niemeyer, 2000).

1.2.1. Metal Nanoparticles (NPs)

Metal NPs have attracted considerable attention because of their unique and fascinating optical, electronic, chemical, and magnetic properties that are strikingly different from those of the individual atoms as well as their bulk counterparts. Of these, Au, Ag and Cu NPs show very intense colour which is attributed to collective oscillation of the free conduction electrons with respect to fixed ionic cores in resonance with interacting electromagnetic field. This phenomenon is commonly known as a localized surface plasmon resonance (LSPR) mode and is illustrated in **Figure 1.1**. The LSPR frequency of metal NPs depends on the size, shape, composition of the metal NP, its surface charge, surface-adsorbed species, interparticle interactions and the refractive index of the surrounding medium (Kreibig and Vollmer, 1995; Kelly et al., 2003). For copper, silver and gold, the absorption band lies in the visible region of the electromagnetic spectrum. The LSPR is responsible for generating enhanced electric fields on NP surface that gives rise to extraordinarily large enhancements of the Raman scattering spectra of adsorbed or adjacent molecules, an effect known as surface-enhanced Raman scattering (SERS). Recently, SERS has become an attractive bioanalytical method for sensing and diagnostics owing to its extremely high sensitivity to single molecule

detection (Nie and Emory, 1997). The optical properties of metal NPs can be easily controlled and tailored for successful use in various areas such as photonics, electronics, biological microscopy, medicine, catalysis, sensors and optoelectronics.

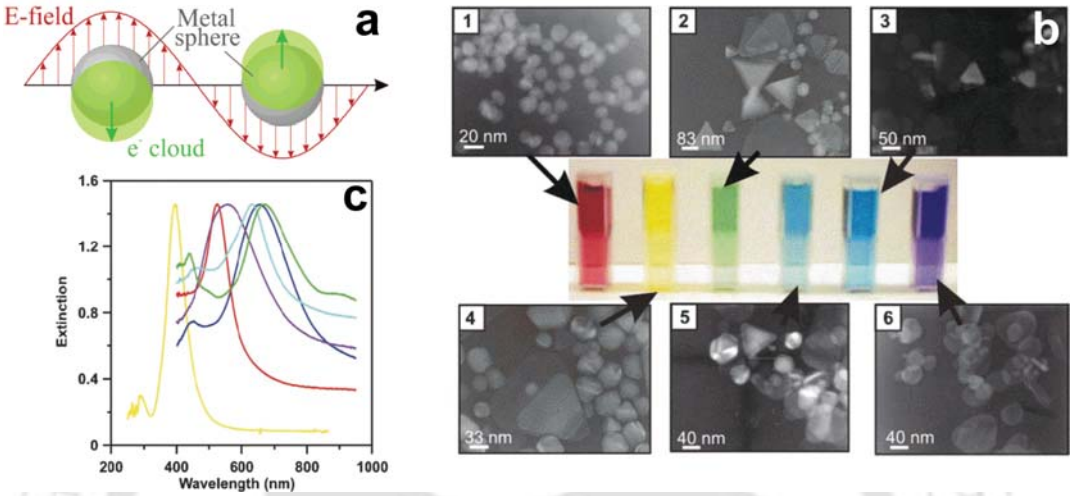

Figure 1.1. (a) Schematic of plasmon oscillation for a sphere, showing the displacement of the conduction electron charge cloud relative to the nuclei. Reprinted with permission from (Kelly et al., 2003). Copyright (2003) American Chemical Society. **(b, c)** Tunable Ag and Au NP solutions. **(b)** Corresponding transmission electron micrographs. *1* The red solution consists of homogeneous Au nanospheres (13-nm diameter). *2* The green solution consists of Ag NPs (nanospheres, trigonal prisms, and polygon platelets). *3* The dark blue solution consists of Ag NPs (trigonal prisms with rounded tips and polygon platelets). *4* The yellow solution consists of inhomogeneous Ag NPs (nanospheres, trigonal prisms, and polygon platelets). *5* The light blue solution consists of Ag NPs (trigonal prisms and polygon platelets). *6* The purple solution is made up of inhomogeneous oblong Ag NPs **(c)** UV-Vis extinction spectra of the corresponding solutions (*color of line* corresponds to solution color) (Courtesy: Haes and Duyne, 2004).

1.2.1.1. Gold Nanoparticles

Au NPs have received much attention since Michael Faraday reported preparation of colloidal gold by reducing gold chloride with phsophors in 1857. In 1908, Mie explained visible absorption of Au NPs using Maxwell's electromagnetic equations. Turkevich et al. in 1951 and Frens in 1973 pioneered synthesis of monodispersed Au

NPs using 'citrate' method. Au colloids have advantages of easy preparation, homogeneity, biocompatibility, rich surface functionalization chemistry, and high photostability. Some of their applications in biology are as follows:

Sensing applications

The gold nanospheres undergo colour change from red to blue on onset of aggregation in colloidal solution. This leads to corresponding broadening and red shift of plasmon resonance due to 3D plasmon coupling owing to reduced interparticle distances. The effect of 3D plasmon coupling has been successfully used for developing colorimetric sensors with DNA-functionalized Au NPs (Elghanian et al., 1997; Li et al., 2004).

Surface-Enhanced Raman Scattering (SERS)

SERS has become promising technique for label-free detection and analysis inside the cells. Souza et al. (2006) reported for the first time, the *in vivo,* non invasive SERS detection using gold colloids aggregated with imidazole in a preclinical tumor-bearing mouse model. Vitol et al. (2009) developed a SERS-active glass nanopipette probe comprised of a glass capillary with a 100-500 nm tip coated with Au NPs which was used to collect spectrum from the nucleus and the cytoplasmic regions. Besides, it was used to measure *in situ* cell response to the changes in its environment. Further, in a recent study by Kneipp et al. (2010), a mobile SERS nanosensor made of gold nanoaggregates and 4-mercaptobenzoic acid (pMBA) attached as a reporter was used to monitor changes in local pH of endosomes of living NIH/3T3 cells. Such information is important for study of cancers and biotechnological processes like non viral gene delivery.

Photothermal Therapy

In photothermal therapy, the tumor tissue is destroyed by the heat produced by absorption of light by photothermal agents like natural chromophores in the tissue or dye molecules added from outside. In this regard, gold nanostructures such as gold nanospheres, gold nanorods, gold nanoshells and gold nanocages (El-Sayed et al., 2006; Huang et al., 2006; Takahashi et al., 2006; Huff, 2007; O'Neal et al., 2004; Loo et al., 2005; Chen et al., 2005; Hu et al., 2006) have successfully been used as effective

photothermal agents which due to their SPR oscillations have strongly enhanced absorption in the visible and NIR regions.

Delivery Applications

Au NPs have extensively been used for gene delivery applications owing to their high surface area-to-volume ratio which maximizes the payload/carrier ratio. The charge and hydrophobicity of Au NPs can be tuned easily to enhance the transfection efficiency keeping the toxicity at minimum. It has been demonstrated that Au NPs functionalized with cationic quaternary ammonium groups bind plasmid DNA through electrostatic interaction and protect DNA from enzymatic digestion. The bound DNA can be released on addition of glutathione *in vitro* (McIntosh et al., 2001; Han et al., 2005; 2006a). Furthermore, Sandhu et al., (2002) demonstrated efficient gene delivery by these DNA–Au NP conjugates in mammalian 293T cells with transfection efficiency 8-fold more than polyethyleneimine (PEI). The Au NP-PEI transfection vectors were synthesized by Thomas et al. (2003) who demonstrated that the transfection efficiency of these hybrid vectors in Cos-7 cells were ~12- fold more than the polymer itself. Han et al., (2006b) loaded DNA on the surface of photolabile Au NPs tailored with a photocleavable o-nitrobenzyl ester linker and a quaternary ammonium salt as end-groups. UV irradiation cleaved the nitrobenzyl linkage creating an anionic carboxylate group, causing effective release of complexed DNA and restoration of transcription in T7 RNA polymerase assay *in vitro*. The nucleic acids have also been attached to Au NPs via thiol (–SH) modification for grafting onto NPs. For instance, Oishi et al., 2006 reported use of Au NPs conjugated thiolated siRNA for successful gene silencing in HuH-7 cells.

In addition, Au NPs have also been used as efficient transporters of peptides and proteins. Verma et al. (2004) demonstrated that positively charged tetra-alkyl ammonium functionalized Au NPs recognized the surface of β-galactosidase through complementary electrostatic interaction and inhibited its activity, which was further restored by adding free glutathione thereby releasing the protein. Bhumkar et al. (2007) reported adsorption of insulin on chitosan stabilized Au NPs which were further demonstrated to be effective for transmucosal delivery of insulin.

Besides, Au NPs have also been used for both 'active' and 'passive' targeted delivery of therapeutic drugs. Chen et al. (2007b) demonstrated delivery of methotrexate using methotrexate functionalized Au NPs (MTX-Au NPs). The MTX-Au NPs inhibited tumor growth in a mouse ascites model of Lewis lung carcinoma. Arosio et al. (2011) reported synthesis of cRGD integrin ligand functionalized Au NPs which specifically targeted $\alpha_v\beta_3$ integrin overexpressing human cancer cells. Fuente and Berry (2005) prepared Au NPs functionalized with TAT peptide which is a nuclear localization signal and demonstrated enhanced translocation of these Au NPs into the nucleus.

1.2.1.2. Silver Nanoparticles

Antimicrobial properties

Silver is known for its antimicrobial properties against a wide range of micro organisms since times immemorial. The US Food and Drug Administration approved colloidal silver for wound treatment as early as 1920s. However with the arrival of antibiotics in 1940s, there was decline in the research on therapeutic application of silver (Jain et al., 2009). In 1960s, research in antimicrobial efficacy of silver revived with the use of 0.5% silver nitrate solution in the burn arena by Moyer et al. (1965) and 1% silver sulfadiazine (SSD) cream to treat burn wound infections by Fox (1968). Recent emergence and continuous rise of new strains of antibiotic resistant pathogenic bacteria coupled with increasing developments in nanotechnology has motivated an upsurge in research on antimicrobial efficacy of Ag NPs. Ag nanomaterials have emerged as an effective antimicrobial agent increasingly being used in consumer products (Marambio-Jones et al., 2012).

Sondi et al. (2004) first reported the antimicrobial activity of Ag NPs against *E. coli* as a model Gram negative bacterium. They found that Ag NPs accumulated in the membrane of treated cells thereby causing damage as evident from the formation of pits on cell surface. Baker et al. (2005) reported the antibacterial efficacy of Ag NPs against *E. coli* and related the surface area to volume ratio of NPs to their antibacterial activity. The smaller Ag NPs exhibited higher bactericidal activity owing to larger surface area to volume ratio. Morones et al. (2005) studied the effect of Ag NPs in the range of 1-100 nm on Gram negative bacteria using scanning transmission electron microscopy (STEM) which confirmed the presence of NPs on membrane surface as well as inside

the bacteria. The high angled annular dark field (HAADF) images revealed that the smaller sized NPs (~5 nm) exhibited efficient antibacterial activity, thus concluding the activity of Ag NPs to be size dependent. Ag NPs synthesized in one step protocol by Panacek et al. (2006) were shown to possess high bactericidal activity against both Gram negative and Gram positive bacteria including highly multiresistant strains such as methicillin-resistant *S. aureus*. The antibacterial efficacy of Ag NPs was found to be size dependent with 25 nm sized Ag NPs possessing highest antibacterial activity. Shahverdi et al. (2007) reported the enhancement in antibacterial activity of antibiotics like penicillin G, amoxicillin, erythromycin, clindamycin, and vancomycin in the presence of Ag NPs synthesized by using *Klebsiella pneumonia* against *E. coli* and *S. aureus*. The antibacterial efficacy of Ag NPs was found to be shape dependent by Pal et al. (2007) who synthesized spherical, rod shaped and truncated triangular NPs and studied their interaction with *E. coli*. They found that truncated triangular silver nanoplates with a {111} lattice plane as the basal plane exhibited highest antibacterial activity. Gong et al. (2007) synthesized bifunctional Fe_3O_4@Ag NPs having both superparamagnetic and antibacterial properties against *E. coli*, *S. epidermidis* and *B. subtilis*. The Fe_3O_4@Ag NPs could be reused several times and thus may have application as water disinfectants. Kumar et al. (2008) developed environment friendly Ag NPs embedded paint in a single step from common household paint. The surfaces coated with this paint demonstrated excellent antimicrobial properties against both Gram positive *S. aureus* and Gram-negative *E. coli*. Dankovich et al. (2011) reported the development of Ag NPs impregnated bactericidal paper that killed bacteria (*E. coli* and *E. faecalis*) when suspensions of bacteria percolated through the paper, thereby demonstrating its effectiveness for emergency water treatment. A very recent study by Falentin-Daudré et al. (2012) reported development of Ag NPs containing antimicrobial coating formed by layer-by-layer (LbL) assembly of oppositely charged polyelectrolyte layers, for imparting strong antibacterial activity against *E. coli* to stainless steel. Furthermore, Mahmoudi et al. (2012) presented a new class of ultrathin (~1–2 nm) silver ring-coated superparamagnetic iron oxide NPs (SPIONs) with ligand gaps that were able to penetrate through *S. epidermidis* and *S. aureus* biofilms on application of an external magnetic field. These NPs were shown to be effective against bacterial biofilms while being simultaneously non toxic to human cells.

In this regard, substantial research from our laboratory has also demonstrated antibacterial potential of Ag NPs either alone or in the form of composite. The antibacterial effect of Ag NPs was studied by Gogoi et al. (2006) on GFP expressing *E. coli*. The results indicated that Ag NPs of less than 10 nm made pores on the bacterial cell wall which was evident from TEM investigations, subsequently releasing the cytoplasmic materials to the medium leading to cell death without affecting the intracellular proteins and nucleic acids. Sanpui et al. (2008) reported antibacterial activity of a composite consisting of chitosan and Ag NPs against *E. coli* at very low concentration of individual components. The fluorescence confocal laser scanning and scanning electron microscopy showed attachment of the bacteria to the composite and their subsequent fragmentation without causing any effect on bacterial proteins. Furthermore, a three component antimicrobial iodinated chitosan-Ag NP composite was developed by Banerjee et al. (2010) which exhibited antibacterial activity against *E. coli* at low concentration of its individual components i.e. chitosan, iodine and Ag NPs. While the positively charged chitosan matrix captured negatively charged bacteria on its surface and Ag NPs created pores on the cell wall, the iodine atoms produced on the surface of Ag NPs led to generation of reactive oxygen species (ROS), eventually killing cells. In another study, Sahoo et al. (2011) developed a nanocomposite comprised of p-hydroxyacetanilide (paracetamol) dimer and Ag NPs by reaction of $AgNO_3$ and paracetamol. The composite killed bacteria efficiently in comparison to its individual components. It was proposed that ROS generation led to oxidation of the dimer to N-acetyl-p-benzoquinone imine (NAPQI) which acted as a DNA gyrase inhibitor causing linearization of DNA leading to cell death.

In addition to antibacterial properties, Ag NPs also possess antimicrobial activity against fungi, algae and viruses. Kim et al. (2008b) demonstrated antifungal action of Ag NPs against *Candida albicans* by disrupting membrane integrity. Ag NPs were also shown to be effective against viruses including HIV-1, Hepatitis B virus, herpes simplex virus type 1 and monkey pox virus (Sun et al., 2005; Lara et al., 2010; Lu et al., 2008; Baram-Pinto et al., 2009 and Rogers et al., 2008). The information about toxicity of Ag NPs against algae is very limited with Navarro et al. (2008) demonstrating reduction in the photosynthetic yield of fresh water alga

C*hlamydomonas reinhardtii* by Ag NPs. In this case the toxicity was attributed to silver ions.

Biomedical/Clinical Applications

Research on antimicrobial properties of Ag NPs has paved way to the development of newly designed Ag NPs-based wound dressings to control infections. Impregnation of Ag NPs in wound dressings ensures slow and continual release of Ag NPs thereby improving antimicrobial efficacy and reducing toxicity to human tissue. Maneerung et al. (2008) suggested use of Ag NPs incorporated bacterial cellulose as wound dressing material which was demonstrated to possess efficient antimicrobial activity against *E. coli* and *S. aureus.* Dubas et al. (2011) coated surgical sutures with Ag NPs and demonstrated their antibacterial efficacy against *S. aureus* for use in surgery to prevent bacterial infection. Madhumathi et al. (2009) developed novel chitin/Ag NPs composite scaffolds which possessed bactericidal activity against both *S. aureus* and *E. coli* and also superior blood clotting ability useful for wound healing applications. Jain et al., (2009) developed an antimicrobial gel formulation containing Ag NPs which exhibited efficient antibacterial and antifungal activity as well as complete safety for treating burn wounds. Further, Xing et al. (2010) proposed Ag NPs loaded poly-(3-hydroxybutyrate-*co*-3-hydroxyvalerate) (PHBV) nanofibres to be used in joint arthroplasty due to their inhibitory effect against both Gram positive *S. aureus* and Gram negative *Klebsiella pneumonia* as well as good *in vitro* cell compatibility.

Effect on Mammalian cells

In addition to antimicrobial properties, Ag NPs have also been demonstrated to possess antiplatelet properties (Shrivastava et al., 2009). Besides, they are known to exert cytotoxic effect on mammalian cells, deep understanding of which is required for their successful application in therapeutics. Studies are being pursued to explore the possible mechanisms of cytotoxicity and possible genotoxicity of Ag NPs in mammalian cells (AshaRani et al., 2008; 2009). In this regard, a study conducted by Hussain et al. (2005) reported depletion in the level of glutathione, reduction in mitochondrial potential and increase in ROS level in BRL 3A rat liver cells exposed to Ag NPs which suggested oxidative stress to be the possible mechanism of toxicity of Ag NPs. Similarly, Carlson

et al. (2008) also demonstrated Ag NPs-induced oxidative stress in alveolar macrophages and found toxicity of Ag NPs to be size dependent. Furthermore, the involvement of ROS- and JNK-dependent pathway in Ag NP-induced apoptosis in mouse fibroblast NIH3T3 cells was demonstrated by Hsin et al. (2008). The *in vitro* toxicity study conducted by Arora et al. (2008) suggested a safe range of use of 7–20 nm spherical Ag NPs in human fibrosarcoma (HT-1080) and human skin carcinoma (A431) cells. Besides, Franco-Molina et al. (2010) reported antitumor activity of Ag NPs on MCF-7 human breast cancer cells. In our laboratory, Ag NPs, either by themselves or in combination with gene therapy have been demonstrated to induce apoptosis in mammalian cells (Gopinath et al., 2008; 2010).

Table 1.1. Commercially available medical products containing nanosilver (Chaloupka et al., 2010)

Product	Company	Description	Clinical uses
Acticoat™	Smith & Nephew	Nanocrystalline silver wound dressing	Dressing for a range of wounds including burns and ulcers; prevents bacterial infection and improves wound healing.
Silverline®	Spiegelberg	Polyurethane ventricular catheter impregnated with NS	Neurosurgical drain of CSF for hydrocephalus. Also can be adapted for use as shunts. Antibacterial silver NP coating prevents catheter-associated infections.
SilvaSorb®	Medline Industries and AcryMed	Antibacterial products: hand gels, wound dressings, cavity filler	Wound dressings and cavity filler prevent bacterial infection. Hand gels used to disinfect skin in clinical and personal hygiene purposes.
ON-Q SilverSoaker™	I-Flow Corporation	Silver-NP-coated catheter for drug delivery	Delivery of medication (e.g. local anesthetics or analgesics) per-, peri- or post-operatively for pain management or for antibiotic treatment.

SERS

Ag NPs have also been used for SERS applications. Ivleva et al. (2008) employed colloidal Ag NPs that led to an enhancement factor of up to two orders of magnitude for ultrasensitive chemical analysis of biofilms. Wang et al. (2010b) demonstrated the potential of silver nanospheres formed by the assembly of silver nanocrystals as SERS substrate for detection of three key pathogens *viz. E. coli* O157, *S. typhimurium* and *S. aureus* as few as 10 colony forming units/mL (CFU mL^{-1}). Ren et al. (2010) developed graphene oxide/Ag NP hybrids (GO/PDDA/Ag NPs) for SERS detection of folic acid in water and serum according to the inherent SERS spectra of folic acid. The modified graphene oxide interacted with folic acid molecules electrostatically and the self-assembled Ag NPs enhanced the signal of folic acid. Further, Huang et al. (2011) used SERS based on Ag NPs for the diagnosis of thyroid tissue.

1.2.1.3. Other Metal Nanoparticles

Besides Ag NPs, Cu NPs also possess antibacterial properties. Cioffi et al. (2005) demonstrated antibacterial and antifungal properties of Cu NP-polymer composites. Esteban-Cubillo et al. (2006) reported antibacterial activity of Cu NPs embedded in the matrix of sepiolite. Cu NPs get oxidized very easily which poses a challenge to use them for biological applications. In this regard, recently, an iodine-stabilized Cu NP-chitosan composite was developed by Mallick et al (2012) which was demonstrated to have effective antibacterial activity against *E. coli* at low concentration of Cu NPs. The NPs in the composite were found to be stable. Caruso et al. (2007) synthesized carboxy-terminated water soluble platinum NPs which photoreleased nitric oxide under the control of visible light stimuli. Gao et al. (2007) demonstrated higher potency of FePt@CoS_2 yolk-shell nanocrystals in comparison to cisplatin in killing HeLa cells.

1.2.1.4. Bimetallic Nanoparticles

Bimetallic NPs are a novel class of nanomaterials containing two kinds of metals in a single NP. The bimetallic NPs have unique electronic, optical, chemical, catalytic and biological properties which are distinct and superior to their constituent monometallic counterparts due to new synergistic and bifunctional effects. These properties depend on size, composition as well as arrangement of two elements in NP. Bimetallic NPs are

prepared from respective metal salts by either co-reduction or successive reduction of two metal salts. The co-reduction of two metal ions often leads to formation of alloys and successive reduction of one metal ion after another normally leads to core shell NP. The bimetallic NPs have been explored for a wide range of applications in SERS, sensors, optoelectronics and catalysis. There is enormous scientific data available on the preparation and characterization of bimetallic NPs using various combinations of metals including Au-Pd, Au-Pt, Ag-Pd, Ag-Pt, and Ag-Au. In this context, a three layer (Pd@Au@Pd), four-layer (Ag@Au@Ag@Ag) core-shell structures for gold-palladium and gold-silver systems respectively and Ag-Au core shell NPs with hollow cores and alloyed shells have also been reported (Ferrer et al., 2007; Rodríguez-González et al., 2005; Ferrer et al., 2009).

1.2.2. Polymeric Nanoparticles

Polymeric NPs are colloidal particles ranging in size from 1 nm to 1000 nm which are prepared from synthetic or natural polymeric substances (Hans and Lowman, 2002). The development of polymer-based particulate (micro and nano) drug delivery systems over the last decades has revolutionized the pharmaceutical research giving workhorse solution to manage poor distribution and stability of bare therapeutics.

A representative list of polymers investigated for drug-delivery applications is given in **Table 1.2**. Of particular interest are biodegradable polymers. The polymeric NPs can be constructed either in the form of nanospheres or nanocapsules to achieve desired NP properties and release characteristics for a specific therapeutic application. Nanospheres are matrix systems whose entire mass is solid and drug may be adsorbed at the surface or encapsulated within the particle whereas nanocapsules are vesicular systems in which the drug is confined to a cavity consisting of a liquid core (either oil or water) surrounded by the polymer (Hans and Lowman, 2002; Soppimath et al., 2001). Polymeric NPs have successfully been used to deliver therapeutic genes which interact electrostatically with polymers to yield nanosized ionic complexes called polyplexes (Leong and Wen, 2008). The polymer/DNA complexes protect DNA against nuclease degradation and are more stable than those involving cationic lipids (Gao and Huang, 1996). Encapsulation of proteins and peptides in polymeric NPs for

oral administration protects them from degradation, improves stability and promotes greater absorption in gastrointestinal tract (Allemann et al., 1998).

1.3. Alginate

Alginate is an unbranched, polyanionic polysaccharide composed of 1, 4-linked β-D-mannuronic (M) and α-L-guluronic (G) residues arranged in an irregular blockwise pattern of varying proportions of GG, MG, and MM blocks along the chain (**Figure 1.2.**). It is a natural biopolymer present in brown marine algae (*Phaeophyceae*) and also as an exopolysaccharide of bacteria such as *Pseudomonas aeruginosa*. The first scientific studies on the extraction of alginates from brown seaweed were done by British chemist E. C. Stanford in 1881. Commercially, alginate is extracted from brown algae including *Laminaria hyperborea, Laminaria digitata, Laminaria japonica, Ascophyllum nodosum and Macrocystis pyrifera* by treatment with dilute alkali solutions such as NaOH. The extract is filtered and alginate is precipitated by the addition of either sodium or calcium chloride to the filtrate. The alginate salt is subsequently transformed into alginic acid on treatment with dilute HCl (Lee et al., 2012). The composition, sequence and molecular weights of alginate vary with the source and species from which it is extracted.

Alginate is a cheap, environment friendly biopolymer that has favourable properties like biocompatibility, biodegradability, mucoadhesiveness, and hydrophilicity that makes it suitable for various biomedical applications. It is known to form a hydrogel in the presence of divalent actions whose affinity for alginate decreases in the following order: Pb > Cu > Cd > Ba > Sr > Ca > Co, Ni, Zn > Mn (Mørch et al., 2006). The cations interact ionically with uronic acid residues of G blocks, resulting in the formation of a three-dimensional network usually described as ‘egg-box’ model (Morris et al., 1978). In addition, alginate has large number of free hydroxyl and carboxyl groups that can be easily functionalized to tailor its properties such as solubility, hydrophobicity and physicochemical and biological characteristics.

Table 1.2. Representative list of polymers used in drug delivery (Pillai and Panchagnula, 2001)

Classification	**Polymer**
Natural polymers	
Protein-based polymers	Collagen, albumin, gelatin
Polysaccharides	Agarose, alginate, carrageenan, hyaluronic acid, dextran, chitosan, cyclodextrins
Synthetic polymers	
Biodegradable	
Polyesters	Poly(lactic acid), poly(glycolic acid), poly(hydroxy butyrate), poly(ε-caprolactone), poly(β-malic acid), poly(dioxanones)
Polyanhydrides	Poly(sebacic acid), poly(adipic acid), poly(terphthalic acid) and various copolymers
Polyamides	Poly(imino carbonates), polyamino acids
Phosphorous-based polymers	Polyphosphates, polyphosphonates, polyphosphazenes
Others	Poly(cyano acrylates), polyurethanes, polyortho esters, polydihydropyrans, polyacetals
Non-biodegradable	
Cellulose derivatives	Carboxymethyl cellulose, ethyl cellulose, cellulose acetate, cellulose acetate propionate, hydroxypropyl methyl cellulose
Silicones	Polydimethylsiloxane, colloidal silica
Acrylic polymers	Polymethacrylates, poly(methyl methacrylate), poly hydro(ethyl-methacrylate)
Others	Polyvinyl pyrrolidone, ethyl vinyl acetate, poloxamers, poloxamines

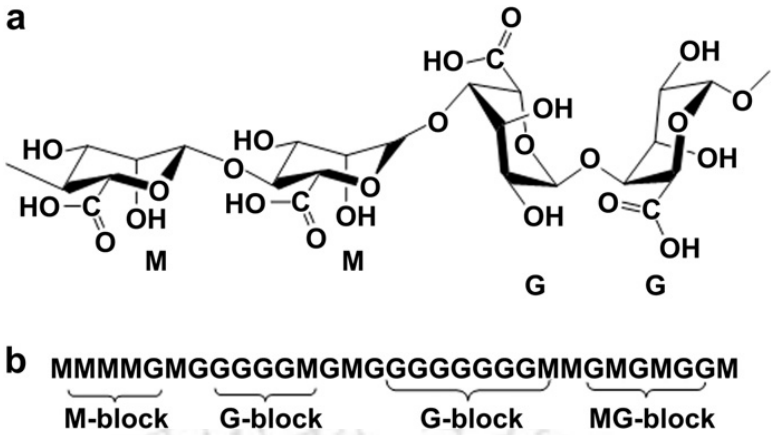

Figure 1.2. Representative alginate structure: **(a)** chain conformation and **(b)** block distribution (Pawar and Edgar, 2012).

Biomedical applications of Alginate and its derivatives

Drug delivery

Alginate gels have extensively been investigated for delivery of small chemical drugs. Bouhadir et al. (2001) synthesized novel alginate hydrogel loaded with three antineoplastic agents' *viz*. methotrexate, doxorubicin, and mitoxantrone for the simultaneous delivery of multiple drugs. Zhang et al. (2010) reported sustained release of theophylline from carbon nanotube (CNT)-incorporated alginate microspheres. The incorporation of CNT increased the mechanical stability of gels. Besides, alginate gels have also been used for the delivery of protein drugs. The proteins are incorporated under relatively mild conditions thereby minimizing denaturation and protected from degradation in the gels until their release (Chan et al. 2010). Recently, Möbus et al. (2012) prepared Zn^{2+} cross-linked alginate microparticles via a simple one-step spray-drying process for controlled pulmonary delivery of BSA as a model protein.

Wound Dressings

Alginate-based products are most commonly employed in wound management. Alginate dressings in dry form absorb wound exudates to form a gel which eliminates fibre entrapment in the wound, a major cause of discomfort for patient during dressing removal. Besides, the gel maintains a physiologically moist microenvironment conducive for rapid healing (Winter et al., 1962). Some examples of commercial

alginate-based wound dressings include Kaltostat™ (dressing calcium/sodium alginate, ConvaTec), Kaltogelw (calcium/sodium alginate gelling fibre, ConvaTec), Seasorbw (calcium/sodium alginate gelling fibre, Coloplast) and Sorbsan™ (dressing calcium alginate, Maersk). Balakrishnan et al. (2006) incorporated dibutyryl cyclic adenosine monophosphate (DBcAMP), a regulator of human keratinocyte proliferation, into partially oxidized alginate wound dressing gel that accelerated the wound healing process due to sustained release of DBcAMP in a rat model. A complete re-epithelialization of full thickness wounds was observed within 10 days. Similarly, Rabbany et al. (2010) demonstrated the effectiveness of alginate gel releasing stromal cell-derived factor-1 in accelerating wound closure rates and reducing scar formation in pigs with acute surgical wounds. Further, Shalumon et al. (2011) developed sodium alginate/poly (vinyl alcohol)/nano ZnO composite nanofibres that were shown to have antibacterial effect against *S aureus* and *E. coli* due to the presence of ZnO, making them suitable as wound dressing material.

Cell culture substrates

In addition, alginate gels are also increasingly being used as either 2D or 3D mammalian cell culture systems by modifying the gels with synthetic peptides specific for cellular adhesion receptors. In this context, arginine-glycine-aspartic acid (RGD)-modified alginate gels have been most frequently used as *in vitro* cell culture substrates till now. Rowley et al. (1999) chemically conjugated RGD peptides to alginate and demonstrated enhancement in adhesion and proliferation of myoblasts cultured on alginate gels in comparison to non-modified alginate gels. The number of cells adherent to the gels and the growth rate were found to be strongly dependent on the bulk RGD density in the gels. Chueh et al. (2009) reported formation of alginate gel in a microfluidic device through UV-triggered release of caged calcium from DM-nitrophenTM. The gel was used as a 3D cell culture substrate for coculture of preosteoblasts (MC3T3-E1) and human umbilical vein endothelial cells demonstrating integration of 3D culture microenvironments into microfluidic systems. Furthermore, alginate gels have been also been used as 3D cell culture substrates for cancer cells and stem cells thereby opening up possibility to gain insights regarding cancer and stem cell biology (Fischbach et al., 2009; Huebsch et al., 2010).

Tissue regeneration

The alginate gels have also been used for the delivery of proteins or cells that can direct the regeneration or engineering of various tissues and organs in the body. These include delivery of angiogenic factors like vascular endothelial growth factor (VEGF) and basic fibroblast growth factor in SCID mice (Lee et al., 2003); bone regeneration factors like bone morphogenetic proteins BMP-2 and BMP-7 (Basmanav et al. 2008) and cell populations like primary chondrocytes and osteoblasts into mice (Alsberg et al., 2002); mesenchymal stem cells for cartilage regeneration in large osteochondral defects (Ma et al. 2003) and also various growth factors and cells for regeneration of other tissues and organs including skeletal muscle, nerve, pancreas, and liver (Borselli et al., 2009; Prang et al., 2006; Calafiore et al., 2003; Dvir-Ginzberg et al., 2003). The alginate gels have also been used for sequential delivery of various growth factors based on their differential binding to various factors. For example, Ruvinov et al. (2011) showed sequential release of insulin-like growth factor-1 (IGF-1) followed by hepatocyte growth factor (HGF) from alginate-sulfate gels in a rat model of acute myocardial infarction.

Other applications of Alginate and its derivatives

Alginate is widely used in food industry as thickening agent, gelling agent, emulsifier and colloidal stabilizer. Furthermore, alginate has also been used in the removal of toxic heavy metals like uranium, lead, zinc, cadmium and nickel from industrial wastes by biosorption (Davis et al., 2003; Gok and Aytas, 2009).

1.4. Chitosan

Chitosan is a polycationic linear copolymer of β-(1–4)-2-acetamido-2-deoxy-β-D-glucose and β-(1–4)-2-amine-2-deoxy-β-D-glucose. Commercially, chitosan is obtained by alkaline deacetylation (NaOH, 40-50%) of chitin (Rabea et al., 2003) which is a structural material present in the shells of marine crustaceans and molluscs such as shrimp, crab, squid, as well as cell wall of fungi. Chitosan is insoluble in water, alkaline pH and organic solvents but is soluble in organic acids with pH < 6 due to protonation of free amino groups on the C-2 position of D-glucosamine residues. Numerous efforts have been made to prepare functional derivatives of chitosan by chemical modifications

to increase the solubility in water (Muzzarelli, 1992; Heras, 2001; Jia et al., 2001; Kurita et al., 2002; Ding et al., 2003; Ramos et al., 2003; Ronghua et al., 2003). Chitosan has found immense applications in fields like biotechnology, pharmaceutics, cosmetics and agriculture owing to its unique properties such as biocompatibility, biodegradability, and no toxicity to mammals. Depending on the use, the physicochemical properties of chitosan such as the degree of deacetylation and molecular weight can be varied.

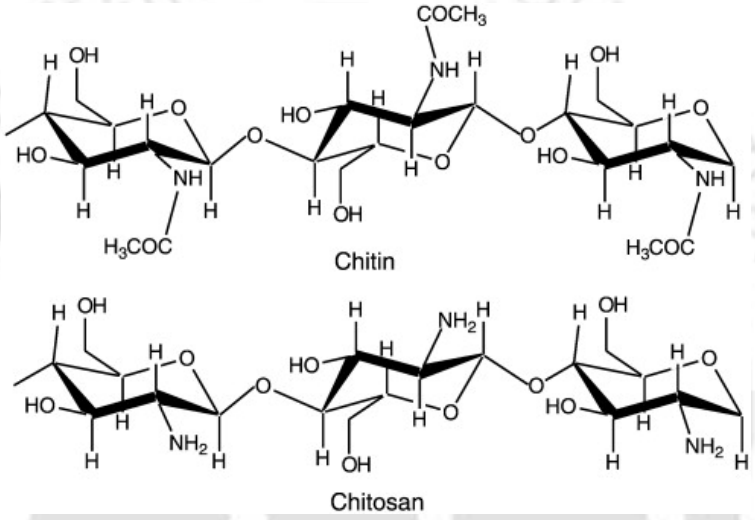

Figure 1.3. Structure of Chitin and Chitosan (Jayakumar et al., 2011).

Antimicrobial properties

Chitosan is well known for its antimicrobial property against a wide range of organisms like algae, bacteria, yeasts and fungi. The antimicrobial property of chitosan is influenced by a number of intrinsic factors such as type of chitosan, degree of chitosan polymerization, host, natural nutrient constituency, chemical or nutrient composition of the substrates or both, and the environmental conditions (Rabea et al., 2003).

Chitosan has been shown to be fungicidal against several fungi with minimum inhibitory concentrations (MICs) ranging from 0.0018% to 1.0% for specific target organisms (Liu et al., 2001). Stössel and Leuba (1984) demonstrated the inhibitory

effect of chitosan against soil borne phytopathogenic fungi. Laflamme et al. (2000) demonstrated successful inhibition of *Fusarium acuminatum*, *Cylindrocladium floridanum* and other pathogens of forest nurseries by chitosan *in vitro*. Roller and Covill (1999) reported efficient inhibition of fifteen yeasts and molds associated with food spoilage including *Mucor racemosus* and *Byssoclamys* spp. by chitosan at various concentrations, pH values, and temperatures. Chitosan has also been successfully used as food wraps (Muzzarelli, 1986). In both Canada and the U.S.A, the use of N, O-carboxymethyl chitin films has been approved for preserving fruits over long periods (Davies et al., 1989).

In addition to fungicidal action, chitosan also possesses antibacterial property against a wide range of bacteria. Chitosan derivatives containing quaternary ammonium salts, such as *N*, *N*, *N*-trimethyl chitosan, *N*-propyl-*N*, *N*-dimethyl chitosan and *N*-furfuryl-*N*, *N*-dimethyl chitosan have also been demonstrated to have antibacterial activity against *E. coli* by Jia et al., (2001). They found that the antibacterial activity of quaternary ammonium chitosan was stronger than that of chitosan and also stronger in acetic acid medium than that in water. Sudarshan et al. (1992) studied the antimicrobial effect of water-soluble chitosan such as chitosan lactate and chitosan hydroglutamate on different bacterial cultures and found that the derivatives were bactericidal against both Gram-positive and Gram-negative bacteria in the range of 1−5 log cycle reductions within 1 h. The authors also reported that chitosan was no longer bactericidal at pH 7 due to absence of a significant proportion of charged amino groups and the poor solubility of chitosan at this pH. In a similar study by Papineau et al. (1991) chitosan lactate (0.2 mg/mL) was shown to be most effective against *E. coli* with population drop of 2 and 4 log cycles within 2 min and 1 h exposure, respectively. They also reported that chitosan glutamate was effective against yeast cultures such as *Saccharomyces cerevisiae* and *Rhodotorula glutensis*.

Biomedical applications of chitosan and chitosan-based composite materials

Chitosan can easily be processed into gel, membrane, nanofibre, film bead, microparticle, nanoparticle, scaffold and sponge forms making it suitable for a wide range of applications such as biosensors, drug delivery systems, wound healing, tissue reconstruction, separation membranes and many more in biomedical field.

The porous structure and cationic nature of chitosan makes it ideal candidate for tissue engineering applications. The porosity and pore morphology of interconnected porous structure of chitosan-based scaffolds is critical for controlling cellular colonization rates and organization within an engineered tissue. The cationic nature of chitosan allows its pH-dependent electrostatic interactions with anionic glycosaminoglycans (GAG) proteoglycans and other negatively charged species. Various types of chitosan derivatives have been used in skin, bone, cartilage, liver, nerve, and blood vessel regeneration (Kim et al., 2008a). In this regard, chitosan has also been combined with other materials to produce 'composite' materials. For example, Risbud et al. (2001) demonstrated the use of chitosan–gelatin hydrogel as a culture substratum for respiratory epithelial cells.

Chitosan is the only positively charged naturally occurring polysaccharide (Muzzarelli, R.A.A., 2009) and thus forms stable complexes with DNA making it suitable for efficient transfection of DNA (Roy et al., 1999; Köping-Höggård et al., 2001; Jiang et al., 2008). Chitosan has also been used for the delivery of proteins and antigens particularly via mucosal routes. It has been found that chitosan (derivatives) interact with mucus and epithelial cells leading to opening of cellular tight junctions and increasing the paracellular permeability of the epithelium (Artursson et al., 1994; Borchard et al., 1996; Schipper et al., 1997).

Chitosan based materials have also been employed for wound healing applications. In this regard, films made from polyelectrolyte complex (PEC) of chitosan and alginate have been investigated as wound dressing materials (Yan et al., 2001).The PEC films were found to promote rapid wound healing in a rat model (Wang et al., 2001). In another study by Hirano et al. (2001), chitosan fibers were combined with acidic gluosaminoglycans (GAGs) to release the GAGs for wound healing.

1.5. Key Areas and Scopes

With the understanding gained by the review of literature in the field of therapeutic implication of nanomaterials, research areas with potential scope were identified and are summarized below:

- Development of new, ecofriendly 'green' methods for the synthesis of metal NPs.
- Development of new, ecofriendly 'green' methods for the synthesis of biocompatible polymer-metal NP nanocomposites.
- Deciphering the fundamental molecular basis of effect of metal NPs and their composites on biological systems including both bacterial and mammalian cells.
- Designing delivery vehicles for potential therapeutic nanomaterials.

1.6. Present Work: Salient Features

The present thesis is divided into seven chapters. The salient features of each chapter of the present thesis are summarized below:

- ❖ The literature on therapeutic applications of metal NPs and polymeric NPs with special emphasis on naturally occurring biopolymers - chitosan and alginate has been reviewed in detail (*Chapter 1*).
- ❖ Enhanced antibacterial efficacy of ~30 nm sized bimetallic gold silver core-shell NPs at low silver concentration against both Gram negative and Gram positive bacteria, with more pronounced effect against Gram negative bacteria was discovered. The core shell NPs were also shown to possess enhanced catalytic efficiency in comparison to their monometallic counterparts (*Chapter 2*).
- ❖ Superior antibacterial activity of chitosan-based nanocarrier of Ag NP nanocomposite in comparison to chitosan NPs or Ag NPs alone was observed against both Gram negative and Gram positive bacteria due to the synergistic effect of chitosan and Ag NPs. The composite was found to be more effective against Gram negative bacteria (*Chapter 3*).
- ❖ A completely 'green' method of synthesis of biocompatible Ag NPs using sodium alginate as both reducing and stabilizing agent was developed. The

alginate stabilized Ag NPs were found to be antibacterial against both Gram negative and Gram positive bacteria (*Chapter 4*).

- A three component film comprising alginate, chitosan and Ag NPs was developed, which was demonstrated to possess effective bactericidal activity against both Gram positive and Gram negative bacteria with more efficacy against Gram positive bacteria *(Chapter 4*).
- Novel, biodegradable alginate-chitosan based nanocarrier of Ag NPs was developed in a new 'green' method (*Chapter 5*).
- The nanocarrier was employed for efficient delivery of Ag NPs in refractory human glioblastoma cancer cells to induce apoptosis by Ag NPs. The apoptosis occurred at very low Ag NP concentration, thereby minimizing toxicity (*Chapter 5*).
- Generation of ROS, loss of mitochondrial potential and DNA damage, in the Ag NP induced apoptosis was established (*Chapter 5*).
- Reversibility in the aggregation behaviour of alginate stabilized Ag NPs was achieved via alginate gel formation and breakage (*Chapter 6*).

|Chapter 2|

Bimetallic Gold-Silver Core-shell Nanoparticles as Antibacterial and Catalytic Agents

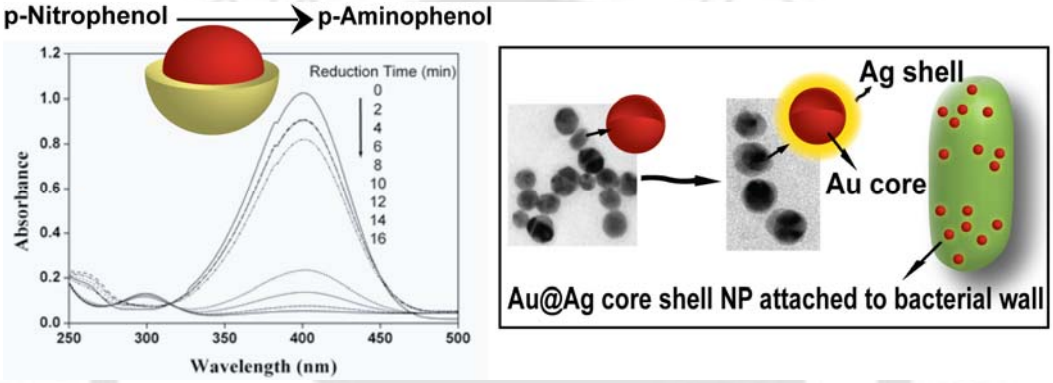

Banerjee, M., Sharma, S., Chattopadhyay, A. & Ghosh, S. S. *Nanoscale* **3**, 5120- 5125 (2011).

Chapter 2

BIMETALLIC GOLD-SILVER CORE-SHELL NANOPARTICLES AS ANTIBACTERIAL AND CATALYTIC AGENTS

2.1. Introduction

In recent years, bimetallic nanoparticles (NPs), containing two kinds of metals in a single NP have attracted attention as a novel class of nanomaterials owing to their unique electronic, optical, chemical and catalytic properties which are distinct and superior to their constituent monometallic counterparts due to new synergistic and bifunctional effects (Toshima and Yonezawa, 1998). The bimetallic NPs, in the form of alloys or core-shell structures, have potential applications in sensors, optoelectronics and catalysis. Bimetallic core-shell NPs are nanostructures, where one metal element forms an inner core and is surrounded by concentric shell of another metal. Of these, noble core-shell NPs containing gold and silver have received immense interest. Au colloids have advantages of easy preparation, homogeneity and biocompatibility with biomolecules like antigen, antibody, DNA, etc in contrast to Ag NPs which are not biocompatible and less stable under biological conditions (Chandran et al., 2007). But the extinction coefficient of the surface plasmon band of Ag NP is approximately four times as large as that for an Au NP of same size (Cao et al., 2001). Several groups have made efforts to deposit silver on gold to obtain Au@Ag core-shell NPs that have homogeneity and stability of gold and optical properties of silver (Freeman et al., 1996; Rivas et al., 2000; Hodak et al., 2000; Mallik et al., 2001; Lu et al., 2002; Selvakannan et al., 2004; Mandal et al., 2004; Chandran et al., 2007; Pande et al., 2007; Yang et al., 2008). Importantly, they serve as useful surface-enhanced Raman spectroscopy (SERS) active substrates, which display SERS activity greater than individual AgNPs and AuNPs. In addition, studies have also been done on the synthesis of inverted Ag@Au core-shell NPs (Mulvaney et al., 1993; Srnová-Šloufová et al., 2000; Cao et al., 2001; Cui et al., 2006), which have been explored for biological applications, such as,

oligonucleotide conjugation and SERS based immunoassay.

In addition, core-shell nanostructures showing antibacterial properties have also been investigated (Rana et al., 2005; Rosemary et al., 2006; Kim et al., 2007b; Jang and Kim, 2008). Ag NPs have strong bactericidal properties and substantial research has been done to use them either alone or in composite with polymer (Morones et al., 2005; Gogoi et al., 2006; Sanpui et al., 2008; Banerjee et al., 2010; Banerjee et al., 2011). Though the antibacterial core-shell NPs comprising of silver shell supported on organic and inorganic cores have been studied, the antibacterial efficacy of bimetallic core-shell NPs containing silver remains largely an unexplored area.

2.2. Outline of the Research Work

1) Bimetallic Au@Ag core-shell NPs were synthesized at room temperature where Au NPs served as the seeds for continuous deposition of Ag atoms on their surfaces.
2) A series of characterizing techniques including transmission electron microscopy (TEM), energy dispersive X-ray (EDX) analysis and X-ray diffraction (XRD) were performed systematically to determine the morphology of the NPs. High resolution transmission electron microscopy (HRTEM) combined with EDX analysis confirmed the formation of Au@Ag core-shell structure.
3) Au@Ag core-shell NPs demonstrated superior catalytic efficiency in comparison to similar sized monometallic counterparts, viz. Au NPs and Ag NPs.
4) Au@Ag core-shell NPs were found to be antibacterial against both Gram negative and Gram positive bacteria at low concentration of Ag present in the shell, with more efficacy against Gram negative bacteria.
5) TEM and flow cytometric studies showed that the core-shell NPs attached to the bacterial surface and caused membrane damage leading to cell death.

2.3. Experimental Section

2.3.1. Chemicals, Bacterial strains, Growth media and conditions

Silver nitrate and hydrogen tetrachloroaurate (III) were purchased from Sigma Aldrich chemicals, USA. Ascorbic acid, cetyl trimethylammonium bromide (CTAB) was

obtained from Merck India Pvt. Ltd, Mumbai, India. Luria-Bertani Broth (LB), nutrient broth (NB), brain-heart infusion (BHI), and de Man Rogosa and Sharpe (MRS) growth media were purchased from Hi Media, Mumbai, India. The strain of lactic acid bacteria (LAB) *Pediococcus acidilactici* CFR K7 was propagated in MRS medium under static condition at 37 °C. *Enterococcus faecalis* MTCC 439 was grown in BHI broth medium at 37 °C at 180 rpm for 12 h, whereas *Pseudomonas aeruginosa* MTCC 2488 was grown in NB medium at 37 °C at 180 rpm for 12 h. GFP expressing recombinant *E. coli* was grown in LB medium at 37 °C at 180 rpm for 12 h.

2.3.2.GFP Construct

The recombinant GFP-expressing *E. coli* (DH5α) was generated by cloning the GFP gene into an ampicillin-resistant pUC-derived plasmid vector as described previously (Gogoi et al., 2006).

2.3.3. Synthesis of Au NPs

The Au NPs were prepared following Frens (1973) method. In brief, 100 mL solution containing 0.01 g $HAuCl_4 \cdot 3H_2O$ was heated to boiling. Then, a freshly prepared sodium citrate solution (3 mL, 1%) was added to the boiling solution. A few minutes later, the colour of the solution changed from colorless to deep wine-red. The solution was further boiled for 40 min and then left to cool to room temperature.

2.3.4. Synthesis of Au@Ag core-shell NPs

The Au@Ag core-shell NPs were synthesized by modifying the procedure of Lu et al. (2002). In brief, in 20 mL water containing 0.2 mL of 25 mM CTAB and 1 mL of 100 mM ascorbic acid, 0.1 mL of 10 mM $AgNO_3$ was added. Afterwards, 2 mL of Au NP seed solution was added and 0.1 mL of 1 M NaOH was added drop by drop to the above solution while stirring. Throughout the experiment, the temperature was maintained at room temperature. Within 1–10 min, the colour of the solution was changed from pink to orange-yellow to yellow, suggesting the formation of composite NPs.

2.3.5. Characterization of Au@Ag core-shell NPs

UV–Vis spectra of the Au@Ag core-shell NPs were obtained using a spectrophotometer (Lambda 45; Perkin-Elmer, Fremont, CA, USA). Transmission electron microscope (TEM) measurements were done using a JEM 2100; Jeol, Peabody, MA, USA machine operating at an accelerating voltage of 200 kV. 5 µL of each sample was drop coated onto a carbon coated copper TEM grid followed by air drying and the grid was then analyzed under TEM. The XRD measurement of core-shell NPs was carried out using a Bruker D8 ADVANCE (Bruker AXS Inc.) XRD machine using Cu Kα ((λ= 1.54 Å) source.

2.3.6. Catalytic activity of Au@Ag core-shell NPs

In order to study the catalytic activity of Au@Ag core-shell NPs, the NPs were centrifuged and redispersed in MilliQ water. To 1.85 mL of water in a 1.0 x 1.0 cm quartz optical cuvette, 0.1 mL of 4-nitophenol (4-NP) and 0.3 mL of freshly prepared aqueous solution of $NaBH_4$ (100 mM) were added. The quartz cuvette was then settled in the cuvette holder of the spectrophotometer (Perkin-Elmer Lambda-25). Thereafter, 0.4 mL of the redispersed Au@Ag core-shell NPs was added and the catalytic reaction was followed by recording the UV-Vis spectra of the reaction mixture every 30 s, immediately after the addition of the NPs. The spectra were recorded at room temperature using a UV-Vis spectrometer in the range 250–500 nm. The amount of sodium borohydride was 50-fold excess of p-nitrophenol, so the reaction was treated as pseudo-first-order reaction. The apparent rate constant *k* of the reaction was calculated by fitting the obtained data using the equation $\log A_{400} = -kt + \log A_{400,\ t=0}$, where, t, A_{400} and $\log A_{400,\ t=0}$ represented the elapsed time, the absorbance at 400 nm at an elapsed time t, and the initial absorbance at 400 nm, respectively.

2.3.7. Antibacterial activity assessment

For antibacterial activity test, *Enterococcus faecalis* and *Pediococcus acidilactici* were selected as representatives of Gram positive bacteria and *Escherichia coli* and *Pseudomonas aeruginosa* as representatives of Gram negative bacteria. Different concentrations of Au@Ag core-shell NPs were used to determine the minimum inhibitory concentration (MIC) and minimum bactericidal concentration (MBC). The bacteria (10^8 CFUs mL^{-1}) were grown in media in the presence of different

concentrations of Au@Ag core-shell NPs for 12 h. The lowest concentration at which there was no visual turbidity was taken as MIC value of core-shell NPs. The cultures that lacked turbidity were tested further for determining MBC. 100 µL from each of the samples without visible growth was spread onto agar plates and incubated at 37 ºC for 12 h. The lowest concentration of Au@Ag core-shell NPs that was bactericidal to ≥99.9% of original inoculum was taken as MBC. The concentration of silver ions (Ag^+) released from core-shell NPs was measured by using Fast Sequential Atomic Absorption Spectrometer (Varian, AA240FS). For this, the core-shell NPs at MIC were incubated in aqueous media under shaking condition and after different time points, the NPs were centrifuged to collect supernatants containing Ag^+ for analysis by spectrometer.

2.3.8. Microscopy

The effects of Au@Ag core-shell NPs and Ag NPs on GFP-expressing *E. coli* were monitored using a fluorescence microscope (Axioskop2MAT, Karl Zeiss) at different time points. 50 µL aliquots of bacterial cultures were withdrawn from the appropriate media and placed on microscope slides, air-dried and observed under the microscope. The excitation wavelength was 445-495 nm, and the observation filter had a long-pass filter wavelength above 515 nm.

2.3.9. Flow cytometric assay of cell membrane damage using GFP-PI combination

The viability of GFP expressing recombinant bacterial cells and assessment of cell membrane damage was done using propidium iodide (PI) dye. 500 µL of 10^6 cells mL^{-1} of the recombinant GFP expressing *E. coli* cells were incubated with different concentrations of core-shell NPs at 25°C. After different time points, 1.5 µL of 0.2 mM PI was added to each tube, mixed, diluted with 150 mM NaCl and analyzed by a flow cytometer (BD FACS calibur System, BD Biosciences, San Jose, CA). The samples were illuminated with a 15 mW argon ion laser (488 nm), and the fluorescence was detected via 525 ± 10 nm (green) and 620 ± 10 nm (red) bandpass filters. Signals were amplified with the logarithmic mode for side scattering, forward scattering, and fluorescence.

2.4. Results and Discussion

2.4.1. Synthesis and Characterization of Au@Ag core-shell NPs

In the present study, Au@Ag core-shell NPs were synthesized by growing Ag nanoshells onto pre synthesized citrate stabilized Au NPs (~12 nm) that served as nucleation sites (**Figure 2.1.**). Ag shells of different thickness were deposited on fixed concentration of Au NPs by varying the amount of $AgNO_3$. The colour of the solution changed from red (due to Au NPs) to pink-red, orange-yellow and yellow depending on the extent of coverage of Ag atoms onto the surface of Au NPs.

The UV-Vis extinction spectra of monometallic citrate stabilized Au NPs showed a band at 520 nm (**Figure 2.2a**). For bimetallic core-shell NPs, the Au band blue shifted and a plasmon band appeared at 420 nm due to plasmon resonance of Ag shell that red shifted upon increasing the ratio (v/v) of $AgNO_3$ to Au NPs (Lu et al., 2002). This was probably because as the amount of $AgNO_3$ increased, the amount of Ag reduced on Au NPs increased, forming larger NPs with thicker Ag shell. For further experiments, the final concentration of Au NPs seed and $AgNO_3$ was 0.02 mM and 0.04 mM, respectively. The mixture of Au NPs and Ag NPs both prepared independently showed well defined typical bands at 520 nm and 420 nm for Au NPs and Ag NPs, respectively (**Figure 2.2b**) indicating that the synthesized NPs were core-shell structures and not merely a mixture of Au and Ag NPs.

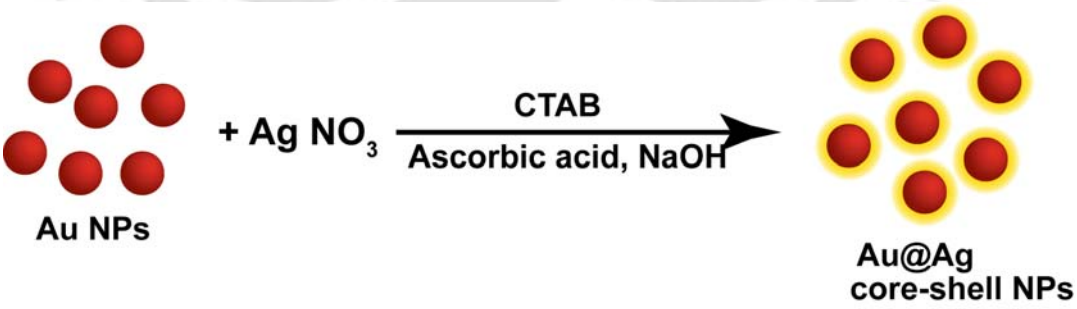

Figure 2.1. Schematic showing synthesis of Au@Ag core-shell NPs from Au NP seeds.

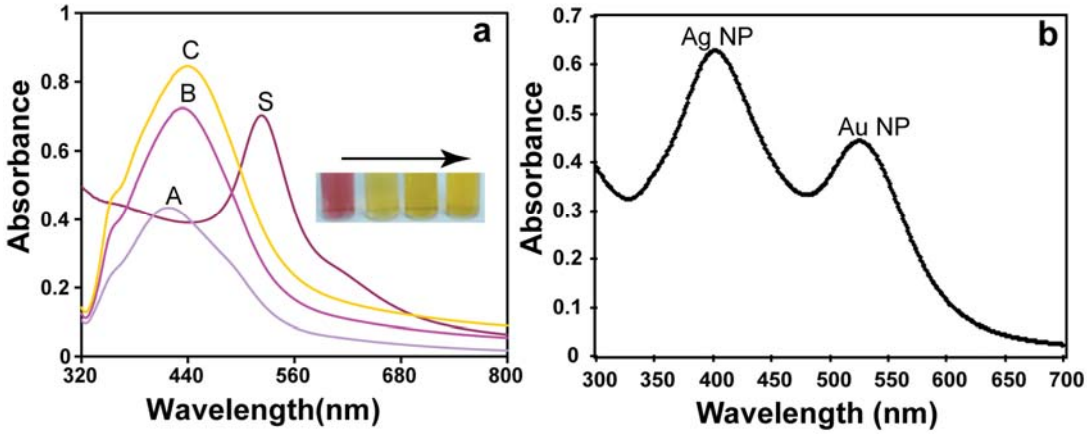

Figure 2.2. UV-visible spectra of **(a)** pure Au NPs (S) and citrate-gold spheres with different coverage of silver on the surface (A–C), resulting from different silver to citrate-gold ratios. Condition: For A, B and C, 0.1, 0.2 and 0.3 mL of 10^{-2} M Ag NO_3 were used, respectively; [Au NPs seed] = 0.02 mM in all cases and **(b)** mixture of Au NPs and Ag NPs.

To further confirm the core-shell structure, the bimetallic solution was mixed with increasing volumes of concentrated HNO_3 (approx. 16 M) and changes in absorbance values were measured spectrophotometrically. The colour of the solution changed from yellow to fairly pink with increasing volume of HNO_3 indicating dissolution of Ag shell revealing gold core. In UV-Vis spectroscopy, the initial bimetallic colloidal solution showed a broad band at 406 nm and a small shoulder at 500 nm. After treatment with HNO_3, the intensity of plasmon band at 406 nm decreased with appearance of band at 520 nm characteristic of Au NPs (**Figure 2.3.**) supporting the formation of core-shell structures.

The TEM and HRTEM images revealed distinct variation in contrast between the dark Au core and the lighter Ag shell (**Figure 2.4a and 2.4b**).The Ag shell was not perfectly uniform although the final shape was nearly spherical. There was no particle-particle aggregation and the average size distribution was 30 ± 3.7 nm (**Figure 2.4c**). Importantly, there was no evidence for the formation of separate Ag NPs in any TEM images. In addition, the EDX spectra revealed presence of both Au and Ag signals in the composite (**Figure 2.4d**). The X-ray diffraction pattern of core-shell NPs (**Figure 2.4e**) showed peaks at 38.2º, 44.3º and 64.5º corresponding to (111), (200) and (220) planes of the cubic structure of metallic Ag (Gong et al, 2007).

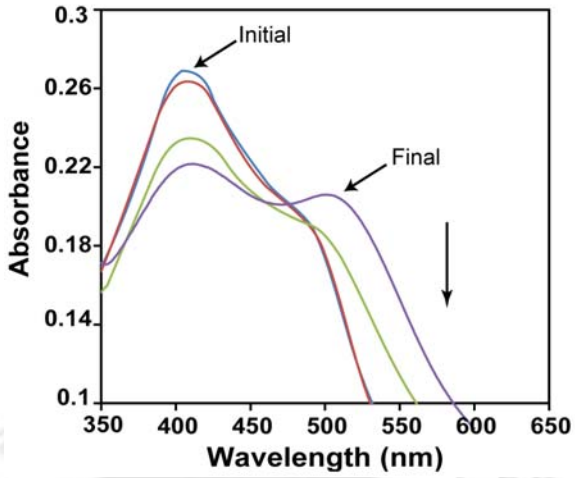

Figure 2.3. Au@Ag core-shell NPs treated with increasing volumes viz.. 60, 150 and 300 mL of ~16 M HNO_3. Different volumes were added to 3 mL of NPs solution and the spectra were recorded within 10 min after acid addition.

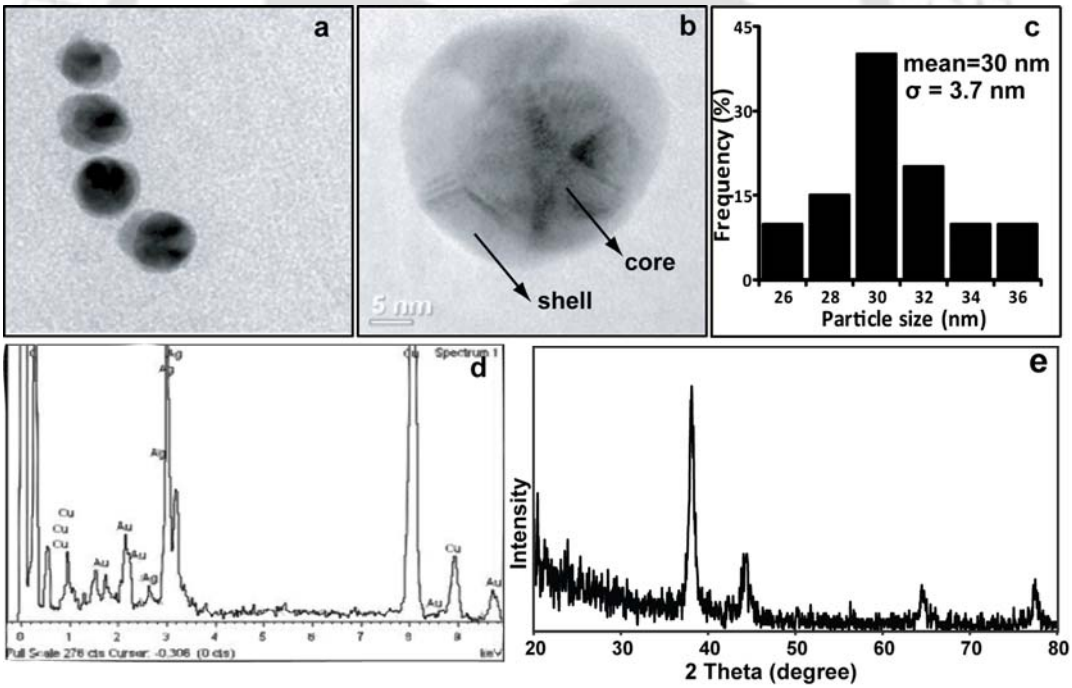

Figure 2.4. Representative **(a)** TEM, **(b)** HRTEM images of Au@Ag core–shell bimetallic NPs, **(c)** particle size distribution calculated based on TEM images **(d)** EDX spectrum confirming the presence of both gold and silver in the Au@Ag core–shell bimetallic NPs and **(e)** XRD pattern of Au@Ag core-shell NPs showing lattice planes of both gold and silver.

2.4.2. Catalytic activity of Au@Ag core-shell NPs

The catalytic activity of Au@Ag core-shell NPs was investigated using a model reaction i.e. reduction of 4-nitrophenol (4-NP) to 4-aminophenol (4-AP) in the presence of excess $NaBH_4$ (Pradhan et al., 2002; Lu et al., 2006; Murugadoss and Chattopadhyay, 2008). In $NaBH_4$ medium (pH>12.0) the peak corresponding to 4-NP at 317 nm is red shifted to 400 nm due to formation of 4-nitrophenolate ion and the peak at 400 nm remains unaltered in the absence of any catalyst. The addition of Au@Ag core-shell NPs in the reaction mixture caused the disappearance of characteristic yellow colour of the 4-NP in aqueous solution indicating its reduction to 4-AP. Time-dependent UV-Vis absorption spectra of the reaction mixture showed that the peak intensity at 400 nm gradually decreased and a new peak at around 290 nm appeared due to reduced product, 4-AP (Lu et al., 2006) whose intensity continued to increase with time (**Figure 2.5a**).

The rate kinetics of the present catalytic reaction was considered to be of pseudo-first order with respect to the concentration of 4-NP as the concentration of $NaBH_4$ used was in large excess in comparison to that of 4-NP. The catalytic rate constant of Au@Ag core-shell NPs was evaluated from the plot of Log A (A = absorbance at 400 nm) vs time (**Figure 2.5b**). The catalytic efficiency of the Au@Ag core-shell NPs was compared with Au NPs and AgNPs of similar size (**Figure 2.5c, 2.5d**). The amount of catalysts in these three groups had same metal loading. It was found that the catalytic activity of core-shell NPs was ~18 and ~12 times higher than similar sized monometallic Au NPs and Ag NPs, respectively.

2.4.3. Antibacterial Activity of Au@Ag core-shell NPs

The antibacterial activity of Au@Ag core-shell NPs was evaluated against both Gram positive viz. *Enterococcus faecalis* and *Pediococcus acidilactici* and Gram negative viz. *Escherichia coli* and *Pseudomonas aeruginosa* strains. The minimum inhibitory concentration (MIC) and minimum bactericidal concentration (MBC) were determined as shown in **Table 2.1**. It may be mentioned here that the MIC and MBC values presented were in terms of effective Ag concentration in core-shell NPs as Ag shell is responsible for the antimicrobial action. The MIC values in terms of effective Ag

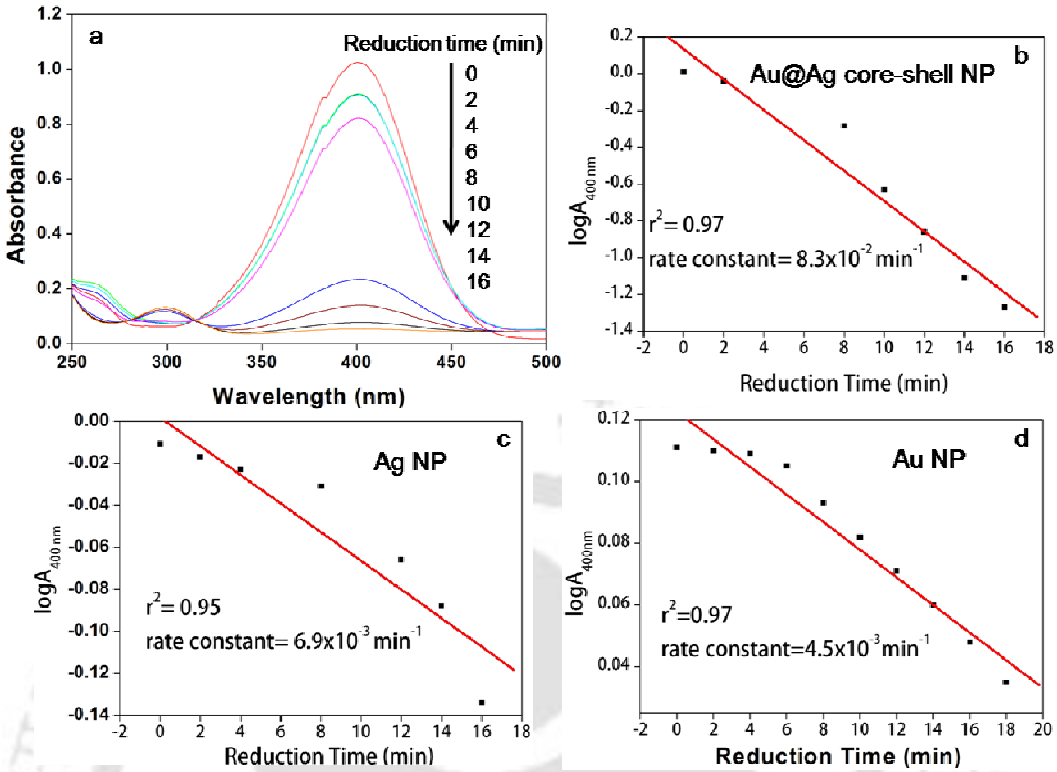

Figure 2.5. (a) UV-visible spectra for the successive reduction of 4-NP by $NaBH_4$ catalyzed by Au@Ag core-shell NPs. Plots of logarithm of absorbance at 400 nm versus time for the reduction of 4-NP by **(b)** Au@Ag core-shell NPs, **(c)** Ag NPs and **(d)** Au NPs.

concentration in core-shell NPs for Gram positive strains were 2.5 µg mL^{-1} for *Enterococcus faecalis* and 2.81 µg mL^{-1} for *Pediococcus acidilactici* and Gram negative strains were 1.56 µg mL^{-1} for *Escherichia coli* and 1.88 µg mL^{-1} for *Pseudomonas aeruginosa*. These values were significantly lower than 22.64 µg mL^{-1} which was the reported MIC of Ag NPs only (Gogoi et al., 2006). Also, the low concentration (0.2 mM) of CTAB used for stabilizing core-shell NPs did not exert any antibacterial activity.

From Table **2.1.**, it is evident that the effect of Au@Ag core-shell NPs was more pronounced against Gram negative than Gram positive bacteria. This is because of difference in membrane structures of Gram positive and Gram negative bacteria (Murray et al., 1965). The Gram-negative bacteria have an outer membrane of lipopolysaccharide, followed by a thin (about 2-3 nm) peptidoglycan layer. On the

other hand, the Gram-positive bacteria lack the outer membrane, but have a thick (about 30 nm) layer of peptidoglycan, consisting of linear polysaccharide chains cross-linked by short peptides to form a three dimensional rigid structure. This rigid structure provides very few anchoring sites for NPs in the cell wall, thus leading to difficulty in penetration. In the present case, the Au@Ag core-shell NPs were positively charged due to the presence of CTAB as stabilizing agent. The positively charged Au@Ag core-shell NPs interacted more strongly electrostatically with Gram negative bacteria due to presence of abundant negative charges of lipopolysaccharide, thereby killing them more effectively than Gram-positive bacteria.

Table 2.1. Ag concentration in MIC and MBC values of Au@Ag core–shell NPs against different bacterial strains

Bacterial strain	**Ag concentration in MIC value (μg mL^{-1})**	**Ag concentration in MBC value (μg mL^{-1})**
Gram positive		
Enterococcus faecalis	2.50	3.44
Pediococcus acidilactici	2.81	3.44
Gram negative		
Escherichia coli	1.56	1.95
Pseudomonas aeruginosa	1.88	3.13

From Table **2.1.**, it is evident that the effect of Au@Ag core-shell NPs was more pronounced against Gram negative than Gram positive bacteria. This is because of difference in membrane structures of Gram positive and Gram negative bacteria (Murray et al., 1965). The Gram-negative bacteria have an outer membrane of lipopolysaccharide, followed by a thin (about 2-3 nm) peptidoglycan layer. On the other hand, the Gram-positive bacteria lack the outer membrane, but have a thick (about 30 nm) layer of peptidoglycan, consisting of linear polysaccharide chains cross-linked by short peptides to form a three dimensional rigid structure. This rigid structure provides few anchoring sites for NPs in the cell wall, thus leading to difficulty in penetration. In the present case, the Au@Ag core-shell NPs were positively charged

due to the presence of CTAB as stabilizing agent. The positively charged Au@Ag core-shell NPs interacted more strongly electrostatically with Gram negative bacteria due to presence of abundant negative charges of lipopolysaccharide, thereby killing them more effectively than Gram-positive bacteria.

In addition, time dependent antibacterial activity of Au@Ag core-shell NPs (at MIC and MBC values) was monitored against GFP expressing recombinant *E. coli* by measuring optical density (OD) at 595 nm at various time points (**Figure 2.6.**). The relative antibacterial activity of Ag NPs of size similar to that of core-shell NPs (~30 nm) at Ag concentration corresponding to Ag in growth inhibitory concentration of core-shell NPs was also determined. The results indicated that Ag NPs of 30 nm size did not inhibit bacterial growth at Ag concentration at which similar sized Au@Ag core-shell NPs inhibited bacterial growth. The experiments were performed thrice to ensure reproducibility. This result was further substantiated with time dependent fluorescence microscopic study with GFP expressing recombinant *E. coli* treated with Au@Ag core-shell NPs and Ag NPs of similar size (**Figure 2.7.**). The results showed less cell population at MIC of Au@Ag core-shell solution at 3 h in comparison to that of Ag NP treated sample which was almost similar to untreated control sample. Further, the bacterial cell number increased normally with time for untreated sample as well as for Ag NP treated sample unlike core-shell treated sample where the cells did not grow.

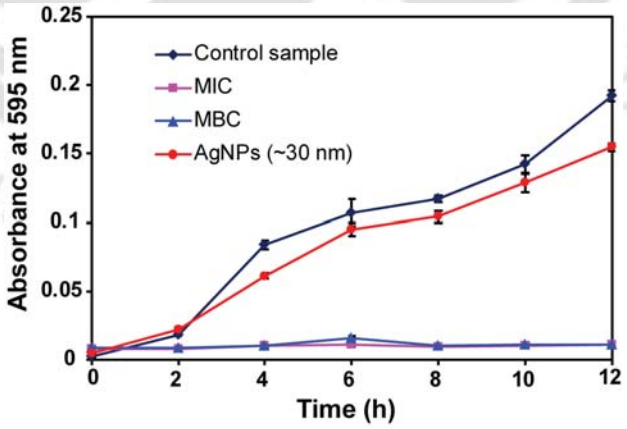

Figure 2.6. Effect of different concentrations of Au@Ag core-shell NPs and Ag NPs on the growth of GFP expressing recombinant *E. coli*.

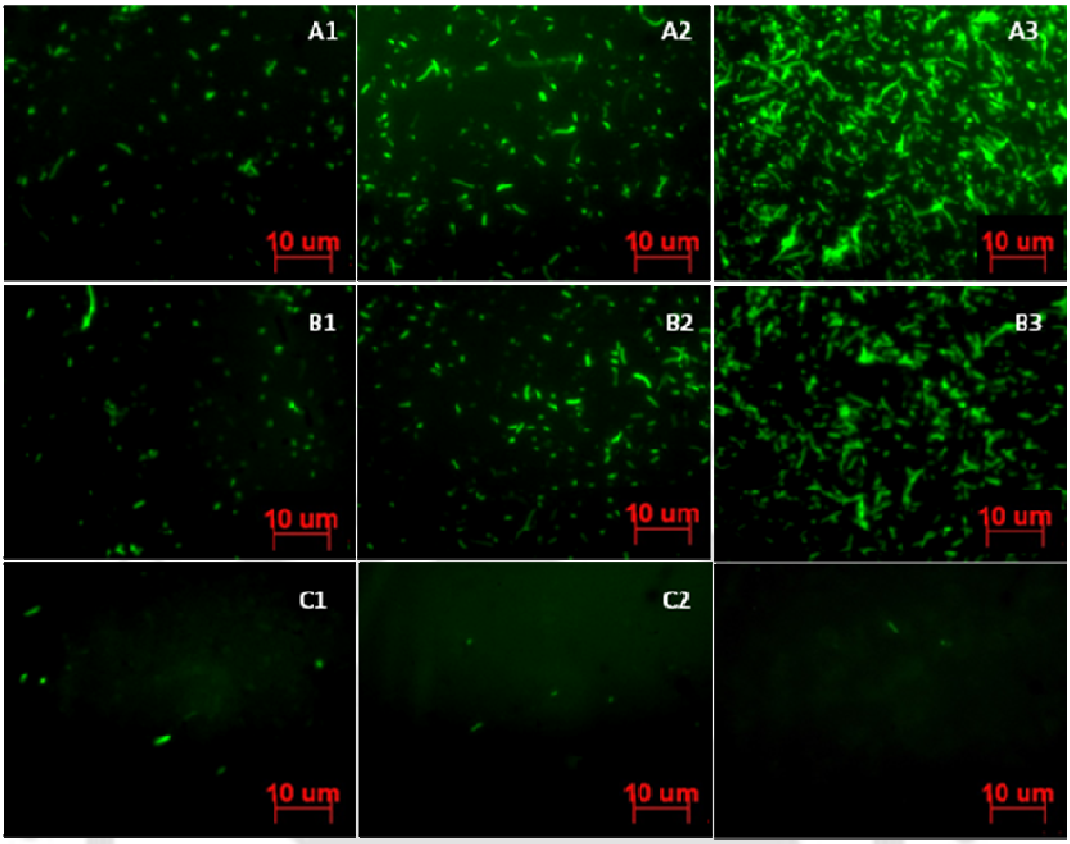

Figure 2.7. Time-dependent fluorescence micrograph of GFP expressing recombinant *E. coli*. Series **A**, **B**, **C** refer to control, Ag NPs and Au@Ag core-shell NPs (at MIC) treated samples, respectively, while series **1**, **2**, **3** refer to the samples at 3, 6 and 12 h time points, respectively.

The enhanced antibacterial activity of Au@Ag core-shell NPs in comparison to Ag NPs of similar sizes could be due to highly active surface Ag atoms in the shell around the Au core in core-shell NPs as compared to silver atoms in monometallic Ag NPs. Also, it may be possible that high activity of Ag atoms in the shell is because of electronic effect by Au atoms in the core on surface Ag atoms by charge transfer (Pande et al., 2007). The Au is more electronegative than Ag causing it to withdraw electrons from Ag shell. Thus, the electronic ligand effect in bimetallic NPs may be responsible for superior antibacterial activity of Au@Ag core-shell NPs. However, since the thickness of the Ag layer over Au core was more than a monolayer, the electronic ligand effect may not be as effective here. On the other hand, the thinness of

the Ag shell surrounding Au core might make the free energy of the surface Ag atoms high and thus more reactive in comparison to similar sized Ag NPs.

2.4.4. Effect of silver ions (Ag^+)

In order to probe the contribution of Ag^+ to the antibacterial activity of Au@Ag core-shell NPs, the concentration of Ag^+ released from Au@Ag core-shell NPs was determined by atomic absorption spectroscopy (AAS). It was found that the maximum concentration of Ag^+ released was ≤ 0.1 ppm after 12 h (**Figure 2.8.**) which did not inhibit bacterial growth. Gogoi et al. (2006) have previously demonstrated that there was no observable effect on the growth of bacteria at Ag^+ concentration = 0.1 ppm (10^{-6} M). In the literature, the MIC of Ag^+ ranges from 5-40 ppm, depending on the growth media (Malcher et al., 2008). Thus, the higher antibacterial activity of Au@Ag core-shell NPs was not due to Ag^+, though the ions possibly had impact on the overall bactericidal activity.

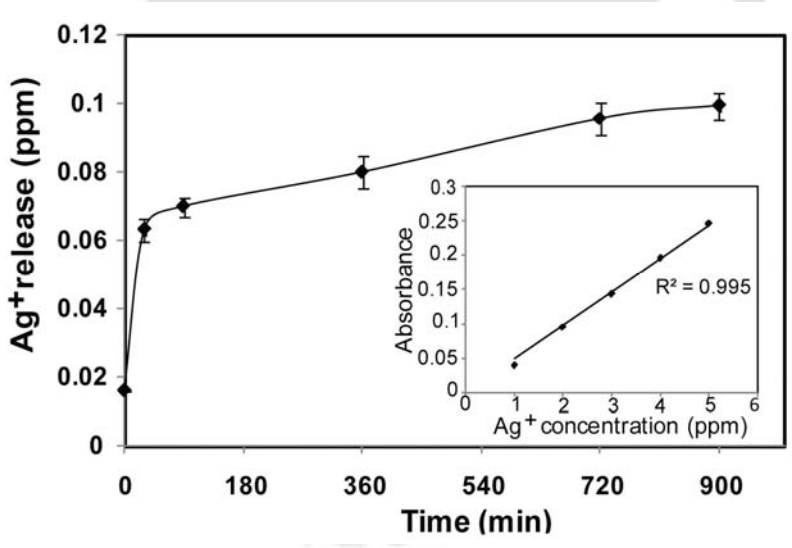

Figure 2.8. AAS measurement of Ag^+ released from core-shell NPs (at MIC) at various time points. (Inset) Standard curve obtained using various concentrations of Ag^+.

2.4.5. TEM studies

The interaction of Au@Ag core-shell NPs with bacteria was studied by TEM. GFP expressing recombinant *E. coli* was incubated with Au@Ag core-shell solution for 3 h followed by deposition on copper grid for observation. The TEM images showed that the core-shell NPs attached to the bacterial surface (**Figure 2.9.**). The HRTEM (**inset, Figure 2.9.**) of the adherent particles showed typical core-shell structures.

2.4.6. Cytometric Assay of Cell Membrane damage

In order to study the effect of Au@Ag core-shell NPs on bacteria, flow cytometric assay was done to investigate the cell membrane damage. It is already known that propidium iodide (PI), a nucleic acid dye, enters a bacterial cell only if the membrane is damaged which indicates change in membrane potential leading to cell death. The PI does not enter a normal intact cell and hence, the intact live bacteria show only green fluorescence (from GFP of the recombinant *E. coli*). The PI enters a compromised cell having membrane damage and binds to DNA to fluoresce red. Thus, the compromised cells show both red and green fluorescence. In dead cells, the GFP leaks out of the cell and thus only red fluorescence is observed. The lysed cells do not show any fluorescence.

In the present study, as depicted in **Table 2.2.**, bacteria when treated with MIC of Au@Ag core-shell NPs for 15 min, more than 50% of cell population appeared to be compromised. In contrast, the bacteria treated with Ag NPs of similar sizes of core-shell NPs, exhibited very less percentage of compromised cells which was more or less identical to that present in case of untreated control bacteria. The above results indicated that Au@Ag core-shell NPs attached to bacteria and caused membrane damage as early as 15 min following treatment.

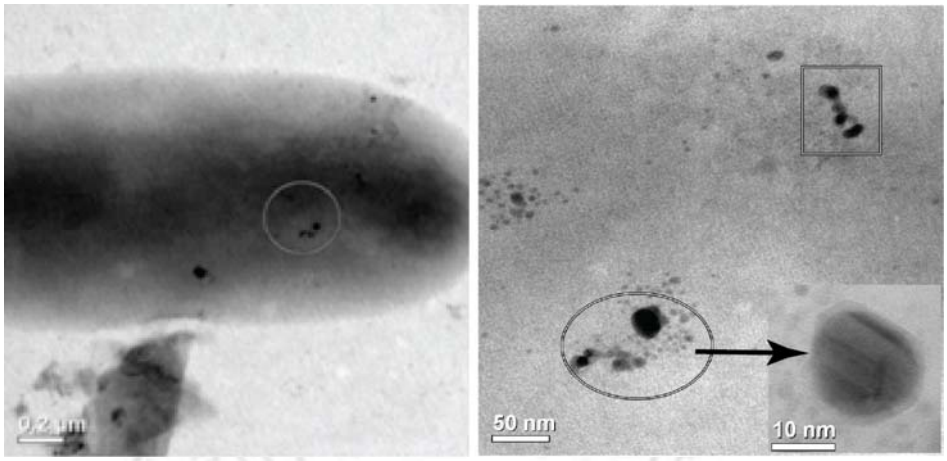

Figure 2.9. Sample TEM micrographs showing interaction of Au@Ag core-shell NPs with bacteria. Inset is an expanded view of a core-shell NP.

Table 2.2. Percentage of GFP expressing recombinant *E. coli* cells untreated and treated with Au@Ag core–shell NPs and Ag NPs at different time points as measured by flow cytometry.

Time		**Untreated**	**Ag NPs**	**Au@Ag < MIC**	**Au@Ag MIC**	**Au@Ag > MIC**
15 min	Live	84.6	85.4	45.2	17.0	2.8
	Compromised	5.2	5.0	40.3	68.3	79.9
	Dead	2.3	2.8	8.0	8.3	8.0
	Lysed	7.8	6.8	6.5	6.4	9.2
30 min	Live	85.4	85.2	37.1	6.5	3.4
	Compromised	5.2	6.8	42.7	72.5	78.8
	Dead	2.2	2.6	13.5	12.5	12.4
	Lysed	7.2	5.3	6.6	8.4	5.6
60 min	Live	86.9	83.3	40.8	5.8	6.3
	Compromised	2.9	6.6	38.6	68.0	68.3
	Dead	1.7	2.5	12.6	14.9	10.7
	Lysed	8.4	7.6	8.0	11.3	14.7

2.5. Conclusion

In the present study, bimetallic Au@Ag core-shell NPs have been shown to be catalytic and antibacterial agents. The Au@Ag core-shell NPs were synthesized at room temperature by reducing silver nitrate onto pre synthesized Au NPs, which provided large surface for effective growth of Ag shells. The core-shell NPs demonstrated higher catalytic efficiency as compared to similar sized monometallic Au NPs and Ag NPs. In addition, Au@Ag core-shell NPs exhibited excellent antibacterial properties against both Gram-positive and Gram-negative bacteria, at low Ag concentration. The Gram-negative bacteria were killed more easily than Gram-positive bacteria. The bactericidal efficiency of the core-shell NPs was much higher than that of similar sized Ag NPs. The results indicated that the core-shell NPs adhered to bacterial surface causing irreparable membrane damage leading to cell death. The enhanced antibacterial properties of Au@Ag core-shell NPs was possibly due to more active Ag atoms in the shell surrounding Au core due to high surface free energy of the surface Ag atoms owing to shell thinness in the bimetallic NP structure. Finally, the present work shows the promise of combining nanotechnology and biotechnology in deciphering the fundamental molecular basis of the interaction between nanomaterials and biological systems. In this regard, it is important to develop biocompatible NPs and investigate their effects on the prokaryotic as well as eukaryotic cells with the aim of finding promising candidates for therapeutic applications.

|Chapter 3|

Enhanced Antibacterial Property of Silver Nanoparticles Immobilized In a Chitosan Nanocarrier

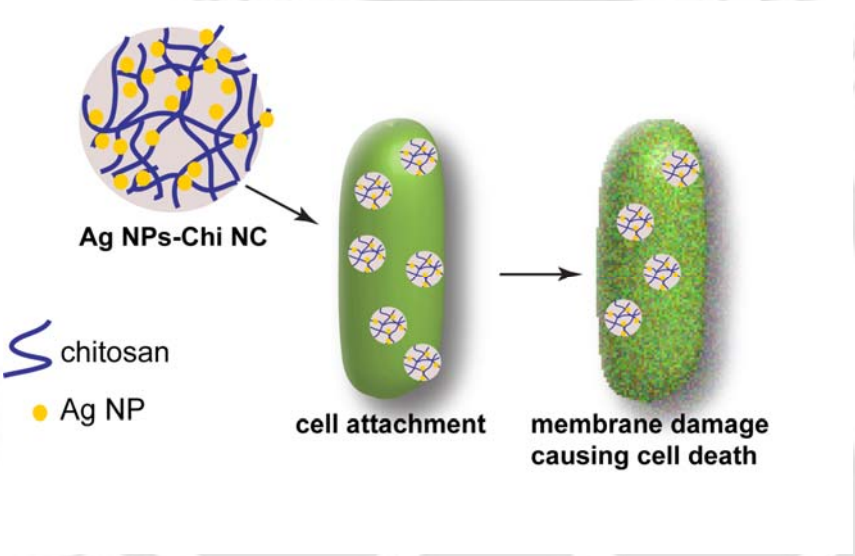

Chapter 3

ENHANCED ANTIBACTERIAL PROPERTY OF SILVER NANOPARTICLES IMMOBILIZED IN A CHITOSAN NANOCARRIER

3.1. Introduction

Silver nanoparticles (Ag NPs) have gained widespread attention in biotechnological and biomedical fields as catalysts, biosensors, antibacterial and anticancer agents. In principle, the synthesis of Ag NPs involves reduction of a Ag salt with reducing agent in the presence of a stabilizer that prevents aggregation of NPs. Generally, chemical reductants like sodium borohydride, hydrazine, dimethylformamide and stabilizers such as polyaniline (PANI) and polyvinylpyrrolidone (PVP) are used (Gogoi et al., 2006; Kim et al., 2007a; Nickel et al., 2000; Pastoriza-Santos and Liz-Marzán, 1999; Kang et al., 2006; Chou and Lai, 2004). However, they are generally associated with biological and environmental risks owing to their toxicity and non biocompatibility. Hence, the development of eco friendly 'green' processes using naturally occurring carbohydrate based biopolymers as templates, for synthesis as well as stabilization has gained impetus because of their excellent biocompatibility (Raveendran et al., 2003; He et al., 2003; Božanić et al., 2011).

Chitosan is an important poly-cationic biopolymer composed of β-(1–4)-2-acetamido-2-deoxy-β-D-glucose and β-(1–4)-2-amine-2-deoxy-β-D-glucose, mainly obtained by deacetylation of chitin which is a natural polysaccharide present in crustacean shells (Rabea et al., 2003). Owing to its biodegradability, biocompatibility and antimicrobial properties, chitosan has attracted considerable interest in a variety of areas such as biomedicine (Khor and Lim, 2003; Berger et al., 2004; Langer and Tirrell, 2004), pharmaceuticals (Dodane and Vilivalam, 1998), metal chelation (Guibal et al.,

2001; Varma et al., 2004), and other industrial applications (Kurita, 1998; Kumar, 2000). The antibacterial property of chitosan and its derivatives has been extensively studied and it is known to exhibit pronounced antibacterial effect against both Gram positive and Gram negative bacteria. The pK_a of chitosan is around 6.5 and thus at low pH, there is protonation of its amine groups making chitosan positively charged. Although the precise mechanisms of antimicrobial action of chitosan are yet to be elucidated, it is generally accepted that the polycationic chitosan binds to negatively charged bacterial cell wall causing subsequent destabilization of cell envelope leading to leakage of intracellular constituents (Rabea et al., 2003; Helander et al., 2001; Liu et al., 2004; Wang et al., 2004). Chitosan is insoluble at neutral and alkaline pH and thus it precipitates and is rendered inactive when added to bacterial medium (pH ~7.2). Therefore, conventional tests for assessing antibacterial activity of chitosan are generally done at low pH conditions (~5.5) (Holappa et al., 2006; Rúnarsson et al., 2007; Másson et al., 2008).

In recent years, chitosan NPs have emerged as potential carriers for delivery of drugs ranging from small organic molecules to proteins and nucleic acids (Janes et al., 2001; Amidi et al., 2010). However, there are fewer reports on the antibacterial studies of chitosan NPs and their derivatives (Qi et al., 2004; Shi et al., 2006; Xing et al., 2008; Anitha et al., 2009; Du et al., 2009; Chávez de Paz et al., 2011). The chitosan NPs can be easily dispersed in distilled water or aqueous buffers of neutral pH and exhibit higher antibacterial efficacy in comparison to chitosan (Qi et al., 2004; Larsen et al., 2009). Although there are reports on the antibacterial activity of chitosan and Ag NP composites (Sanpui et al., 2008; Potara et al., 2011), the antibacterial efficacy of Ag NPs containing chitosan nanocarrier is still unexplored.

3.2. Outline of the Research Work

1) Chitosan based nanocarriers containing Ag NPs were synthesized by ionotropic gelation of Ag NP-chitosan with tripolyphosphate.
2) The nanocarriers were well dispersed in distilled water and characterized by using UV-Vis spectroscopy, transmission electron microscopy (TEM), selected area electron diffraction pattern (SAED) and dynamic light scattering (DLS).

3) The nanocarriers exhibited superior antibacterial property against both Gram negative and Gram positive bacteria in comparison to either chitosan or Ag NPs alone.
4) TEM studies showed interaction of Ag NPs containing chitosan nanocarriers with bacteria that caused membrane damage, which was evaluated by flow cytometry studies.

3.3. Experimental Section

3.3.1. Chemicals, Bacterial strains, Growth media and conditions

Chitosan (high MW, >75% deacetylated) and sodium tripolyphosphate were obtained from Sigma-Aldrich Chemical Pvt. Ltd., Kolkata, India. Acetic acid (glacial, 99–100%) was purchased from Merck India Ltd, Mumbai, India. The strains of *Enterobacter aerogenes* MTCC 2822 and *Bacillus cereus* 1305 were grown in NB medium at 37 °C at 180 rpm for 12 h. The growth conditions of GFP expressing recombinant *Escherichia coli*, *Pseudomonas aeruginosa* and *Enterococcus faecalis* have been described in Experimental Section in Chapter 2.

3.3.2. Synthesis of Silver Nanoparticle-Chitosan Nanocarrier (Ag NP-Chi NC)

For the preparation of Ag NP-chitosan nanocarrier (Ag NP-Chi NC), chitosan stabilized Ag NPs (Chi-Ag NPs) were synthesized as described previously (Sanpui et al., 2008). Briefly, 4×10^{-4} M freshly prepared $AgNO_3$ solution was added to 50 mL of 2 mg mL^{-1} chitosan solution under constant stirring at 95 ºC. The appearance of yellow colour after the addition of NaOH to the reaction mixture indicated the formation of Ag NPs. The yellow coloured precipitate was collected, filtered and washed several times with water to remove NaOH and residual Ag^+ ions, if any present in the preparation, completely. The filtrate was dried in vacuum and 2 mg mL^{-1} solution of Chi-Ag NPs was prepared in 0.1 % (v/v) glacial acetic acid. The pH of the above solution was set to 4.8 (by adding few drops of NaOH) for synthesizing Ag NP-Chi NC.

The Ag NP-Chi NC was synthesized by an ionic gelation method described previously (Sanpui et al., 2011). The NPs were formed by adding 2.5 mL of aqueous TPP solution (1.6 mg mL^{-1}) dropwise to 7.5 mL of Chi-Ag NPs solution under

magnetic stirring at room temperature. The solution turned turbid indicating formation of NPs. After 30 min, the samples were centrifuged twice at 16000 rcf for 20 min at 10 ºC (Sigma Sartorius 3K30 centrifuge). The pellets of NPs were resuspended in MilliQ water. Similarly, blank chitosan nanocarriers (Chi NCs) were also prepared following same procedure with chitosan solution, instead of Chi-Ag NPs composite.

3.3.3. Characterization of Ag NP-Chi NCs

UV-Vis spectrum of the NCs was obtained using a spectrophotometer (Lambda 45; Perkin-Elmer, Fremont, CA, USA). The particle size and zeta potential of the NCs were assessed on the Zeta Sizer Nano ZS90 (Malvern Instruments) by dynamic light scattering measurements (DLS) and laser Doppler electrophoresis, respectively. The analysis was performed at a scattering angle of 90º under 25 ºC. Transmission electron microscopy (TEM) measurements were done using a JEM 2100; Jeol, Peabody, MA, USA machine operating at an accelerating voltage of 200 kV. 5 µL of each sample was drop coated onto a carbon coated copper TEM grid followed by air drying and the grid was then analyzed under TEM. The selected area electron diffraction (SAED) pattern of NCs was also recorded using the same instrument. The histograms for particle size distribution were constructed analyzing several frames of similar images.

3.3.4. Antibacterial activity of Ag NP-Chi NCs

For antibacterial assessment of NCs, *Bacillus cereus* MTCC 1305 and *Enterococcus faecalis* MTCC 439 were selected as representatives of Gram positive bacteria and *Escherichia coli, Enterobacter aerogenes* MTCC 2822 and *Pseudomonas aeruginosa* MTCC 2488 as representatives of Gram negative bacteria. Freshly grown bacterial inoculum (10^8 CFUs mL^{-1}) of all the strains were added to liquid media in presence of range of concentrations of NC for 12 h. The lowest concentration at which there was no visual turbidity was taken as the MIC value of NC. The cultures that lacked turbidity were tested further for determining MBC.100 µL from each of the samples without visible growth was spread onto agar plates and incubated at 37 ºC for 12 h. The lowest concentration of the NC that was bactericidal to ≥99.9% of original inoculum was taken as MBC. The experiments were performed three times to ensure reproducibility. The bacterial growth was monitored by measuring optical density (OD) at 595 nm using a

UV-visible spectrophotometer (Lambda 25; Perkin-Elmer, Fremont, CA, USA) at different time points.The concentration of Ag^+ released from Ag NP-Chi NCs was measured by using a fast sequential atomic absorption spectrometer (Varian, AA240FS). For this, the NCs at MIC were incubated in aqueous media under shaking condition and after different time points, the NPs were centrifuged to collect supernatants containing Ag^+ for analysis by spectrometer.

3.3.5. Flow cytometric assay of cell membrane damage using GFP-PI combination

The assessment of cell membrane damage of GFP expressing recombinant *E. coli* cells after treatment with NCs was done using the protocol described in Experimental Section of Chapter 2.

3.4. Results and Discussion

3.4.1. Characterization of Ag NP-Chi NCs

The Ag NPs containing Chi NCs were synthesized by ionotropic gelation of bulk Chi-Ag NPs with tripolyphosphate. The UV-Vis absorption spectra of Chi-Ag NPs composite and NCs synthesized from this composite exhibited peak at around 409 nm, which is characteristic of surface plasmon resonance (SPR) of Ag NPs. (**Figure 3.1a**). The unaltered position of SPR band of Ag NPs in NCs and the starting material (Chi-Ag NPs bulk composite) indicated that the size and shape of Ag NPs were unaffected during encapsulation in chitosan NC. The blank Chi NC did not exhibit any SPR peak due to absence of Ag NPs.

Table 3.1. presents the average hydrodynamic diameter, polydispersity index and zeta potential values of blank and Ag NP containing NCs. The prepared NCs were positively charged and stable as the zeta potential values were greater than ± 30 mV which is required as a minimum for a physically stable nanosuspension stabilized solely by electrostatic repulsion (Müller et al., 2001). TEM analysis (**Figure 3.1b**) showed that the Ag NP-Chi NCs were spherical in shape and well dispersed without aggregation. The average particle size calculated from TEM images was found to be 162.3 ± 35 nm (**Figure 3.1d**), which was different from 379.2 ± 5.16 nm as measured by DLS. This was expected as in TEM, the particles were in dried form on TEM grid

whereas in DLS, the hydrodynamic diameter of the swelled particles due to dispersion in water media, is measured. The SAED pattern of Ag NPs (**Figure 3.1c**) confirmed the presence of crystalline Ag NPs in the composite.

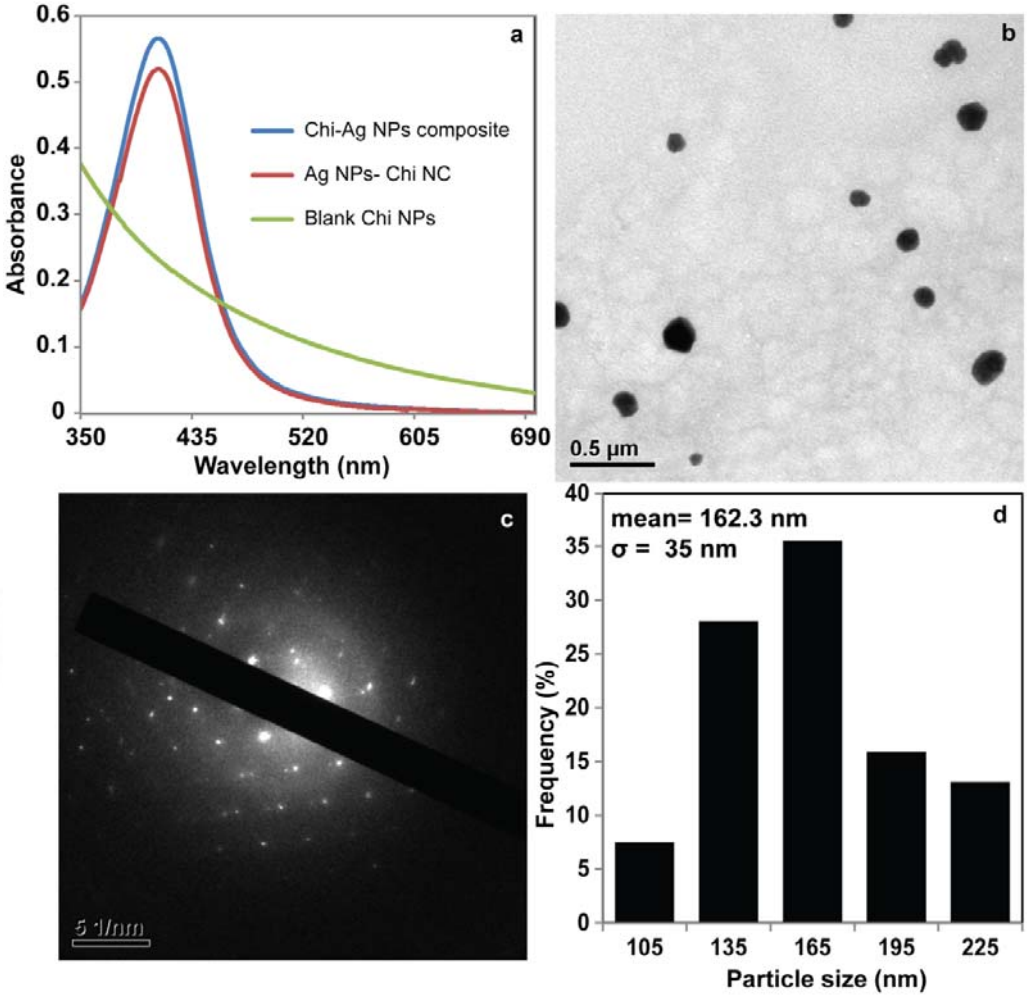

Figure 3.1. (a) UV-Vis absorption spectra of Chi-Ag NPs composite, Ag NP-Chi NCs and blank chitosan nanocarriers (Chi NCs), **(b)** Representative TEM image of Ag NP-Chi NCs, **(c)** corresponding SAED pattern and **(d)** Particle size distribution of Ag NP-Chi NCs.

Table 3.1. Particle size and surface charge of Nanocarriers

Nanoparticles	Mean Diameter (nm)[a]	Zeta Potential (mV)
Blank NCs	356.1 ± 7.68 (0.223)	40.1 ± 2.26
Ag NP-Chi NCs	379.2 ± 5.16 (0.474)	33.85 ± 1.34

[a]Values in parentheses represent the polydispersity index.

3.4.2. Antibacterial activity of Ag NP-Chi NCs

The antibacterial activity of Ag NP-Chi NCs was evaluated against two Gram positive strains viz. *Bacillus cereus* MTCC 1305 and *Enterococcus faecalis* MTCC 439 and three Gram negative strains viz. *Escherichia coli*, *Enterobacter aerogenes* MTCC 2822 and *Pseudomonas aeruginosa* MTCC 2488. The MIC and MBC values of Ag NP-Chi NCs and corresponding Ag NPs concentration for different strains were determined and are presented in **Table 3.2**. The concentration of Ag NPs in Ag NP-Chi NCs was calculated by determining loading of Ag NPs in Ag NP-Chi NCs by AAS measurements which was found to be 1.5% (w/w), in agreement with the previously reported value (Sanpui et al., 2011). The results indicated that the concentration of Ag NPs in MIC and MBC values of Ag NP-Chi NCs was much less than earlier reported values for Ag NPs only (Gogoi et al., 2006).

Further, from **Table 3.2.**, it is evident that Ag NP-Chi NCs were more effective against Gram negative bacteria than Gram positive bacteria. This was probably because Ag NP-Chi NCs were positively charged and since Gram negative bacteria have comparatively higher negative surface charge (Chung et al., 2004), the NCs interacted more strongly electrostatically with Gram negative bacteria thereby killing them more effectively in comparison to Gram positive bacteria. In addition, the effect of Ag NP-Chi NCs on the growth of GFP expressing *E. coli* was investigated through a time-dependent turbidity measurement by monitoring optical density at 595 nm at various time points. **Figure 3.2.** compares the effect of Ag NP-Chi NCs (at MIC and MBC) and blank Chi NCs at concentration corresponding to chitosan in MIC of Ag NP-Chi NCs i.e. 189.12 μg mL^{-1}. The growth curves revealed that blank Chi NCs exhibited limited inhibitory effect on the growth of bacteria. However, when present with Ag NPs in Ag

NP-Chi NCs, the growth was completely inhibited indicating synergy between Ag NPs and Chi NCs against bacteria.

Table 3.2. MIC and MBC values of Ag NP-Chi NCs for different strains. The values are in μg mL^{-1}

Strains	**Ag NP-Chi NC**		**Ag NPs in NC**	
	MIC	**MBC**	**MIC**	**MBC**
Gram negative				
Escherichia coli	192.07	204	2.88	3.06
Enterobacter aerogenes	172.10	308.05	2.58	4.62
Pseudomonas aeruginosa	193.32	285.8	2.89	4.28
Gram positive				
Bacillus cereus	274.56	367.19	3.22	5.50
Enterococcus faecalis	232.66	378	3.49	5.67

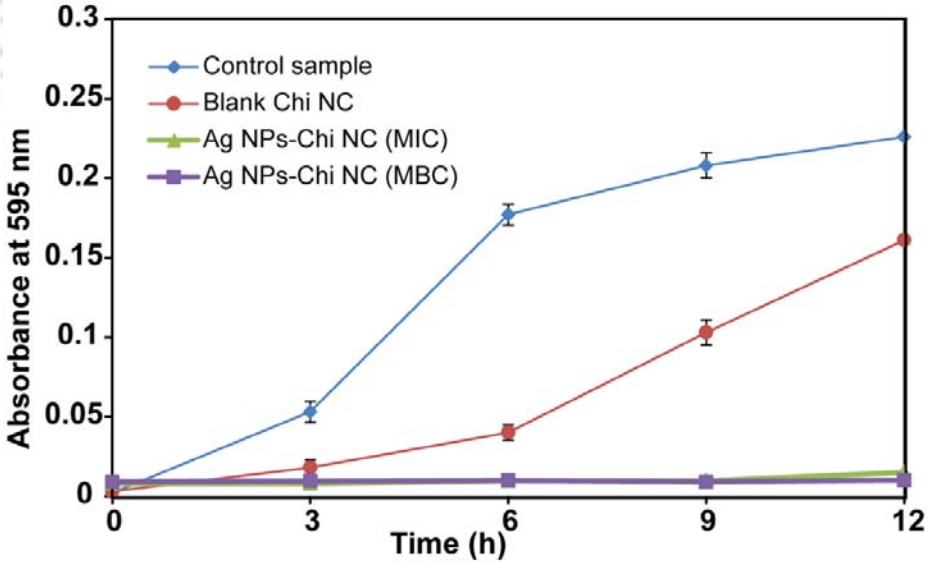

Figure 3.2. Effect of different concentrations of Ag NP-Chi NCs and Blank Chi NCs on the growth of GFP expressing recombinant *E. coli.*

3.4.3. Effect of Ag^+

AAS measurements (**Figure 3.3.**) revealed that the maximum concentration of Ag^+ released from Ag NP-Chi NCs was ~1 ppm after 12 h which was earlier reported to show no inhibitory effect on bacterial growth (Gogoi et al., 2006). This was further confirmed by testing the growth of bacteria in presence of 1 ppm $AgNO_3$, which showed growth of bacteria. As mentioned in Results and Discussion in Chapter 3, the MIC of Ag^+ is typically found in the range of 5–40 ppm depending on the growth media (Malcher et al., 2008). Thus, it was concluded that Ag^+ released from NCs did not play major role on the antibacterial potency of Ag NP-Chi NCs though the ions certainly had impact on the overall antibacterial activity.

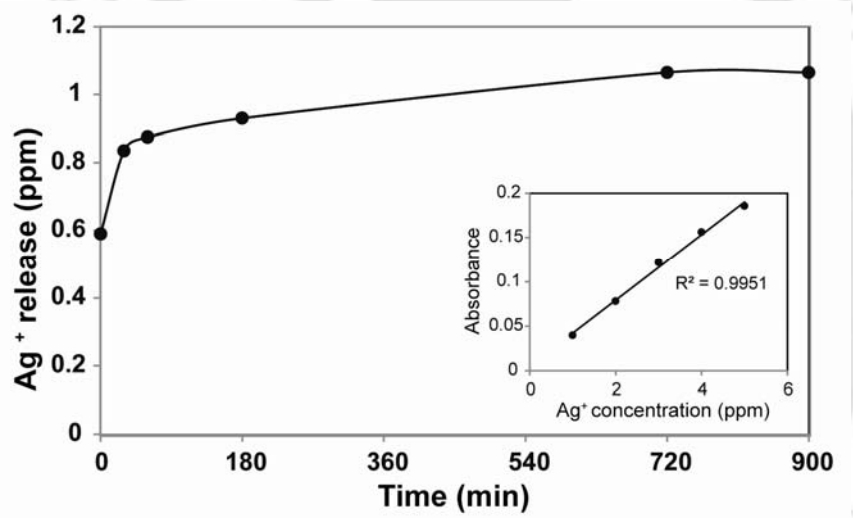

Figure 3.3. AAS measurement of Ag^+ released from Ag NP-Chi NCs (at MIC) at various time points. (Inset) Standard curve obtained using various concentrations of Ag^+.

3.4.4. TEM analysis

TEM analysis of treated GFP expressing recombinant *E. coli* showed that Ag NP-Chi NCs adhered to the bacterial surface suggesting interaction of NCs with bacteria (**Figure 3.4.**). Further, the SAED pattern (**inset, Figure 3.4d**) confirmed the presence of Ag NPs on bacterial surface. As evident from **Figure 3.4.**, the cells were disrupted

on contact with NCs. It could thus be inferred that the positively charged NCs attached to negatively charged bacterial surface causing destruction of membrane leading to outburst of cell materials.

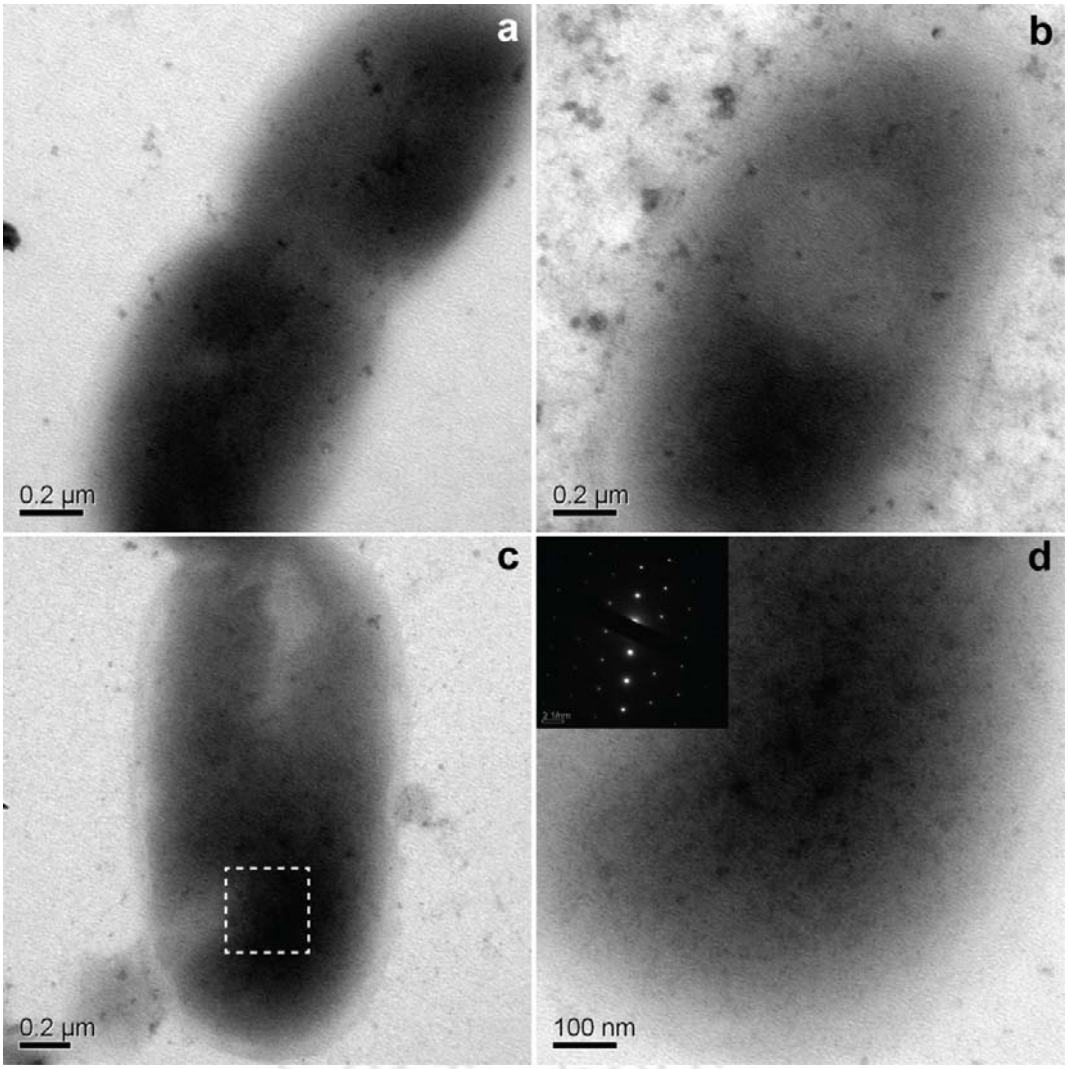

Figure 3.4. Sample TEM micrographs showing interaction of Ag NP-Chi NCs with *E. coli* treated with MIC in liquid medium for 3 h. **Inset** is corresponding SAED pattern.

3.4.5. Cytometric assay of cell membrane damage

To further gain insight into the mechanism of cell death by Ag NP-Chi NCs, membrane damage was studied by flow cytometry. For this, the bacterial cells were treated with MIC and >MIC (200 µg mL^{-1}) of Ag NP-Chi NCs and blank Chi NCs at concentration corresponding to that of chitosan in MIC of Ag NP-Chi NCs (189.12 µg mL^{-1}) for different time periods (30 min, 1h, 3h and 6 h) followed by PI staining and flow cytometry. It is evident from **Figure 3.5.**, that there was a gradual shift of population from viable to compromised cells with increase in concentration of NCs and time of treatment. For example, the percentage of compromised cells dramatically increased to 28.18 % for MIC of Ag NP-Chi NCs in comparison to 14.97 % for blank NCs treated bacteria at 6 h. The results are further mentioned in detail in **Table 3.3**. It is already known that positively charged Chi NPs interact with bacteria causing subsequent membrane damage followed by leakage of intracellular components leading to cell death (Qi et al., 2004; Larsen et al., 2009; Chávez de Paz et al, 2011). Ag NPs are also known to penetrate the barrier of cell wall resulting in compromised permeability (Morones et al., 2005; Gogoi et al., 2006). Thus, Ag NPs containing Chi NCs demonstrated superior antibacterial efficacy in comparison to blank Chi NCs. It was also expected that NCs due to their high surface area and reactivity interacted more strongly with bacterial surface causing disruption of membrane integrity.

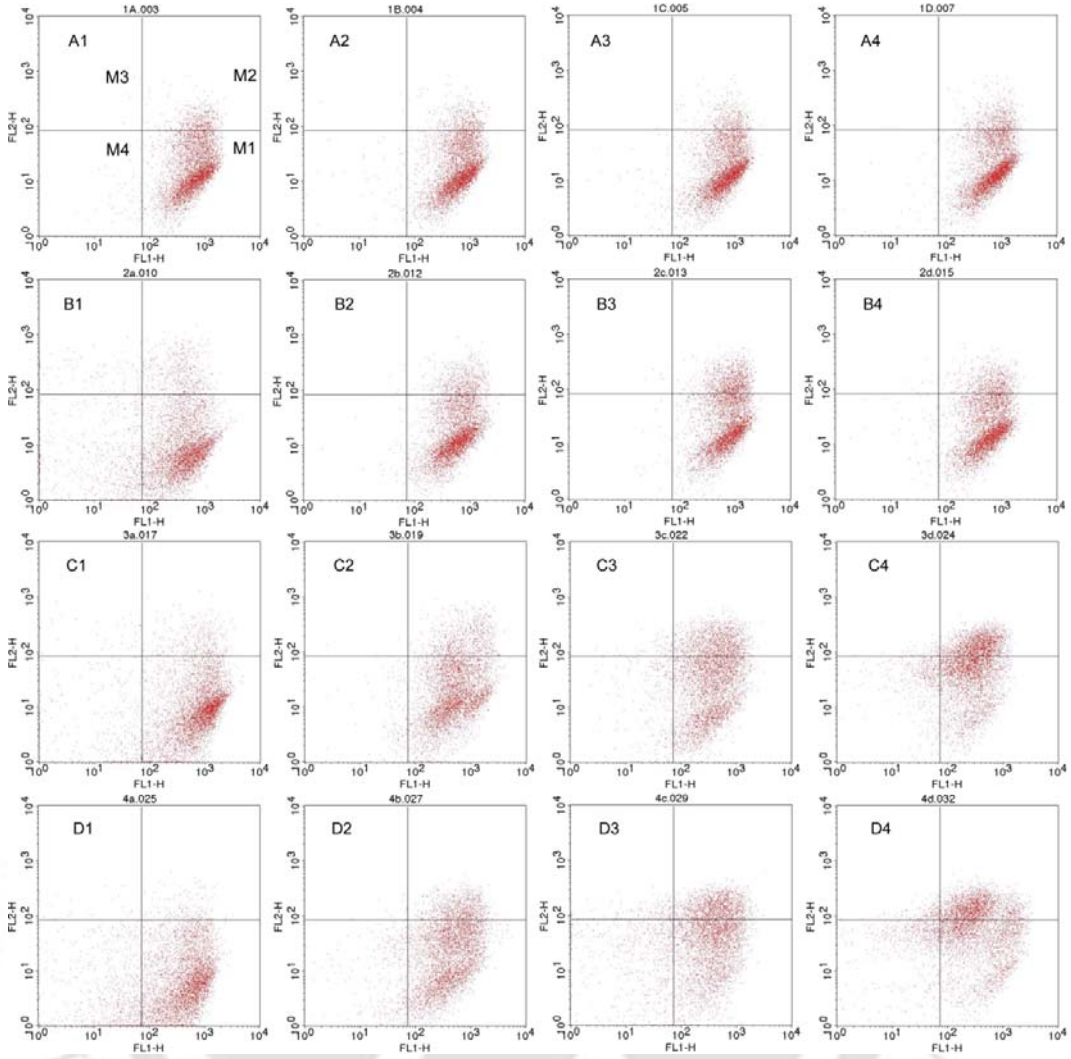

Figure 3.5. Dot plots showing populations of PI stained GFP containing recombinant *E. coli* cells at different viability stages, measured by flow cytometry at different time points. Series **1** refers to untreated , series **2** to blank Chi-NCs, series **3** to MIC of Ag NP-Chi NCs and series 4 to > MIC dose (200 µg mL^{-1}) of Ag NP-Chi NCs and **A**, **B**, **C** and **D** refer to samples at 30 min, 1 h, 3 h and 6 h, respectively. Different viability stages are denoted as M1 (live), M2 (compromised), M3 (dead), and M4 (lysed).

Table 3.3. Percentage of GFP expressing recombinant *E. coli* cells untreated and treated with blank Chi NCs and Ag NPs- Chi NCs at different time points as measured by flow cytometry.

Time		Untreated	Blank Chi NC	Ag NP-Chi NC (MIC)	Ag NP-Chi NC (>MIC)
30 min	Live	89.76	90.14	91.08	88.68
	Compromised	9.04	8.95	8.00	10.54
	Dead	0.03	0.06	0.05	0.04
	Lysed	1.17	0.85	0.87	0.74
1 h	Live	78.44	89.05	78.69	85.40
	Compromised	8.11	10.18	20.69	13.39
	Dead	1.59	0.07	0.12	0.14
	Lysed	11.86	0.70	0.50	1.07
3 h	Live	87.35	82.97	67.32	54.97
	Compromised	5.33	14.56	25.92	35.56
	Dead	0.64	0.12	1.42	1.12
	Lysed	6.68	2.35	5.34	8.36
6 h	Live	81.84	78.45	56.59	45.59
	Compromised	2.48	14.97	28.18	40.59
	Dead	0.49	0.34	2.75	3.01
	Lysed	15.20	6.24	12.48	10.81

3.5. Conclusion

Chitosan based NCs containing Ag NPs were synthesized that were well dispersed in distilled water. The NCs exhibited superior antibacterial properties against both Gram negative bacteria and Gram positive bacteria at low Ag NPs concentration with more activity against Gram negative bacteria. TEM studies showed Ag NP-Chi NCs interacted with bacteria causing membrane damage. The advantage of using Chi NCs over bulk form was that the antibacterial tests could be easily done in bacterial medium pH (~7.2) unlike chitosan that precipitates at this pH. The present study demonstrates

antibacterial potential of a hybrid nanocomposite containing polymer chitosan and Ag NPs at low Ag NP concentration. Next, it will be interesting to develop 'green' method of synthesis of Ag NPs embedded biocompatible polymers.

|Chapter 4|

Alginate mediated 'Green' Synthesis of Silver Nanoparticles and Fabrication of Antibacterial Silver Nanoparticle-Sodium Alginate-Chitosan Composite Films

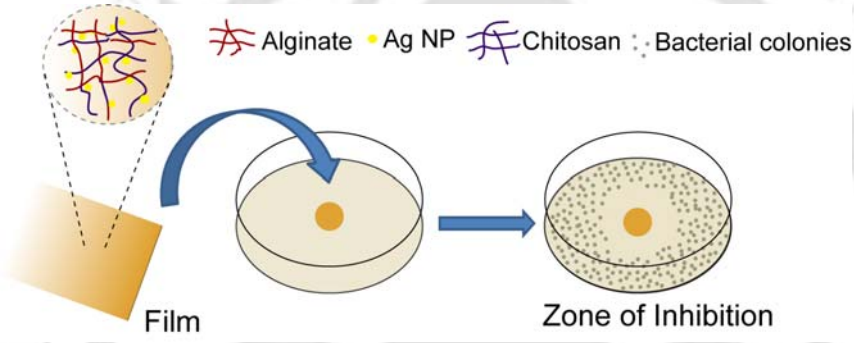

Sharma, S., Sanpui, P., Chattopadhyay, A. & Ghosh, S. S. *RSC Advances* **2**, 5837-5843 (2012).

Chapter 4

ALGINATE MEDIATED 'GREEN' SYNTHESIS OF SILVER NANOPARTICLES AND FABRICATION OF ANTIBACTERIAL SILVER NANOPARTICLE-SODIUM ALGINATE-CHITOSAN COMPOSITE FILMS

4.1. Introduction

Alginate is a naturally occurring poly-anionic polysaccharide derived from brown marine algae and composed of 1, 4-linked β-*D*-mannuronic and α-*L*-guluronic residues in varying proportions. It is a cheap, biocompatible and an environmentally benign biopolymer having numerous applications in biotechnology industry as non-toxic food additive, thickening agent, gelling agent, emulsifier and colloidal stabilizer (Tønnesen and Karlsen, 2002). However, very few studies have been done on using alginate for synthesizing metal nanoparticles (NPs). For instance, Liu et al. reported the synthesis of Ag NPs using sodium alginate as a stabilizer under gamma radiation (Liu et al., 2009). Here, isopropanol was added as a scavenger of hydroxyl radical. On the other hand, Pal et al. (2005) synthesized Au NPs using sodium alginate by UV photoactivation. However, both the methods mentioned above involve usage of high-energy irradiation, which may not be favorable.

Due to the poor binding affinity with various surfaces, Ag NPs are usually incorporated in some matrix or solid supports for practical applications. Several studies, in this context, have demonstrated successful incorporation of Ag NPs in food packaging films and coatings on medical devices as antimicrobial agent (Tankhiwale and Bajpai, 2009; Yoksan and Chirachanchai, 2010; Roe et al., 2008; Dubas et al., 2011). Alginate has a potential to form edible films, which exhibit poor water resistance due to hydrophilicity owing to presence of carboxylic and hydroxyl groups. To overcome this, alginate has been crosslinked with polyvalent metal cations like Ca^{2+}

or polyamines like chitosan that ionically interact with it to produce strong gels or insoluble polymers. The polyelectrolute complex (PEC) obtained from the ionic interactions between the protonated amino groups of chitosan and carboxylate groups of alginate, has been shown to have reduced tendency of swelling and enhanced mechanical properties as compared to their constituent polymers (Smitha et al., 2005).

4.2. Outline of the Research Work

1) A novel and simple 'green' method of synthesis of Ag NPs using sodium alginate as both reducing and stabilizing agent has been developed.
2) The Ag NPs were characterized using UV-Vis spectroscopy, transmission electron microscopy (TEM) and selected area electron diffraction pattern (SAED) and found to be antibacterial against both Gram positive and Gram negative bacteria.
3) The synthesized NPs were then blended with varying amounts of chitosan to form polyelectrolyte complex that was cast into stable films.
4) The films were characterized by field emission scanning electron microscope (FESEM), optical microscopy, Fourier transform infrared spectroscopy (FTIR) and X-ray diffraction (XRD). The water uptake and mechanical properties of the films were also studied.
5) The blended film demonstrated excellent antibacterial activity against both Gram negative and Gram positive bacteria with more activity against Gram positive bacteria.
6) Thus, the developed films have a potential to be used for various antibacterial applications in biotechnology and biomedical fields.

4.3. Experimental Section

4.3.1. Chemicals, Bacterial strains, Growth media and conditions

Alginate was obtained from Loba Chemie Pvt. Ltd., Mumbai, India. Acetone was purchased from Merck India Ltd, Mumbai, India. The growth media and conditions of GFP expressing recombinant *Escherichia coli*, *Enterobacter* aerogenes, *Pseudomonas aeruginosa*, *Bacillus cereus* and *Enterococcus faecalis* have been described in detail in Experimental Section in Chapters 2 and 3.

4.3.2. Preparation of alginate capped Ag NPs (Alg-Ag NPs) composite

Alg-Ag NPs composite was synthesized by adding 2 mL of freshly prepared 1.0×10^{-2} M $AgNO_3$ solution to 50 mL of 0.2 % (w/v) alginate solution, with constant stirring at 90 °C. The appearance of brown colour after an hour indicated formation of Ag NPs.

4.3.3. Characterization of the composite

The formation of Ag NPs was monitored by making UV-Vis spectroscopic measurements using a spectrophotometer (Lambda 45; Perkin-Elmer, Fremont, CA). For transmission electron microscopy (TEM), 5 µL of the sample was drop-cast onto a carbon-coated copper TEM grid, which was subsequently air-dried. The drop-coated grid was analyzed by a high resolution transmission electron microscope (JEM 2100; Jeol, Peabody, MA, USA) operating at an accelerating voltage of 200 kV. The selected area electron diffraction (SAED) pattern of Ag NP was also recorded using the same instrument. The histograms for particle size distribution were constructed analyzing several frames of similar images. The zeta potential of Ag NPs was measured using Delsa ™ Nano C particle analyzer.

4.3.4. Bactericidal activity of the composite

The antibacterial activity of Alg-Ag NPs was tested against *Escherichia coli* and *Bacillus cereus* MTCC 1305 as representative strains of Gram negative and Gram positive bacteria, respectively by well diffusion method. The suspensions of bacterial cultures in the range of 10^5-10^6 CFU mL^{-1} were made and streaked over the surface of agar plates to obtain uniform growth. After the plates were dried for 5 min, 4 distinct wells were punctured into the agar plates and filled with Alg-Ag NPs solution and alginate solution as control. The zones of inhibition were observed after incubation at 37°C overnight.

4.3.5. Preparation of alginate-Ag NPs-Chitosan (Alg-Ag NPs-Chi) blended Films

Films were prepared by varying the ratio of alginate and chitosan to 1:1, 2:1, 4:1. In detail, 1:1 film was prepared by adding 6 mL of chitosan solution (0.1 % w/v in a 1:1 v/v solvent mixture of 2 % aqueous acetic acid and acetone) to 3 mL of above Alg-Ag NPs solution under vigorous stirring at room temperature for 20 min. This was repeated five times; the resultant suspension (45 mL after pooling) was cast into a polyethylene

petri dish and dried for 24 h at 37 °C in an incubator (Reico Equipment & Instrument Pvt. Ltd.). By a similar casting method, control films of chitosan and sodium alginate were also prepared. All films were stored in dessicator at room temperature until use.

4.3.6. Characterization of films

The surface morphology of the films was examined by field emission scanning electron microscopy (FESEM) and light microscopy. For FESEM, the films were sputter-coated with gold film using a sputter coater (SC7620"Mini", Polaron Sputter Coater, Quorum Technologies, Newhaven, England) and imaged under FESEM (Carl Zeiss, SIGMA VP). Optical microscopy images were acquired with a Carl Zeiss Axioskop 2 Mat Microscope fitted with a digital camera. The Fourier transform infrared (FTIR) spectra of the films were recorded using a Perkin-Elmer Spectrum one spectrometer. X-ray diffraction (XRD) patterns of the solid product of Alg-Ag NPs obtained after drying the colloidal dispersion and films were recorded with a Bruker D8 ADVANCE (Bruker AXS Inc.) XRD machine using Cu Kα (λ= 1.54 Å) source.

4.3.7. Water uptake studies

Triplicate samples of each film were weighed by using a weighing balance (GR-202, A&D Company Ltd.) and equilibrated in 15 mL of PBS (pH 7.4) at room temperature. After 24 h, the films were retrieved, blotted of excess water and weighed immediately. The procedure was repeated until the membrane attained constant weight. The % uptake was determined by following equation:

% uptake = [(wet weight - dry weight)/dry weight] x 100

4.3.8. Mechanical properties

The mechanical properties of films were measured using a Deben MICROTEST (Gatan) machine running at a speed of 5 mm min^{-1}. Tensile strength was calculated by dividing the maximum force at break by the cross-sectional area of film (Newton m^{-2} = Pascal). Percent elongation at break was calculated on the basis of length extended as compared to the original length of the film. The reported film properties were average of measurements on three different films. The film thickness was measured by FESEM (Carl Zeiss, SIGMA VP) and the average of eight measurements was reported.

4.3.9. Antibacterial activity of films

The agar diffusion method was used to determine the antimicrobial effects of films on bacterial strains. The suspensions of bacterial cultures in the range of 10^5 - 10^6 CFU mL^{-1} were made and streaked over the surface of agar plates to obtain uniform growth. After the plates dried for 5 min, films of diameters 1 cm, 1.5 cm and 2 cm were placed on the top of swabbed agar. The zones of inhibition were measured after incubating plates at 37 °C overnight. The reported values were average of three independent experiments carried out with each strain.

4.4. Results and Discussion

4.4.1. Synthesis and Characterization of Alg-Ag NPs

In the present study, Ag NPs were synthesized in a 'green' method using natural biopolymer alginate by simply heating an aqueous mixture of sodium alginate and $AgNO_3$. Here, alginate played dual role of both stabilizer and reducing agent. In the presence of alginate, the band at ~301 nm exhibited by $AgNO_3$ in aqueous solution disappeared indicating possible chelation of Ag^+ by the adjacent hydroxyl and carboxylic groups of alginate (**Figure 4.1.**). The Ag^+ chelate produced Ag (0) on heating. The synthesis was carried out at ambient conditions. This method was found to produce Ag NPs reproducibly.

In order to optimize the synthesis of Ag NPs, the concentration of alginate was varied (0.05, 0.1, 0.2, 1.0, 2.0 wt %) while keeping $AgNO_3$ concentration and reaction temperature constant at 4×10^{-4} M and 80 °C, respectively. After one hour of reaction, the colour of the reaction mixture changed varying from yellow to light brown to dark brown with increasing alginate concentration indicating the formation of Ag NPs. The UV–Vis absorption spectroscopy of the samples revealed the appearance of peak at 407 nm, which is characteristic of surface plasmon resonance (SPR) of Ag NPs. As evident from **Figure 4.2a**, the intensity of the peak increased as the concentration of alginate increased till it became constant at an alginate concentration of 0.2% (w/v) or more, indicating complete reduction of Ag^+ at those concentrations of alginate.

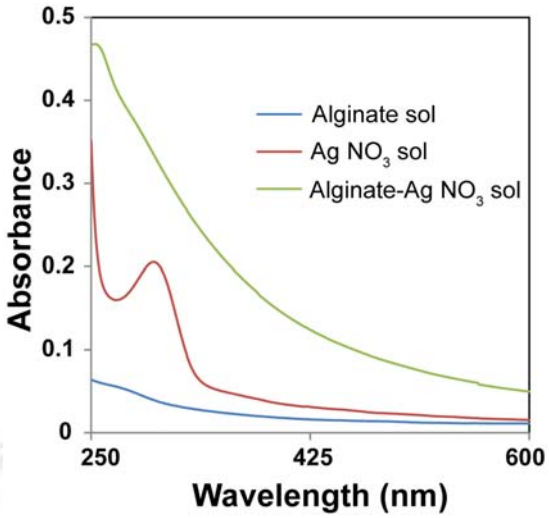

Figure 4.1. UV-Vis spectra of alginate, $AgNO_3$ and mixture of alginate and $AgNO_3$ solutions.

Next, the influence of reaction temperature on the synthesis of Ag NPs was investigated at constant $AgNO_3$ (4×10^{-4} M) and alginate concentration (0.2%, w/v). **Figure 4.2b** compares the UV-Vis absorption spectra of Ag NPs obtained at different temperatures. The absence of SPR band in UV-Vis spectrum indicated that no Ag NPs were formed at 60 °C. As the temperature was raised to 70 °C or above, a well defined plasmon band appeared at 407 nm. At temperature 90 °C, the intensity of the SPR peak increased with a concomitant shift to lower wavelength of 402 nm indicating the formation of smaller Ag NPs. Also, the peak was sharp and symmetric indicating a narrow size distribution of Ag NPs synthesized at 90 °C.

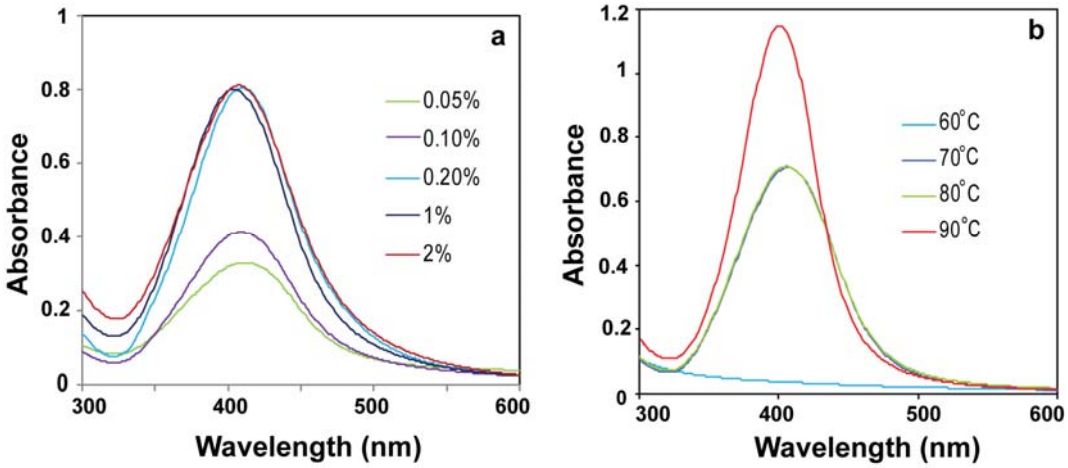

Figure 4.2. UV-Vis spectra of **(a)** Ag NPs synthesized using different concentrations of alginate at 80 ^{0}C and **(b)** Ag NPs at different temperatures keeping alginate concentration 0.2 % (w/v).

TEM analysis (**Figure 4.3a**) showed that the Ag NPs were well-dispersed and spherical in shape. The particle size distribution, shown in **Figure 4.3d**, revealed that the size of the particles was in the range of 5 nm to 21 nm with mean diameter of 14 ± 3 nm. The observed lattice fringes in the HRTEM image (**Figure 4.3b**) indicated the crystalline structure of Ag NPs. Also, the selected area electron diffraction pattern (SAED) of Ag NPs (**Figure 4.3c**) supported the formation of polycrystalline Ag NPs. The XRD pattern of Alg-Ag NPs (**Figure 4.4**) showed peaks at 38.2º and 44.3º corresponding to the (111) and (200) planes of the cubic structure of metallic Ag.

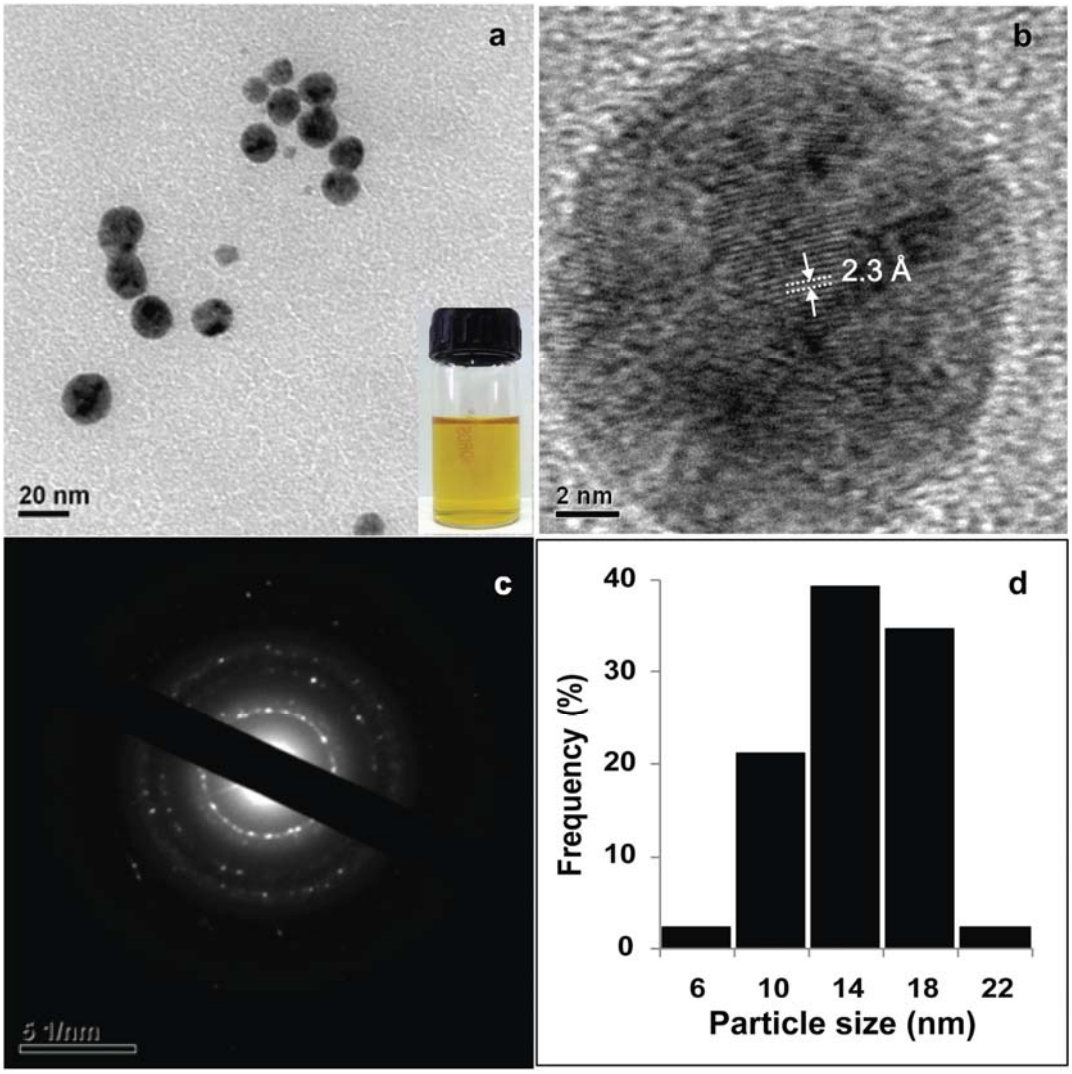

Figure 4.3. (a) TEM image of Ag NPs synthesized using 0.2 % alginate at 90 °C, **inset** shows the photo of Ag NPs **(b)** HRTEM image of a single Ag NP, **(c)** corresponding SAED pattern and **(d)** particle size distribution of Ag NPs.

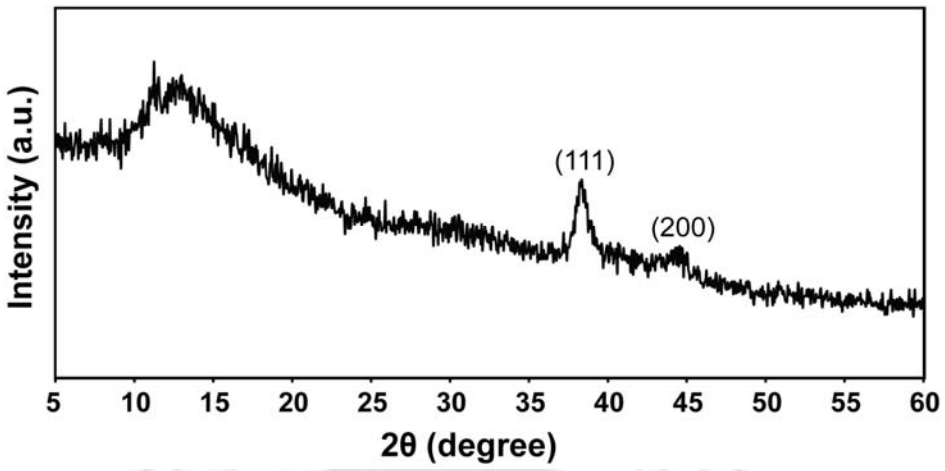

Figure 4.4. XRD pattern of Alg-Ag NPs

Ag NPs were also prepared at higher Ag NO_3 concentrations (2×10^{-3} M and 4×10^{-3} M) keeping alginate concentration and temperature as 0.2 % and 90 °C, respectively. UV-Vis spectra measurements (**Figure 4.5a**) showed broad peaks at ~409 nm and ~413 nm for NPs prepared using 2×10^{-3} M and 4×10^{-3} M $AgNO_3$ concentration, respectively indicating wide distribution of NPs. This was confirmed by TEM measurements. For NPs prepared using 2×10^{-3} M $AgNO_3$ concentration, particles of various shapes were formed (**Figure 4.5c**). The particle size distribution was calculated by measuring diameters of spherical particles. The average size was calculated to be 5.65 ± 2.4 nm (**Figure 4.5b**). In case of NPs synthesized using 4×10^{-3} M Ag NO_3, TEM images showed that the particles of various irregular morphologies were formed (**Figure 4.5d**). Most of the particles were found to be aggregated.

Thus, the optimum reaction conditions (alginate = 0.2 %, $AgNO_3 = 4 \times 10^{-4}$ M at 90 °C) were standardized to obtain uniform Ag NPs for further experiments.

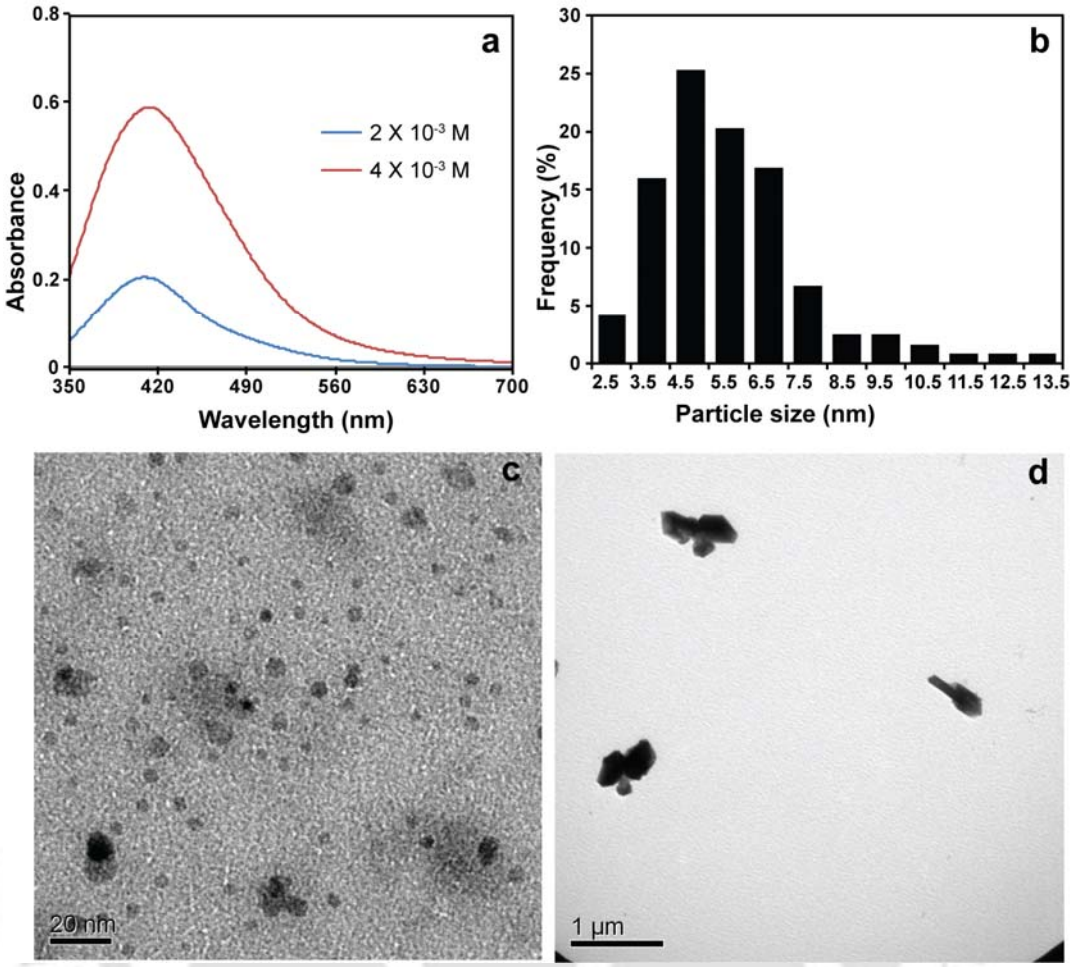

Figure 4.5. (a) UV-Vis spectra of Ag NPs prepared using five times and ten times initial Ag NO_3 concentrations (i.e. 2×10^{-3} M and 4×10^{-3} M, respectively) and 0.2 % alginate at 90 °C. **(b)** Particle size distribution of NPs prepared using 2×10^{-3} M Ag NO_3. TEM images of NPs synthesized using **(c)** 2×10^{-3} M and **(d)** 4×10^{-3} M of Ag NO_3.

4.4.2. Antibacterial activity of Alg-Ag NPs

The Alg-Ag NPs were found to be antibacterial against *Escherichia coli* (Gram negative) and *Baclillus cereus* (Gram positive) strains as indicated by zones of inhibition around the wells loaded with Alg-Ag NPs in bacterial culture plates (**Figure 4.6.**). Also, there was no zone of inhibition around the well containing only alginate solution, indicating no antibacterial activity of alginate.

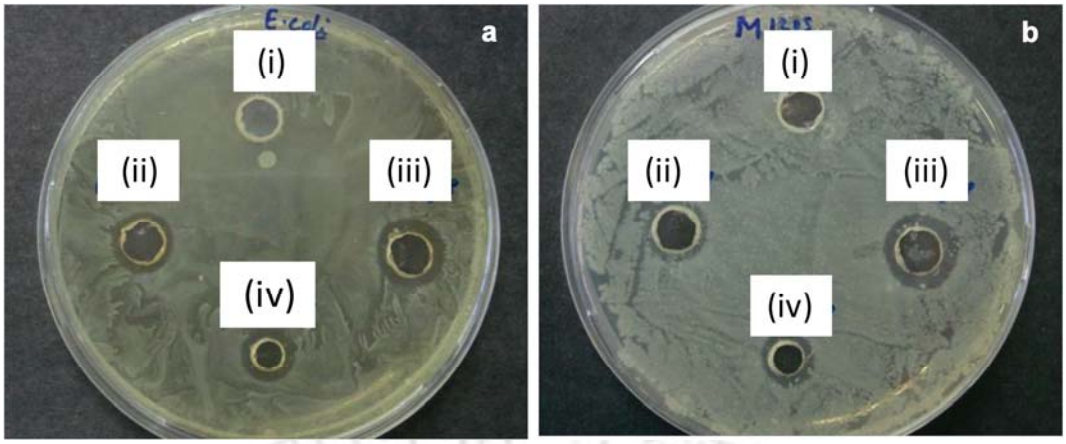

Figure 4.6. Photographs of antimicrobial test results of **(i)** alginate and **(ii-iv)** Alg-Ag NPs against **(a)** *E. coli* and **(b)** *B. cereus* MTCC 1305 strains.

4.4.3. Fabrication and characterization of Alg-Ag NPs-Chi blended films

In view of increasing popularity of Ag NP based biomaterials for antibacterial purposes, the Alg-Ag NPs synthesized in the present study were developed into antibacterial films for practical applications. For this, the Alg-Ag NPs were blended with varying amounts of chitosan to have films with improved properties in comparison to Alg-Ag NPs film. However, the challenge was to have homogenous films with uniform concentration of Ag NPs throughout the film. This is because when chitosan was added to alginate solution, insoluble heterogenous coacervates were formed due to rapid interaction between protonated amino groups of chitosan and carboxylic groups of alginate. Hence, in order to ensure the homogeneity of films, acetone was used as a part of solvent for chitosan. Previously, Yan et al (2000) had successfully used acetone to prepare coacervates for casting into homogenous films. The acetone ensured that chitosan remained in less extended conformation so that its interaction with carboxylic groups of alginate was restricted.

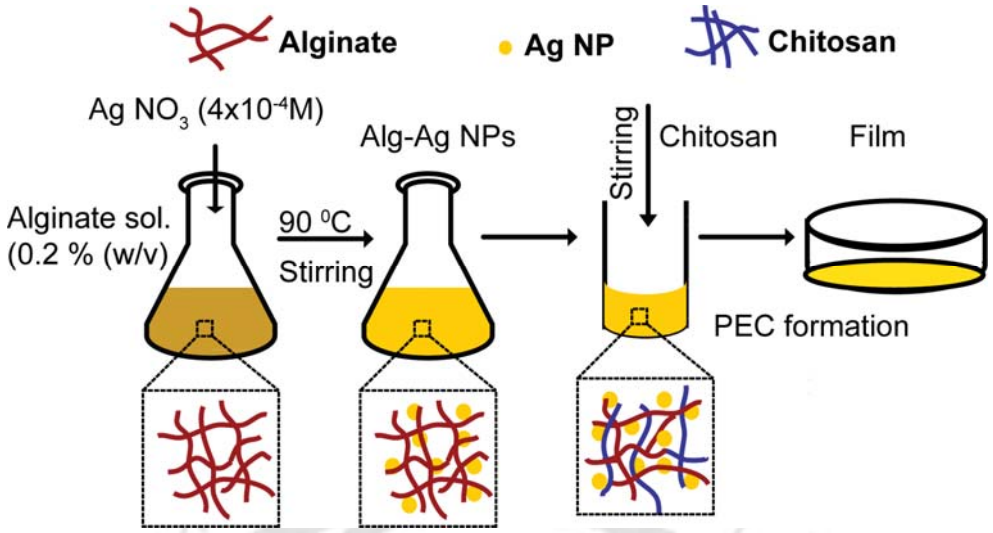

Figure 4.7. Schematic illustration of procedure used for the preparation of Alg-Ag NPs-Chi blended films.

The chitosan blended Alg-Ag NPs films (Alg-Ag NPs-Chi) were prepared according to scheme presented in **Figure 4.7.** with various weight ratios of alginate and chitosan (1:1, 2:1, 4:1). Control films made up of only alginate and only chitosan were also prepared. It was found that with the increase in sodium alginate content, the films became fragile and difficult to handle. Hence, the film prepared with 1:1 ratio of alginate and chitosan was chosen for further studies as it was easier to handle.The control films were colourless and transparent in contrast to blended films, which were yellow in colour due to presence of Ag NPs (**Figure 4.8.**). The colour of the films did not change on storage for several weeks indicating stability of Ag NPs. The NPs were observed in the FESEM image of 1:1 blended film (**Figure 4.9b**) in the form of small particles, which revealed that the NPs were well dispersed throughout the film. On the other hand, the chitosan film did not contain any such small particulate structure (**Figure 4.9a**). The observed cracks in the film could have occured during drying especially in the vacuum. The optical micrographs showed that chitosan and 1:1 blended films had smoother surfaces as compared to 2:1 and 4:1 films which had striated and irregular surface morphology (**Figure 4.10.**).

Figure 4.8. Photograph of different **(C)** chitosan, **(1)** 1:1, **(2)** 2:1 and **(3)** 4:1 films.

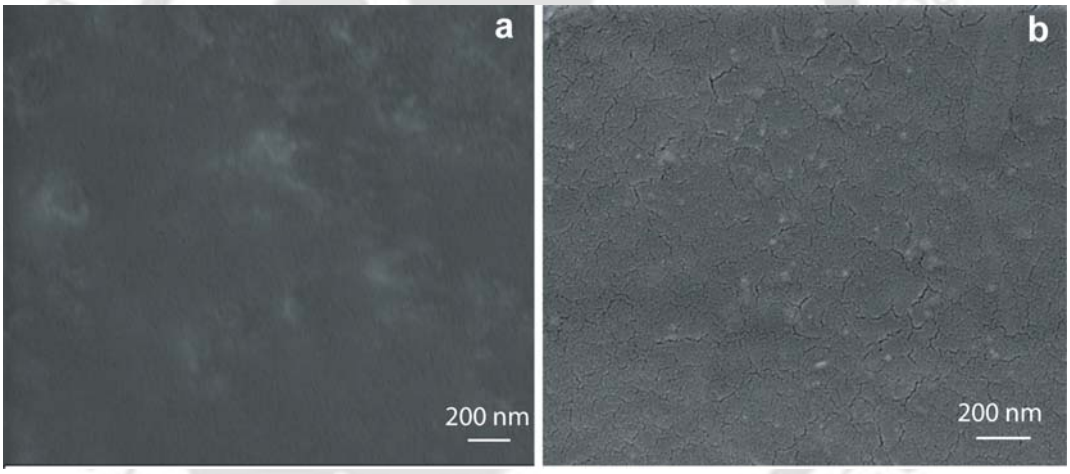

Figure 4.9. FESEM images of **(a)** chitosan film and **(b)** 1:1 blended film showing Ag NPs.

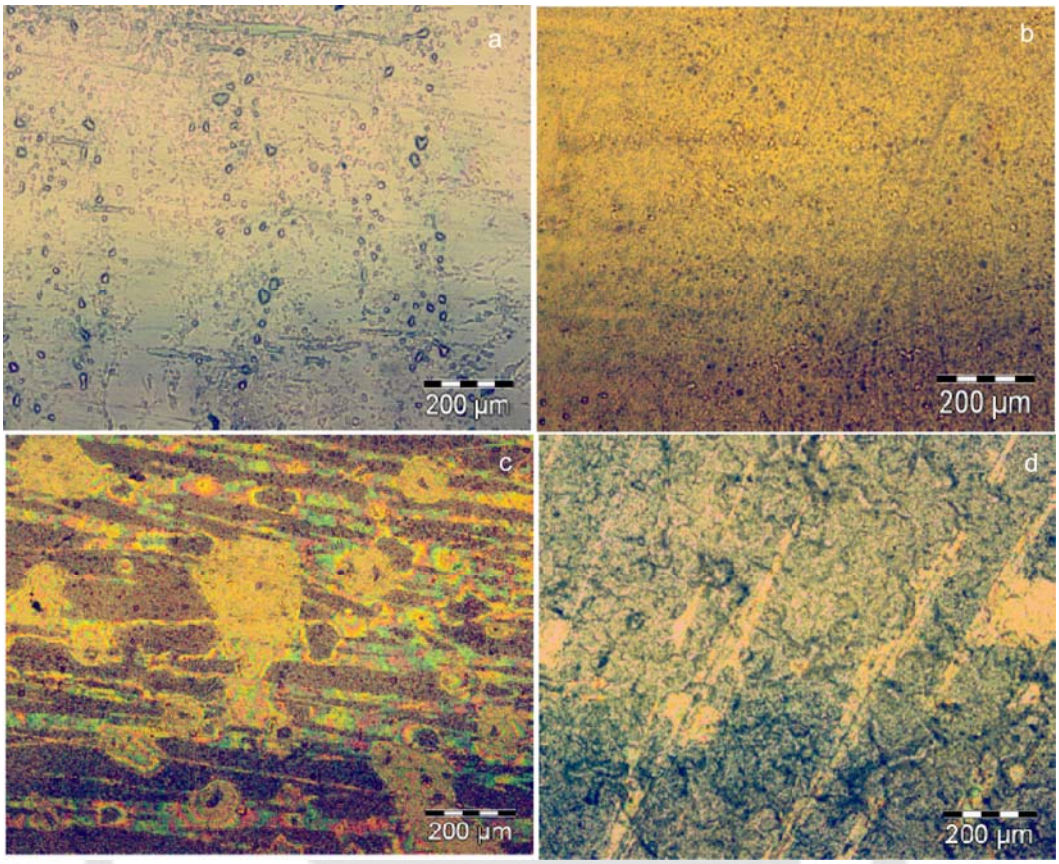

Figure 4.10. Optical micrographs of **(a)** chitosan film **(b)** 1:1, **(c)** 2:1 and **(d)** 4:1 blended films.

4.4.4. FTIR analysis of films

The FTIR studies of the films indicated the interaction between alginate and chitosan polymers (**Figure 4.11.**). The absorption bands at 1607 and 1415 cm^{-1} for alginate film were due to the respective asymmetric and symmetric stretching vibrations of carboxylate anions. The absorption band at 1607 cm^{-1} shifted to 1633 cm^{-1} and 1415 cm^{-1} shifted to 1384 cm^{-1} after alginate reduced Ag^{+} to form Alg-Ag NPs. Also, the broad band at 3366 cm^{-1} corresponding to stretching vibration of O-H groups in alginate shifted to 3428 cm^{-1} in Alg-Ag NPs. The peak shifting could be due to bond formation between silver and oxygen. Thus, from above, it can be inferred that perhaps both hydroxyl and carboxyl groups of alginate were involved in the synthesis and stabilization of Ag NPs. Previously, Kora et al. (2010) have also reported changes in shape and peak positions of hydroxyl and carboxylate groups of gum kondagogu, a

polysaccharide, when used for Ag NPs synthesis. For chitosan film, the absorption bands at 1639, 1558, and 1324 cm^{-1} represented characteristic amide I, amide II and amide III bands, respectively. The FTIR spectra of Alg-Ag NPs-Chi film showed a broad band from 1566 cm^{-1} to 1647 cm^{-1} that arose from overlapping bands from amide of chitosan and carboxyl anions of alginate confirming the interaction between alginate and chitosan (Li et al., 2009).

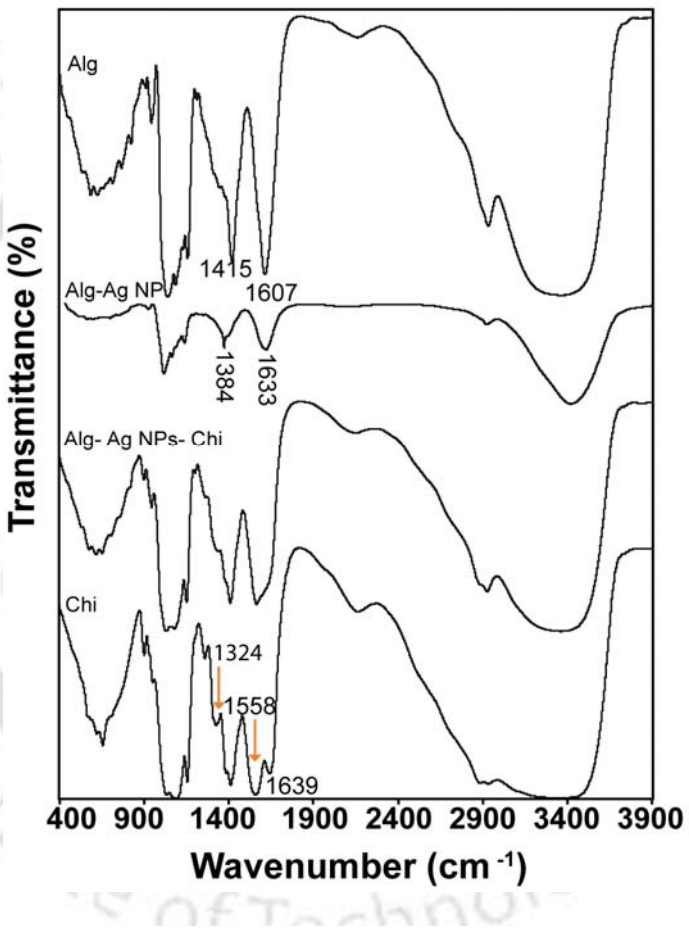

Figure 4.11. FTIR spectra of alginate, Alg–Ag NPs, chitosan and 1: 1 blended (containing Ag NPs) films.

4.4.5. XRD analysis

The XRD patterns of different films are shown in **Figure 4.12**. The chitosan films showed two peaks at 2θ of 9.4° and 11.6° contributed, respectively by hydrated and

anhydrous chitosan crystals. An additional broad peak that extended from 2θ of 15.5° to 24° showed the amorphous region of the film (Yan et al., 2001). The diffractogram of alginate film consisted of two broad bands at 13.5° and 21.5° of low intensity. In Alg-Ag NPs-Chi film, the peaks corresponding to crystalline region of chitosan almost disappeared and broad bands appeared at 14.2° and 21° indicating amorphous morphology of the complex due to strong interactions between alginate and chitosan that destroyed the close packing of polymers (Meng et al, 2010). In addition, the Alg-Ag NPs-Chi film had a well defined characteristic diffraction peak at 38.3°, and weak peaks at 44.2° and 64.5°, respectively, which corresponded to (111), (200) and (220) planes of face centered cubic (fcc) crystal structure of metallic Ag, indicating the presence of Ag NPs in the blended film.

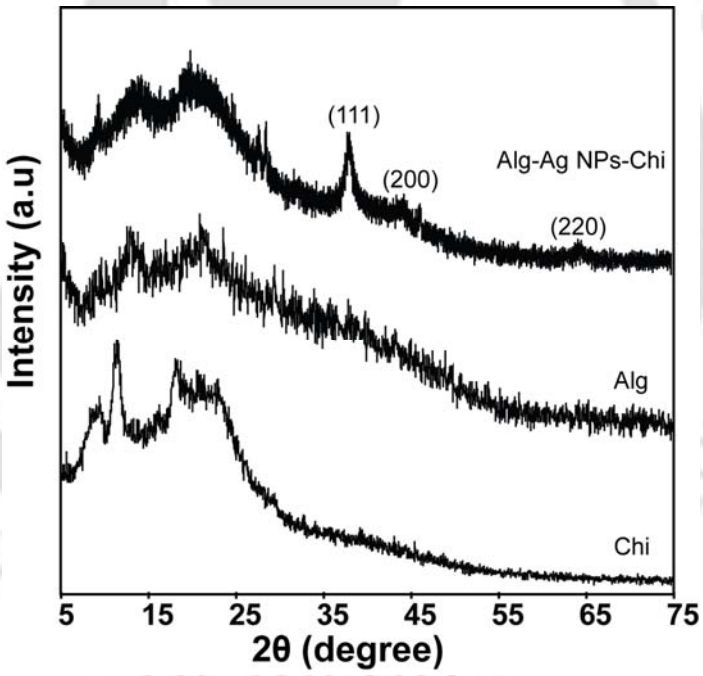

Figure 4.12. XRD of 1: 1 blended (containing Ag NPs), alginate and chitosan films.

4.4.6. Water Uptake studies

As the swelling behaviour of an antibacterial film is an important aspect of its successful biomedical application, the water uptake capabilities of the blended films were investigated. **Table 4.1.** shows the water uptake behaviour of the films in PBS

(pH 7.4) at room temperature. The alginate film completely dissolved in PBS in contrast to blended films that remained stable. The % water uptake of chitosan film was highest as compared to blended films. This indicated that in blended films, there was formation of polyelectrolyte complex between amino groups of chitosan and carboxylic groups of alginate. The polymer chains became more entangled thereby restricting their mobility and thus limiting water uptake (Lin et al., 2005; Pasparakis and Bouropoulos, 2006). Amongst the blended films, 1:1 film demonstrated slightly higher % water uptake than either 2:1 or 4:1 blended films.

Table 4.1. Water uptake of different films

Film	**% Water uptake (Mean ± SD, n=3)**
Alg	_[a]
Chi	45.4± 5.6
1:1	19.8 ± 1.2
2:1	15.3 ± 0.5
4:1	16.6 ± 0.3

[a] Completely soluble in water, hence could not be measured

4.4.7. Mechanical properties

The mechanical properties of the films were studied and are summarized in **Table 4.2.** Tensile strength measures the strength and elongation at break indicates stretchability of the film prior to breakage. The mechanical data of alginate film could not be obtained due to difficulty in peeling off the film from casting plate. On the other hand, the blended films showed improved mechanical properties in comparison to alginate film with 1:1 film demonstrating superior properties than 2:1 film. It was found that the values of tensile strength and Young's modulus for 1:1 blended film were comparatively less than that of chitosan film. However, the elongation at break value for 1:1 film was higher than chitosan film indicating higher elasticity of 1:1 film.

Table 4. 2. Mean mechanical properties of the films

Film	Thickness (µm)[a]	Elongation at break (%)[b]	Tensile Strength (MPa)[b]	Young's Modulus (MPa)[b]
1:1	5.562 ± 0.43	23.80 ± 2.53	16.55 ± 3.62	520 ± 88.82
2:1	5.606 ± 0.38	11.14 ± 0.83	7.42 ± 1.82	398 ± 44.36
Chi	5.547 ± 0.19	10.38 ± 0.39	24.77 ± 6.22	3496 ± 479.6

[a]Mean ± SD (n=8), [b]Mean ± SD (n=3)

4.4.8. Antibacterial activity of Alg-Ag NPs-Chi blended films

In order to evaluate practical applicability of the blended film, the 1:1 film was cut into small circular pieces of diameters 1, 1.5 and 2 cm and tested against two Gram positive viz. *Bacillus cereus* MTCC 1305, and *Enterococcus faecalis* MTCC 439 and three Gram-negative strains viz *Escherichia coli, Enterobacter aerogenes* MTCC 2822, and *Pseudomonas aeruginosa* MTCC 2488. **Table 4.3.** showed the antibacterial effect of blended films in terms of zone of inhibition. The results indicated that the film was antibacterial against both Gram negative and Gram positive bacteria with more inhibition against Gram positive bacteria as revealed by the size of inhibitory zone. The Alg-Ag NPs synthesized in the present study had zeta potential value of -16.37 mV. The Gram positive bacteria have less negative charge on the cell surface as compared to Gram negative bacteria (Chung et al., 2004). The results presented in **Table 4.3.** implied that the net charge on Ag NPs might have remained negative after the addition of chitosan. However, Ag NPs are known to be reactive and thus will interact with the cell-surface of the bacteria eventually killing them. Since the composite was overall negatively charged and Gram negative bacteria have comparatively higher negative surface charge, the composite would interact less with them in comparison to the Gram positive bacteria. Hence the composite will be more effective against Gram positive bacteria, which has been the case herein. Previously Kora et al. (2010) also reported negatively charged Ag NPs to be more effective against Gram positive bacteria. Besides, it was found that the size of inhibitory zone increased with increase in film size due to increase in content of Ag NPs. The control film made of only chitosan did not show any inhibitory zone indicating non-antibacterial activity of the film.The lack

of antibacterial activity of chitosan films in contrast to antibacterial chitosan solutions has already been reported earlier (Foster and Butt, 2010). Also, as expected the film made of alginate and chitosan only without Ag NPs did not show any antibacterial activity.

Table 4.3. Antibacterial activity of 1: 1 blended film for varying film diameter (d_F)

Strains	Zone of inhibition (mm)[a]		
	d_F = 1 cm	**d_F = 1.5 cm**	**d_F = 2 cm**
Gram negative			
Escherichia coli	0.5 ± 0.03	1.5 ± 0.05	1.9 ± 0.05
Enterobacter aerogenes	0.7 ± 0.05	1.4 ± 0.02	1.5 ± 0.07
Pseudomonas aeruginosa	2.5 ± 0.03	2.8 ± 0.05	3.1 ± 0.08
Gram positive			
Bacillus cereus	5.9 ± 0.03	5.9 ± 0.04	6.0 ± 0.03
Enterococcus faecalis	4.7 ± 0.04	4.9 ± 0.05	5.1 ± 0.04

[a]Mean ± SD (n=9)

4.5. Conclusion

The present study demonstrates a new, facile and 'green' method of synthesis of Ag NPs in aqueous medium using sodium alginate as both reducing as well as stabilizing agent. The synthesized Alg-Ag NPs were uniform in size (14 ± 3 nm) and antibacterial. The as-synthesized Alg-Ag NPs were blended with chitosan and cast into stable films having improved properties in comparison to alginate film. The films were characterized and their mechanical properties studied. FTIR, XRD and water uptake studies of blended film indicated interaction between alginate and chitosan polymers. The blended film was stable under storage and demonstrated effective bactericidal activity against both Gram positive and Gram negative bacteria with more efficacy against Gram positive bacteria The present approach of synthesis of Ag NPs utilized green chemistry principles and thus, films prepared from as-synthesized NPs can potentially be used for food packaging, as wound dressings, graftings onto various

implants and several other biotechnological and biomedical applications. Further, the 'green' method developed in the present study can easily be extended to prepare other biocompatible metal NPs, which subsequently be used for fabrication of films for practical applications. Finally, the present work depicts successful practical application and utilization of antibacterial potential of Ag NPs. In this regard, it becomes important to have an in-depth study of interaction of Ag NPs with mammalian cells. To achieve this goal, an effective biodegradable nanocarrier system for Ag NPs has to be developed and its interaction with mammalian cells needs to be investigated for possible therapeutic implications.

|Chapter 5|

Induction of Apoptosis in Human Glioblastoma Cancer Cells by Silver Nanoparticles using Alginate-Chitosan blended Nanocarrier

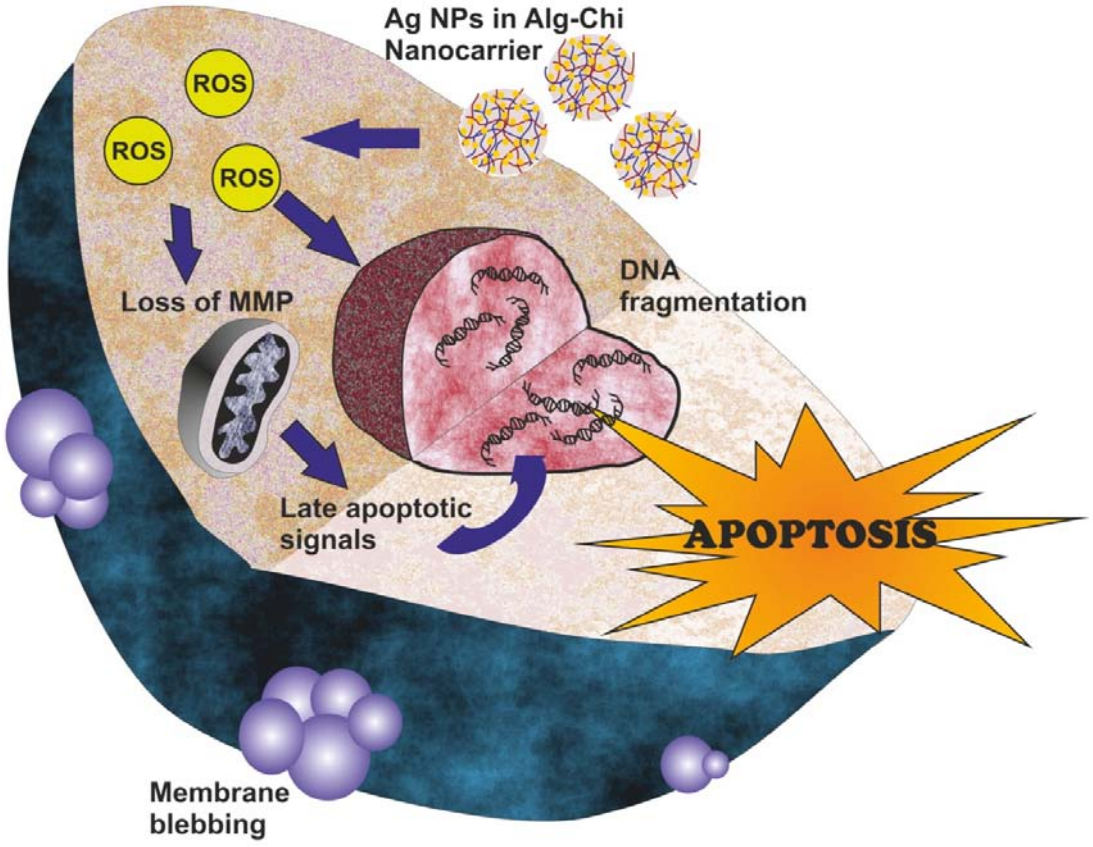

Chapter 5

INDUCTION OF APOPTOSIS IN HUMAN GLIOBLASTOMA CANCER CELLS BY SILVER NANOPARTICLES USING ALGINATE-CHITOSAN BLENDED NANOCARRIER

5.1. Introduction

Recently, our laboratory has explored the possibility of using Ag nanoparticles (NPs) either alone or in combination with gene therapy to induce apoptosis in mammalian cells (Gopinath et al., 2008, 2010; Sanpui et al., 2011). Other groups have also demonstrated apoptosis inducing therapeutic promising aspect of Ag NPs (Arora et al., 2008; Hsin et al., 2008; AshaRani et al., 2009; Franco-Molina et al., 2010; Liu et al., 2010). Apoptosis or programmed cell death is a normal regulated physiological process that maintains balance between cell proliferation and cell death by eliminating unwanted or damaged cells. The cancer cells have mechanisms of evading cell death and hence current clinical approaches aim at inducing apoptosis in these cells (Kasibhatla and Tseng, 2003). In this regard, the therapeutic potential of Ag NPs can be used as an alternative in cancer therapeutics. Over the last decade(s), nanotechnology has emerged as a key technology with immense potential to revolutionize cancer therapeutics (Peer et al., 2007). Several nanocarriers (NCs) including inorganic and polymeric NPs, liposomes, polymeric micelles, dendrimers, carbon nanotubes, biomolecules-such as albumin and gelatin-based particles have been used as drug delivery vehicles for cancer therapy (Lu et al, 2004; Dreis et al., 2007). Drug delivery systems based on natural polymers hold promising prospect owing to their desirable properties like biocompatibility, biodegradability, easy availability, controlled drug delivery and amenability to surface functionalization for possible active targeting. In this regard, alginate and chitosan are both FDA approved natural biopolymers with properties like high drug loading capacity, muco- and bioadhesiveness and enhanced intracellular penetration (Tønnesen and Karlsen, 2002; Hejazi and Amiji, 2003; George and Abraham, 2006). The potential of polyelectrolyte complex of alginate and chitosan

for controlled delivery of proteins, peptides and drugs has already been well established (Mi et al., 2002; Anal et al., 2003; Xu et al., 2007; Li et al., 2007; Goycoolea et al., 2009; Finotelli et al, 2010). However, the NC based on polyelectrolyte complex of alginate and chitosan has not been used for Ag NP delivery. It was speculated that the development of alginate-chitosan blended NC system for Ag NPs could improve bioavailability leading to increased therapeutic index of Ag NPs thereby decreasing overall toxicity.

5.2. Outline of the Research Work

1) A complete 'green' method for the synthesis of a novel biodegradable NC system based on polymers for Ag NPs has been developed.
2) The NC was prepared by a simple and mild ionic gelation method of polyelectrolyte complex formation between alginate and chitosan in aqueous condition at room temperature.
3) The NC was characterized and shown to induce apoptosis in mammalian human glioblastoma cancer cells by Ag NPs (impregnated in the NCs) at a concentration much less than previously reported values.
4) The apoptotic cell death was investigated by conventional acridine orange/ ethidium bromide (AO/EB) dual staining, electron microscopy and finally confirmed by terminal deoxynucleotidyl transferase dUTP nick end labelling (TUNEL) assay.
5) The effect of NC on oxidative stress, mitochondrial membrane potential and cell cycle progression was also evaluated to elucidate the molecular mechanism associated with toxicity.
6) The results indicated that the NC not only delivered Ag NPs efficiently but also enhanced the therapeutic efficacy of Ag NPs in inducing programmed cell death at low concentration thereby minimizing toxicity.

5.3. Experimental Section

5.3.1. Synthesis of Alginate-Chitosan-Ag NP nanocarrier (Alg-Chi-Ag NP NC)

Chitosan stabilized and Alginate stabilized Ag NPs (Chi-Ag NPs and Alg-Ag NPs) were synthesized as described in Experimental Section in Chapters 3 and 4, respectively. Alginate-chitosan blended NCs containing Ag NPs *Alg-Chi-Ag NP NC)* were synthesized by adding 3 mL Chi-Ag NPs (0.05 % w/v, pH 4.9) to 5 mL Alg-Ag

NPs (0.05 % w/v) drop by drop under vigorous stirring at room temperature. The mixture was stirred for 15 min. Blank NCs without Ag NPs (Alg-Chi NCs) were also prepared by following same procedure taking chitosan and alginate solutions respectively, instead of Chi-Ag NPs and Alg-Ag NPs.

5.3.2. Characterization of Alg-Chi-Ag NP NCs

The UV-visible spectra of the samples were recorded using a spectrophotometer (Lambda 45; Perkin-Elmer, Fremont, CA, USA) at room temperature. The surface morphology of the NCs was investigated by a LEO1430VO scanning electron microscope (SEM) by depositing 10 µL of NP sample on a glass slide followed by air drying. The slides were mounted on aluminium stubs, using double sided adhesive carbon tape, and then coated with gold film with a Polaron Sputter Coater before analyzing under SEM. For transmission electron microscopy (TEM), 5 µL of different liquid NP samples were drop cast on carbon-coated copper TEM grids and subsequently air-dried at room temperature. The drop-coated grids were analyzed by a high resolution transmission electron microscope (JEM 2100; Jeol, Peabody, MA, USA) operating at an accelerating voltage of 200 kV. The selected area electron diffraction (SAED) pattern of Ag NP was also recorded using the same instrument. The histograms for particle size distribution were constructed by analyzing several frames of similar images. The particle size and zeta potential of the NCs were assessed on the Zeta Sizer Nano ZS90 (Malvern Instruments) by dynamic light scattering (DLS) measurements and laser Doppler electrophoresis, respectively. The analysis was performed at a scattering angle of 90º under 25 ºC. The Fourier transform infrared (FTIR) spectra of the samples were recorded using a Perkin-Elmer Spectrum one spectrometer. For X-ray diffraction (XRD) patterns, the samples were dried and patterns were recorded with a Bruker D8 ADVANCE (Bruker AXS Inc.) XRD machine using Cu Kα (λ= 1.54 Å) source.

5.3.3. Cell Culture and Alg-Chi-Ag NP NC Treatment

Human glioblastoma U87MG cells were procured from National Centre for Cell Sciences (NCCS), Pune, India and were maintained in Dulbecoo's modified Eagle's medium (DMEM, Sigma-Aldrich, USA) supplemented with 10% (v/v) fetal bovine serum, 50 U mL^{-1} penicillin, 50 mg mL^{-1} streptomycin (all from Sigma Aldrich) at 5% CO_2 in a humidified incubator at 37°C. The cells were treated with different

concentrations of Alg-Chi-Ag NP NCs and blank Alg-Chi NCs. After 6 h and 24 h, the cells were observed under a phase contrast microscope (Nikon ECLIPSE, Ti-U) to identify the morphological changes in comparison to the untreated cells.

5.3.4. Cell Viability Assay

Cells were seeded in a 96 well cell culture plate at a density of ~5 x 10^3 cells/well in serum media. The plate was incubated at 37 ºC overnight for cell attachment. The medium was removed after incubation and replaced with serum free medium containing different concentrations of Alg-Chi-Ag NP NCs ranging from 116 µg mL^{-1} to 222 µg mL^{-1}. After treatment for 12 h, cytotoxicity was evaluated by determining the viability of cells using XTT (Sigma Aldrich) assay according to the manufacturer's instruction. The mitochondrial dehydrogenases of viable cells reduced the tetrazolium ring of XTT (2, 3-bis [2-Methoxy-4-nitro-5-sulfophenyl] - 2H-tetrazolium-5-carboxyanilide inner salt) to form an orange formazan derivative. The amount of formazan product formed was measured by recording absorbance at 450 nm and 690 nm with a multiplate reader (Tecan, Infinite M200). The quantity of formazan product was directly proportional to the number of viable cells in culture. The cell viability was calculated as:

% cell viability= [($A_{450} - A_{690}$) in treated sample/ ($A_{450} - A_{690}$) in control sample] × 100

5.3.5. Transmission Electron Microscopy (TEM) of Alg-Chi-Ag NP NCs treated cells

For TEM, cells grown to 70-80 % confluency in 6-well plate were treated with 139 µg mL^{-1} of Alg-Chi-Ag NP NCs for 12 h. After treatment, the cells were washed with PBS, trypsinized, and pelleted down by centrifugation. The cell pellet was then washed with PBS followed by fixation in glutaraldehyde solution and subsequent dehydration in graded ethanol solutions. Finally, the cells were resuspended in absolute ethanol and 7 µL of cell suspension was drop-cast on TEM grid followed by air drying. The grids were then analyzed by a JEM 2100; Jeol, Peabody, MA, USA instrument.

5.3.6. Acridine orange/Ethidium bromide (AO/EB) Dual Staining

For morphological identification of apoptotic or necrotic nuclei, the cells were stained with dual acridine orange/ethidium bromide (Sigma-Aldrich, USA) dye mixture. Cells grown to 70-80 % confluency in 6-well plates were treated with desired concentrations

of NCs for 6 h. The culture media was removed and the cells were washed twice with PBS. Fresh media containing 2 µg mL^{-1} AO and 6 µg mL^{-1} EB was added to each well and cells were stained for 10 min in the dark. The cells were then washed with PBS thoroughly and visualized under a fluorescence microscope (Nikon ECLIPSE, T*i*-U).

5.3.7. Scanning Electron Microscopy (SEM)

For SEM, cells grown to 70-80 % confluency in 6-well plate were treated with Alg-Chi-Ag NP NCs for 3 h. The cells were then washed with PBS followed by fixation in glutaraldehyde solution. The fixed cells were dehydrated in graded ethanol solutions and air-dried. A heated metal cutter was used to cut out discs from the bottom of the well on which the cells had been grown. The cells attached on discs were coated with gold film in a Polaron sputter coater and examined in LEO 1430VP SEM.

5.3.8. Determination of Reactive Oxygen Species (ROS)

U87MG cells grown in a 6-well plate were treated with different concentrations of Alg-Chi-Ag NP NCs for 45 min. After treatment, the cells were harvested by trypsinization and washed twice with PBS. Finally, the cells were resuspended in 1 mL of DMEM containing 5 µM 2, 7-dichlorofluoresceindiacetate (DCFH-DA; Sigma-Aldrich, USA) dye and incubated for 10 min at 37 °C. DCFH-DA is a membrane permeable, fluorogenic dye which gets deacetylated by cellular esterases to form a non-fluorescent DCFH. DCFH on oxidation by intracellular ROS forms a highly fluorescent dichlorofluorescein (DCF) with excitation and emission maxima at 495 nm and 529 nm, respectively. The samples were incubated with dye for 10 min at 37°C and immediately after incubation the samples were analyzed for DCF fluorescence in a flow cytometer (FacsCalibur, BD Biosciences, NJ). The fluorescence data were acquired and analyzed with the CellQuest Pro (BD Biosciences) software for 10 000 events in each sample. The ROS generation was expressed in terms of percentage of cells with DCF (green) fluorescence.

5.3.9. Determination of Mitochondrial Membrane Potential (MMP)

For determining changes in MMP after treatment, cells grown in a 6-well plate were treated with desired concentrations of Alg-Chi-Ag NP NCs for 1 h. The cells were trypsinized, centrifuged and resuspended in medium containing 10 µg mL^{-1} of 5,5,6,6-tetrachloro-1,1,3,3-tetraethylbenzimidazolylcarbocyanine iodide (JC-1; Sigma- 319

Aldrich, USA) for 10 min in dark at room temperature. After incubation, the cells were washed twice, resuspended in PBS and analyzed with flow cytometer. The JC-1 fluorescence data were recorded with the CellQuest Pro software for 10 000 cells in each sample. Parallelly, a fresh batch of treated cells was stained with JC-1 and washed with PBS before visualization under a fluorescence microscope (Nikon327 ECLIPSE, TS100, Tokyo) equipped with red and green filters.

5.3.10. Cell cycle analysis

Cells grown to 60-70% confluency in 6-well plate were treated with appropriate concentrations of Alg-Chi-Ag NP NCs for 1h. At the end of the treatment period, cells were harvested by trypsinization and fixed with 70% alcohol solution in ice for 15 min. The fixed cells were collected by centrifugation and stained with propidium iodide (PI) staining solution (50µg/mL PI, 0.1mg/mL RNase A and 0.05% triton X-100) at 37°C for 30 minutes in dark. The cell cycle distribution of the cells was then determined by measuring the amount of PI-labeled DNA in flow cytometer (FacsCalibur, BD Biosciences, NJ) for 10000 events in each sample and analysed by Cell Quest Pro software in the same instrument.

5.3.11. Terminal Deoxynucleotidyl Transferase dUTP Nick End Labelling (TUNEL) Assay

The cells were treated with appropriate concentrations of Alg-Chi-Ag NP NCs for 12 h. At the end of treatment, cells were trypsinized and fixed with 1% w/v formaldehyde and then with 70% ethanol. The Br-dUTPs were incorporated in the fragmented DNA followed by staining with FITC-labelled anti-BrdU mAb using BD Pharmingen APO-BRDU^{TM} Kit following manufacturer's instruction. Samples were acquired by BD FacsCalibur and data analysed by Cell quest pro software.

5.3.12. Statistical analysis

The values for all experiments are expressed as mean ± SEM (standard error mean) of three or more individual experiments. The data were analyzed by Student's t test using GraphPad Prism 5.01 and statistically significant values are denoted by * ($p < 0.05$), ** ($p < 0.005$) and *** ($p < 0.001$).

5.4. Results and Discussion

5.4.1. Synthesis and Characterization of Alg-Chi-Ag NP NCs

In the present study, a NC system based on the polyelectrolyte complex of chitosan and alginate for delivery of Ag NPs has been developed. The blended NCs (Alg-Chi-Ag NP NCs) were synthesized by adding pre-synthesized Chi-Ag NPs drop by drop to Alg Ag NPs under vigorous stirring at room temperature in aqueous condition. The solution turned turbid indicating formation of Alg-Chi-Ag NPs blended NCs. Preliminary experiments were performed to standardize the concentrations of Chi-Ag NPs and Alg-Ag NPs in order to avoid the formation of insoluble coacervates that settled at the bottom.

The UV-Vis absorption spectra of Alg-Ag NPs and Chi-Ag NPs exhibited peaks at ~400 nm and ~409 nm, respectively, characteristic of surface plasmon resonance of metallic Ag NPs (**Figure 5.1a**). The Ag NPs containing NCs exhibited band at ~407 nm. The size of Alg-Chi-Ag NP NCs ranged from 233 nm to 410 nm as indicated by SEM images with average size calculated to be 315.1 ± 39.5 nm (**Figure 5.2b**, **5.2d**). In contrast, the average size of blank NCs was found to be 214 ± 59.4 nm (**Figure 5.2a, 5.2c**). The large size of Alg-Chi-Ag NP NCs as compared to blank NCs could be due to presence of Ag NPs. The hydrodynamic diameter and zeta potential values of Alg-Chi-Ag NP NCs were found to be 318.6 ± 4.6 nm and -35.5 ± 0.98 mV, respectively**.** TEM analysis showed that the NC had spherical shape with smooth surface (**Figure 5.1b**). The presence of Ag NPs in NC was confirmed by the energy dispersive X-ray (EDX) spectrum of NC (**Figure 5.1d**). The Ag NPs were polycrystalline as indicated by the SAED pattern (**Figure 5.1c**).

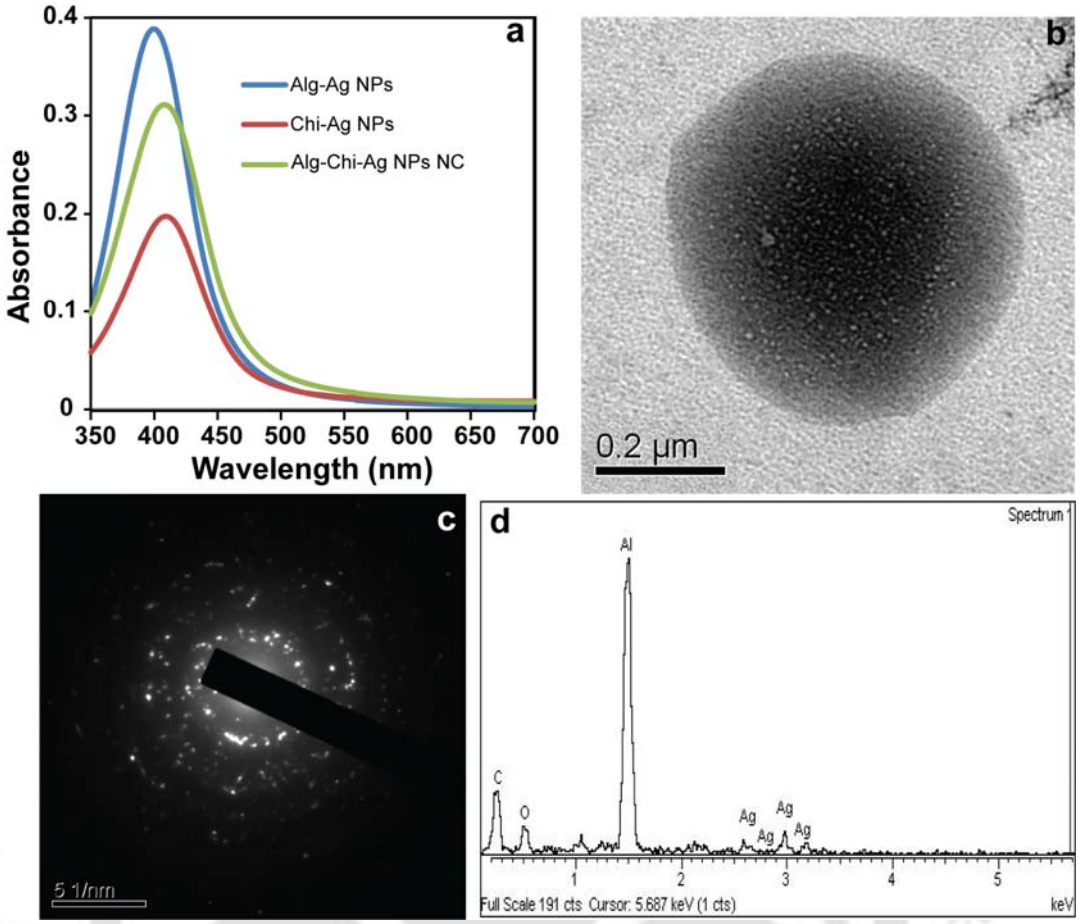

Figure 5.1. (a) UV-Vis spectra of Alg-Ag NPs, Chi-Ag NPs and Alg-Chi-Ag NP NCs, **(b)** Representative TEM image of an Alg-Chi-Ag NP NC **(c)** corresponding SAED pattern and **(d)** EDX spectrum of Alg-Chi-Ag NP NCs showing silver signals.

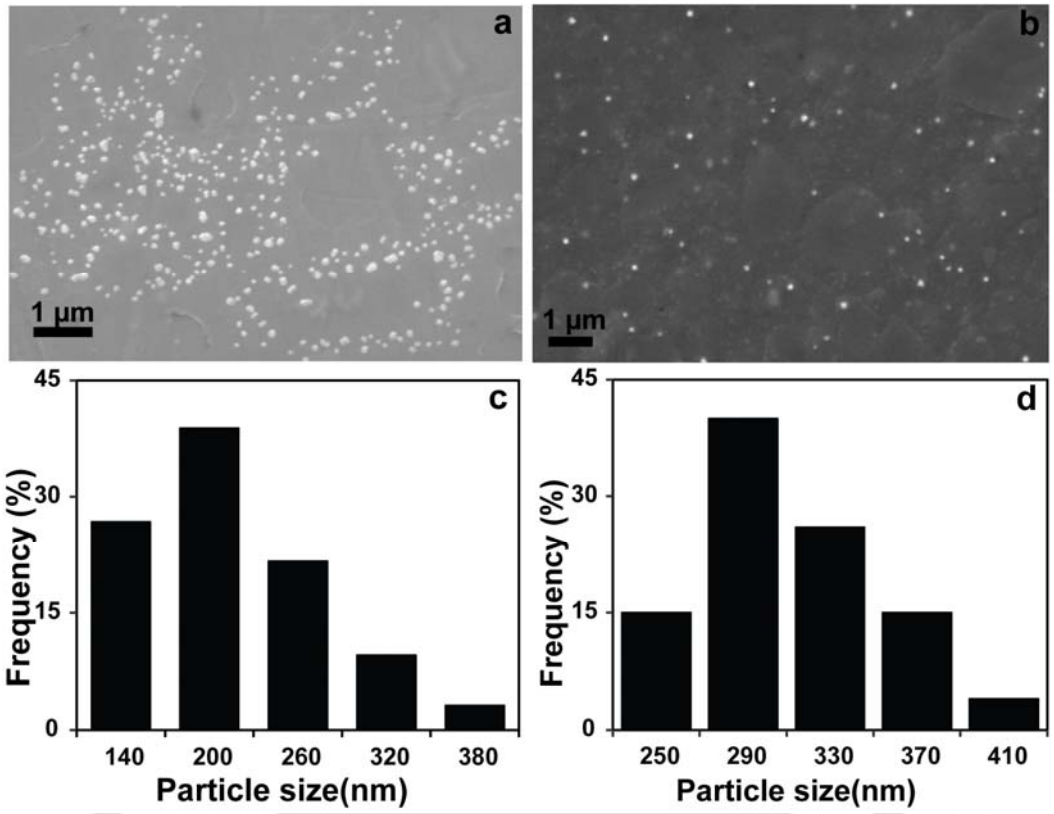

Figure 5.2. Representative SEM images of **(a)** blank Alg-Chi NCs and **(b)** Alg-Chi-Ag NP NCs with particle size distributions as determined by SEM images shown in **(c)** and **(d)**, respectively.

5.4.2. FTIR analysis

The FTIR spectra of Alg-Ag NPs, Chi-Ag NPs and Alg-Chi-Ag NP NCs are shown in **Figure 5.3**. The Alg-Ag NPs showed characteristic absorption bands at 1630 cm^{-1} and 1384 cm^{-1} corresponding to stretching vibrations of carboxylate groups as described previously in Results and Discussion in Chapter 4. The amide groups of Chi-Ag NPs showed absorption band with a slight shoulder at 1635 cm^{-1}. The shifting of peak of Alg-Ag NPs at 1630 cm^{-1} to 1635 cm^{-1}, disappearance of amide shoulder of Chi-Ag NPs and appearance of a new band at 1410 cm^{-1} indicated the formation of complex between chitosan and alginate polymers in Alg-Chi-Ag NP NC. Further, the absorption bands due to stretching vibration of O-H groups at 3433 cm^{-1} in Alg-Ag NPs and at 3431 cm^{-1} in Chi-Ag NPs shifted to a broad band at 3445 cm^{-1} in NC which confirmed the interaction between polymers (Sankalia et al., 2007; Wang et al., 2010a).

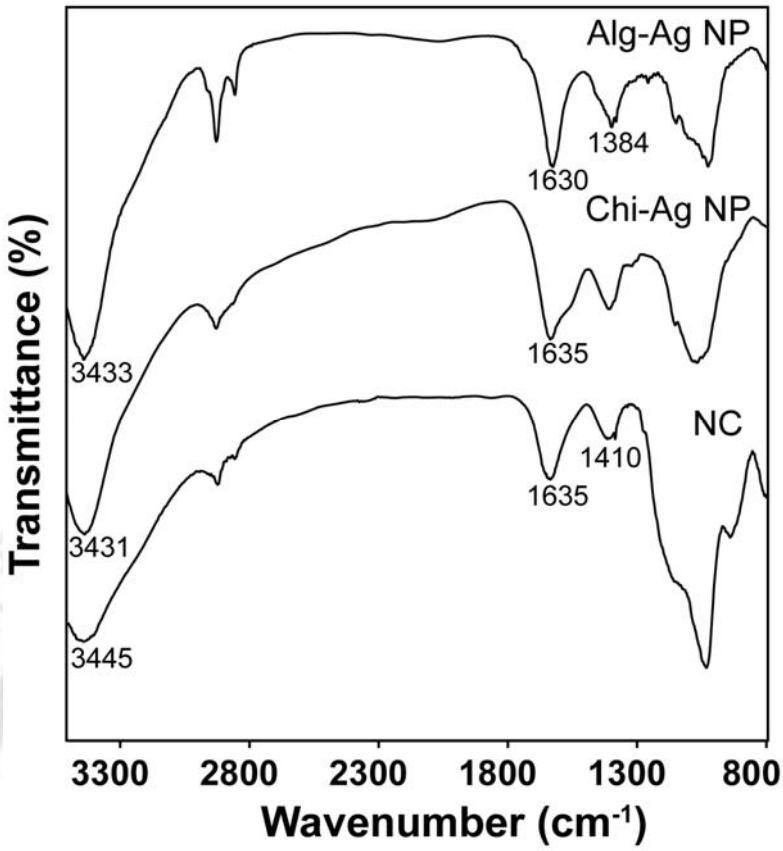

Figure 5.3. FTIR spectra of Alg-Ag NPs, Chi-Ag NPs and Alg-Chi-Ag NP NCs.

5.4.3. XRD analysis

The XRD patterns of samples are presented in **Figure 5.4.** The diffractogram of Chi-Ag NPs consisted of a peak at 10.5° corresponding to chitosan crystals and a broad peak of very low intensity extending from 16.2° to 24.1° corresponding to amorphous region. Alg-Ag NPs showed a broad peak at 11.9°. In NC, the peak corresponding to the crystalline region of chitosan almost disappeared and a prominent broad band appeared at 22.3° due to strong interactions between polymers that destroyed the close packing of polymers (Meng et al, 2010). In addition, Alg-Ag NPs, Chi-Ag NPs and Alg-Chi-Ag NP NCs had a well defined characteristic diffraction peak at 38.3° corresponding to (111) plane of face centered cubic (fcc) crystal structure of metallic Ag indicating the presence of Ag NPs.

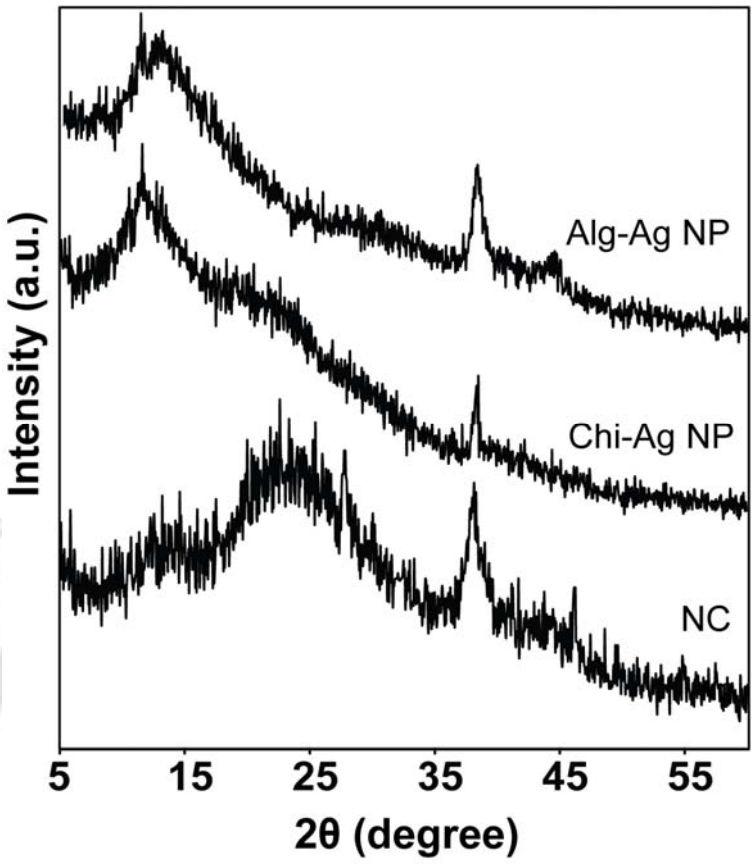

Figure 5.4. XRD patterns of Alg-Ag NPs, Chi-Ag NPs and Alg-Chi-Ag NP NCs.

5.4.4. Stability of NCs

Before carrying out cell based experiments, the stability of Alg-Chi-Ag NP NCs in cell culture medium was checked by incubating NCs in DMEM at 37 °C followed by TEM studies. It was found that the NCs were stable in medium for 12 h ((**Figure 5.5a)** However after 24 h, the NC began to degrade revealing Ag NPs confined inside the core of NC (**Figure 5.5b**) thereby demonstrating successful encapsulation of Ag NPs in the Alg-Chi blended NC. The SAED pattern indicated polycrystalline Ag NPs (**Figure 5.5c**). The average size of encapsulated Ag NPs was calculated to be 10.3 ± 6.8 nm (**Figure 5.5.d**).

5.4.5. Cytotoxicity of Alg-Chi-Ag NP NCs on U87MG cells

In order to examine the effect of Alg-Chi-Ag NP NCs on cells, the U87MG cells were treated with varying concentrations of NCs for different time periods and observed under phase contrast microscope. Distinct dose and time dependent changes in

morphology were observed in treated cells, which clearly demonstrated the toxicity of NCs (**Figure 5.6.**). It was found that with the increase in concentration, more cells became rounded and shrunk in size. The cells detached from the surface and began to float. The number of floating cells increased with time at higher concentrations. On the other hand, cells treated with blank NCs without Ag NPs maintained their elongated spindle-like shape indicating healthy and normal morphology as that of control untreated cells.

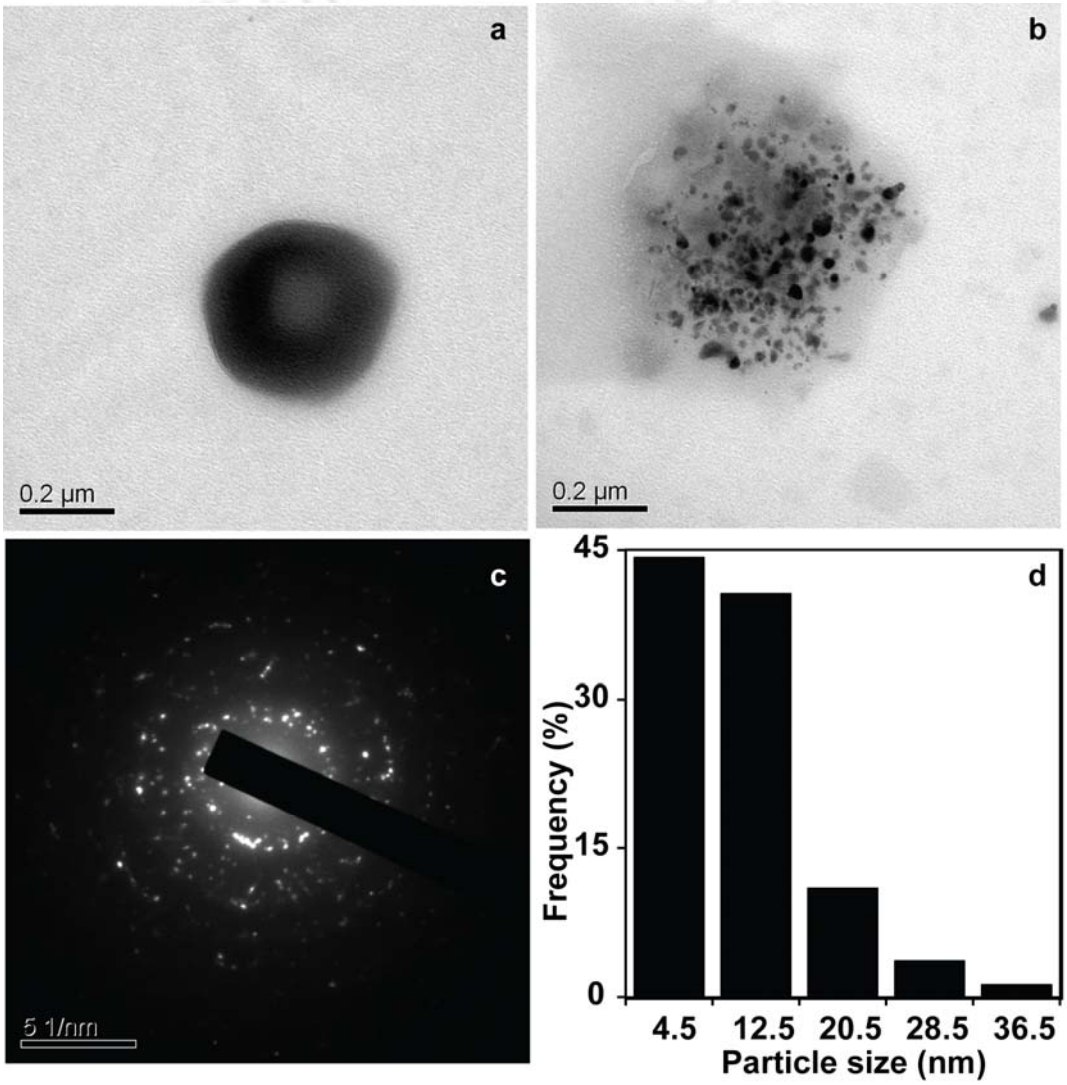

Figure 5.5. Representative TEM images of Alg-Chi-Ag NP NC incubated in cell culture medium for **(a)** 12 h and **(b)** 24 h, **(c)** SAED pattern of Alg-Chi-Ag NP NC incubated in medium for 24 h and **(d)** particle size distribution of Ag NPs confined in NC.

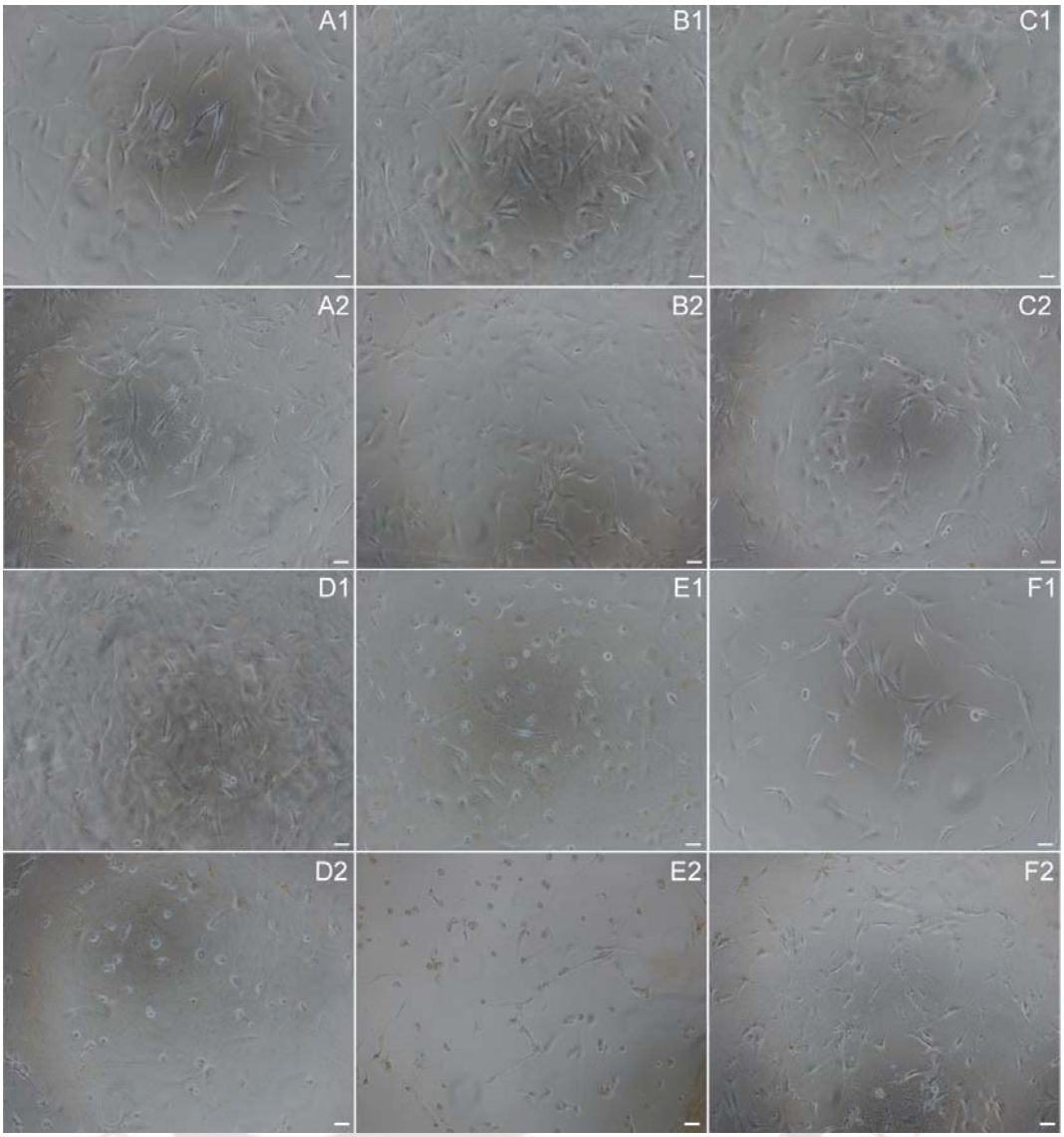

Figure 5.6. Morphology of U87MG cells untreated (**A1, A2**) and treated with 116 µg mL^{-1} (**B1, B2**), 233 µg mL^{-1} (**C1, C2**), 350 µg mL^{-1} (**D1, D2**), 466 µg mL^{-1} (**E1, E2**) of Alg-Chi-Ag NPs beads for 6 h (**A1-E1**) and 24 h (**A2-E2**). Morphology of cells treated with 466 µg mL^{-1} of blank Alg-Chi beads (**F1**, 6 h and **F2**, 24 h) is also shown. Scale bar: 50 µm

5.4.6. Cell Viability

The cell viability of Alg-Chi-Ag NP NCs treated cells after 12 h was determined quantitatively by XTT assay. The results shown in **Figure 5.7.** clearly indicated that the viability of cells decreased with increase in concentration of Alg-Chi-Ag NP NCs. The mean IC_{50} value of Alg-Chi-Ag NP NCs was found to be 139 µg mL^{-1}. The concentration of Ag NPs at IC_{50} value of NCs was calculated to be 2.4 µg mL^{-1} which is

very less than previously reported values (Gopinath et al., 2008; Arora et al., 2008; Hsin et al., 2008; AshaRani et al., 2009; Jain et al., 2009; Hussain et al., 2005). For instance Gopinath et al. (2008) reported IC_{50} for medium stabilized Ag NPs to be 27 µg mL^{-1} for HT 29 and BHK 21 cells. The probable reason for high cytotoxicity at such low Ag NP concentration is that in the present system, Ag NPs were not free but confined in a biodegradable polymeric NC. As a result, Ag NPs were prevented from premature interaction with biological environment, thereby having improved bioavailability. The blank Alg-Chi NCs did not affect the viability of cells, not even at a high concentration of ~222 µg mL^{-1} demonstrating non cytotoxicity of blank NCs.

Glioblastoma is a highly aggressive brain cancer generally refractory to conventional chemotherapeutic agents (Hegde et al., 2004; Castino et al., 2011). In the present case too, U87MG glioblastoma cells showed poor therapeutic responsiveness to conventional anticancer drugs viz. 5-fluorouracil (5-FU) and cisplatin as revealed by cell viability data after 48 h treatment (**Figure 5.8.**). Treatment with 50 µM of 5-FU for 48 h resulted in drop in cell viability to only 60 % which remained unchanged even for high concentrations of 5-FU. Cisplatin, on the other hand, killed cells, but at high concentrations. The IC_{50} value for cisplatin was found to be 4 ug mL^{-1} after 48 h. However, with the present system, the cells were killed at low concentration of Ag NPs after 12 h demonstrating its superior efficacy.

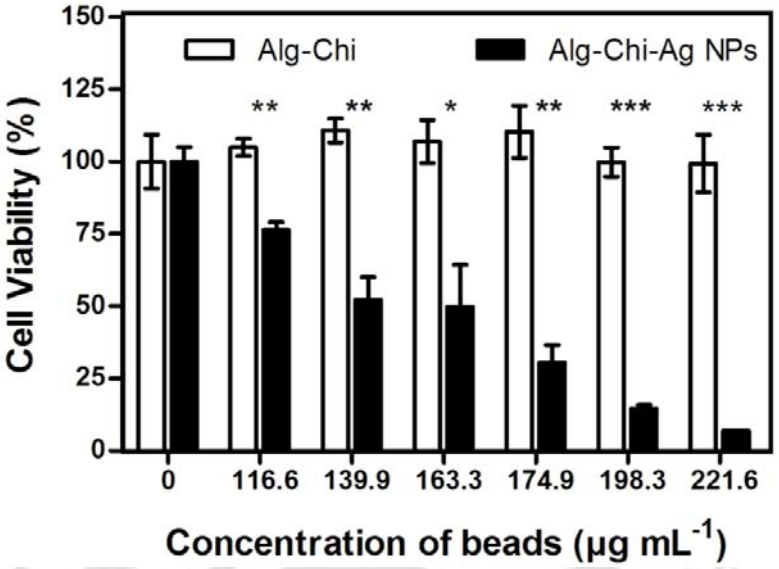

Figure 5.7. Cell viability of U87MG cells after 12 h treatment with different concentrations of Alg-Chi-Ag NP NCs, as calculated from the XTT assay. The values are represented as mean ± SEM of three individual experiments. Statistical significance between samples treated with Alg-Chi Ag NPs NCs and blank NCs is denoted by * ($p < 0.05$), ** ($p < 0.005$) and *** ($p < 0.001$).

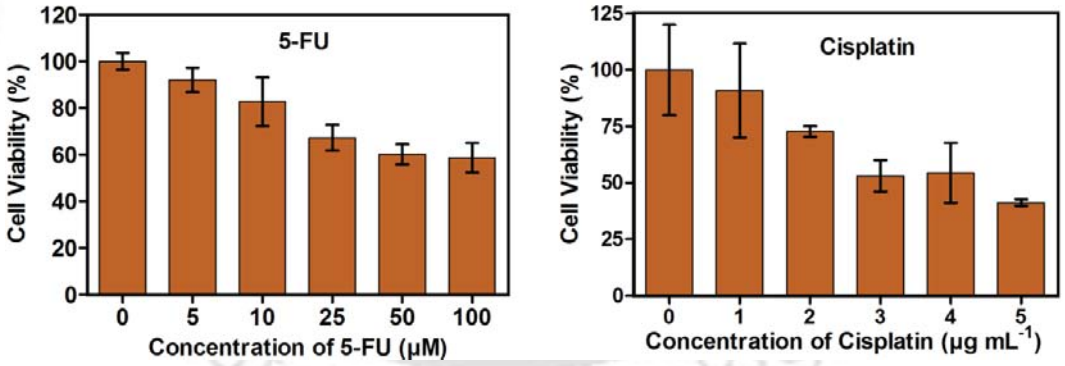

Figure 5.8. Cell viability of U87MG cells after 48 h treatment with different concentrations of 5-FU and cisplatin as calculated from the XTT assay.

Further, TEM investigations with Alg-Chi-Ag NP NCs treated cells showed Ag NPs as black contrasted dots inside the cells (**Figure 5.9.**). The SAED pattern (**inset**, **Figure 5.9b**) showed hexagonal pattern confirming presence of Ag NPs in the cells. The sizes of Ag NPs were similar to that of Ag NPs in the core of NC in **Figure 5.5b**.

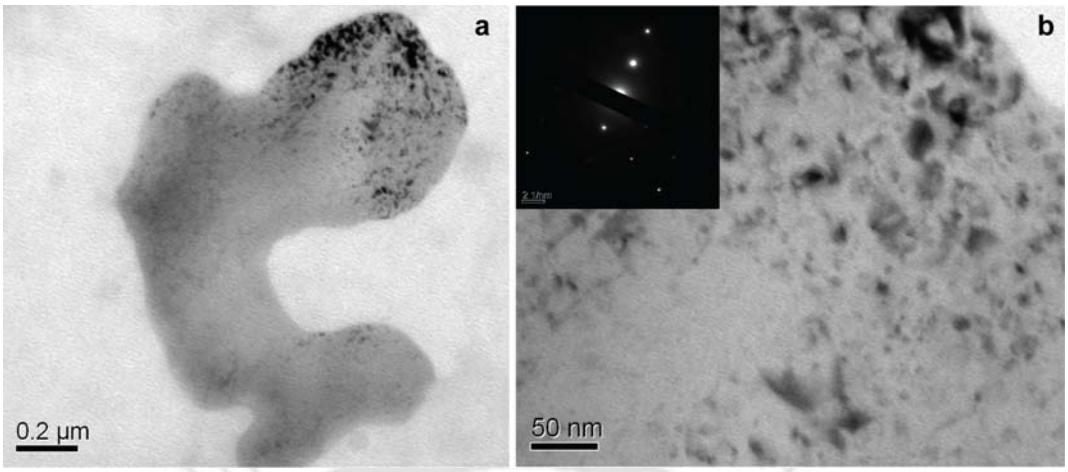

Figure 5.9. Representative TEM images of U87MG cells treated with Alg-Chi-Ag NP NCs (139 µg mL $^{-1}$) at **(a)** lower and **(b)** higher magnification showing presence of Ag NPs in the cell, **inset** shows corresponding SAED pattern.

5.4.7. AO/EB Dual Staining

In order to determine the mode of cell death by Alg-Chi-Ag NP NCs, the treated cells were stained with fluorescent DNA intercalating dyes namely acridine orange (AO) and ethidium bromide (EB) and were observed under a fluorescence microscope. It is known that AO is taken up by all cells (both viable as and non-viable cells) and emits green fluorescence on binding with double stranded DNA and red fluorescence on binding with RNA and single stranded DNA. On the other hand, EB enters only membrane compromised cells and emits orange fluorescence on binding with double stranded DNA and red with RNA. Based on this difference of permeation ability of both labeling dyes, it is possible to distinguish live, apoptotic and necrotic cells by double staining with AO and EB (Castilho, 2008). The live cells show uniformly green coloured nucleus due to AO. An early apoptotic cell in which apoptosis has started but membrane is still intact shows green granules corresponding to condensed and fragmented chromatin in nuclear region. The membrane integrity is lost in late apoptotic cells and thus they become permeable to EB. As a result, cells appear reddish orange with orange granules in the nuclear region. Necrotic cells have orange nucleus of regular size or larger without any condensation or fragmentation of chromatin.

In the present case, as is evident from **Figure 5.10.**, the cells treated with 69.5 µg mL^{-1} (0.5 IC_{50}) Alg-Chi-Ag NP NCs, like untreated cells, had uniformly stained

green nuclei indicating healthy viable cells. However cells treated with 139 µg mL^{-1} (IC_{50}) of NCs showed green and orange stained condensed nuclei indicating the presence of both early and late apoptotic cells. At higher concentration of 278 µg mL^{-1} ($2IC_{50}$) of NCs, more number of cells in late apoptotic stage and few necrotic cells were seen. Thus, AO/ EB staining results indicated induction of apoptosis in cells treated with Alg-Chi-Ag NP NCs.

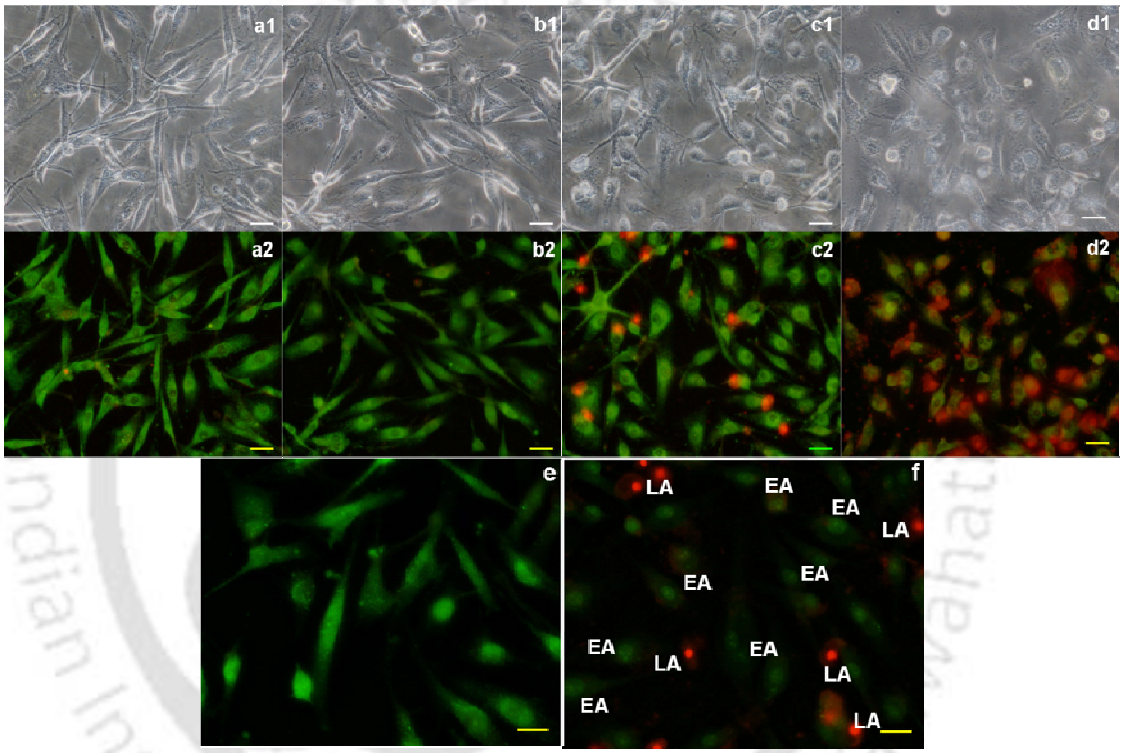

Figure 5.10. Representative images of AO/EB dual staining of **(a1, a2)** untreated, **(b1, b2)** 69.5 µg mL^{-1} (0.5 IC_{50}), **(c1, c2)** 139 µg mL^{-1} (IC_{50}) and **(d1, d2)** 278 µg mL^{-1} (2 IC_{50}) Alg-Chi-Ag NP NCs treated U87MG cells after 6 h of treatment. The images in the upper panel **(a1-d1)** are corresponding bright field images. High magnification representative images of **(e)** untreated and **(f)** 139 µg mL^{-1} (IC_{50}) Alg-Chi-Ag NP NCs treated U87MG cells after 6 h of treatment. Scale bar: 50 µm

5.4.8. SEM studies

SEM studies were further performed with Alg-Chi-Ag NP NCs exposed cells to observe any morphological changes associated with apoptosis. As is evident from **Figure 5.11.**, the treated cells had a distinct shape change and shrinkage in contrast to untreated cells that displayed normal morphology. The treated cells appeared spherical with minimal cellular extensions and restricted spreading patterns contrary to untreated cells that were well connected to each other through slender extensions. Besides, membrane blebbing and formation of apoptotic bodies which are characteristics of apoptosis (Rello et al., 2005) were also observed in case of treated cells suggesting apoptotic cell death.

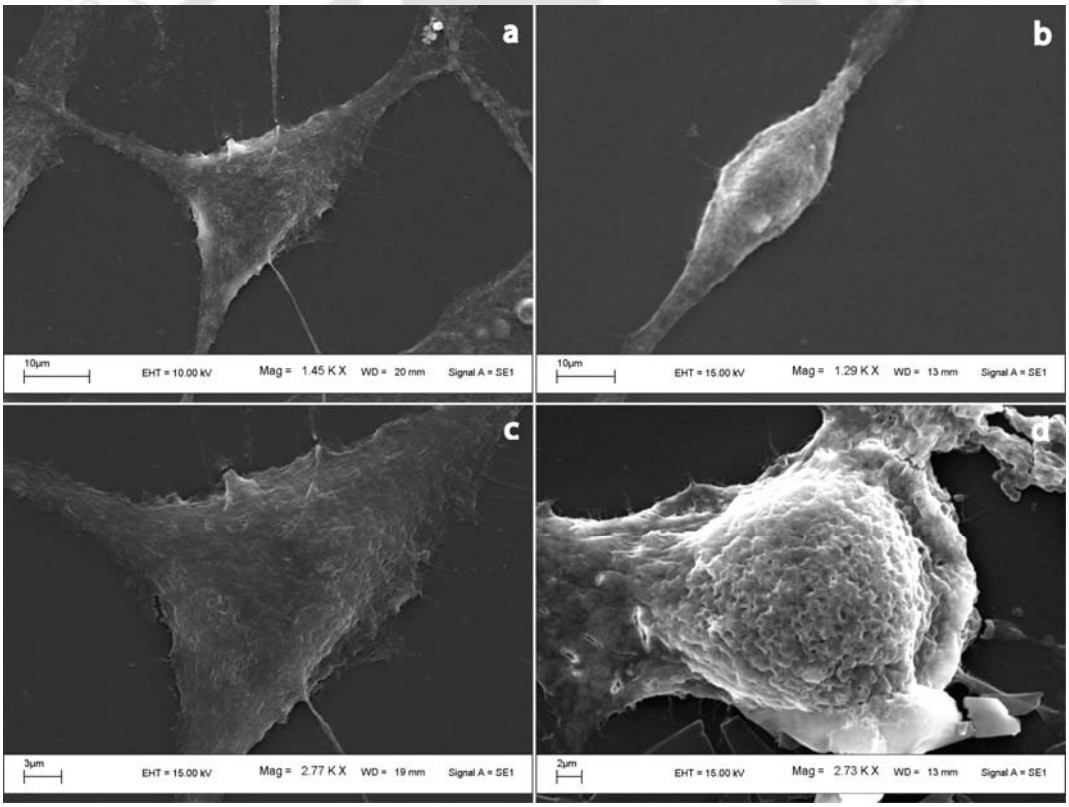

Figure 5.11. Representative SEM images of **(a, c)** untreated and **(b, d)** treated U87MG cells with Alg-Chi-Ag NP NCs.

5.4.9. Role of ROS

Cells have an inherent anti-oxidant defence mechanisms and oxidative stress occurs when the generation of ROS exceeds the tolerable limits within the cells. Earlier studies have emphasized the role played by oxidative stress in apoptosis induced by Ag NPs in mammalian cells (Hsin et al., 2008; AshaRani et al., 2009; Piao et al., 2011; Carlson et al., 2008). It has been shown that the level of glutathione, a key molecule responsible for maintaining cellular oxidation-reduction homeostasis (Sies, 1999) gets depleted in cells exposed to Ag NPs. To evaluate possible role of oxidative stress in inducing apoptosis in the present case, ROS level was measured by DCFDA staining using a flow cytometer (**Figure 5.12.**).The results indicated that cells treated with 69.5 µg mL^{-1} (0.5 IC_{50}) of Alg-Chi-Ag NP NCs had more or less same ROS level as that of untreated cells. At 139 µg mL^{-1} (IC_{50}) of Alg-Chi-Ag NP NCs, there was a significant increase in ROS level which however decreased slightly at the highest concentration of 278 µg mL^{-1} (2 IC_{50}). This could be probably due to loss of DCF from dead cells. The results suggested that Ag NPs induced oxidative stress in the cells by evoking ROS.

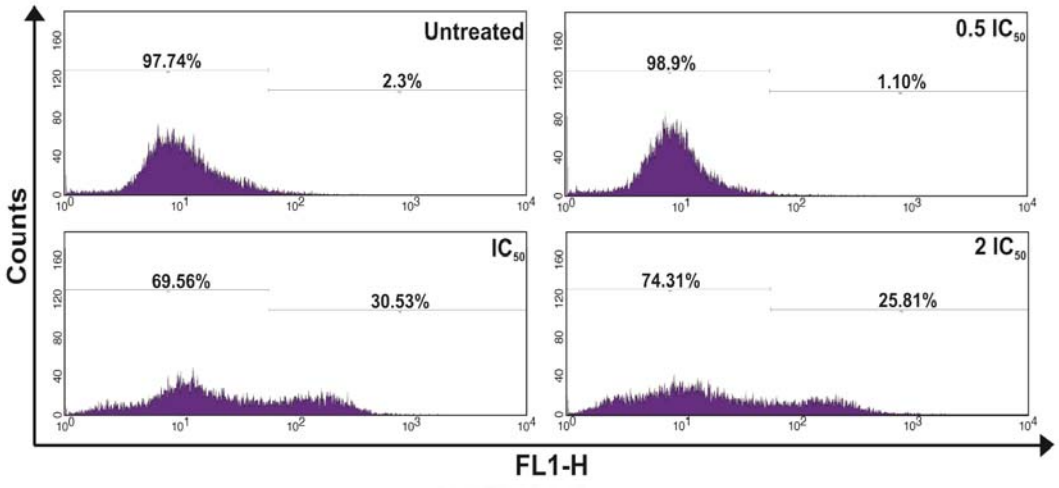

Figure 5.12. Flow cytometric analysis of ROS production in cells treated with different concentrations of Alg-Chi-Ag NP NCs

5.4.10. Measurement of mitochondrial membrane potential (MMP)

Intracellular ROS play an important role in the signal transduction pathways leading to mitochondria-dependent apoptosis (Kamata and Hirata, 1999; Ueda et al., 2002). In this context, loss of mitochondrial transmembrane potential ($\Delta\Psi_m$) is an important early apoptotic event. The effect of Alg-Chi-Ag NP NCs on mitochondrial potential was evaluated by JC-1 staining. JC-1 dye is a cationic lipophilic molecule that selectively enters into mitochondria. It is a dual fluorescence probe whose monomeric and aggregated forms emit green and red fluorescence, respectively, when excited at 488 nm (Cossarizza et al., 1993). In healthy cells, MMP is high and thus JC-1 spontaneously aggregates whereas in the apoptotic cells due to depolarization of mitochondrial membrane, JC-1 remains in its monomeric form. Thus, the ratio of red to green fluorescence is decreased in cells undergoing apoptosis as compared to healthy cells.

In the present study, treated cells exhibited loss of MMP as revealed by fluorescence microscopy images (**Figure 5.13.**). The untreated control cells showed completely polarized mitochondria as red dots due to J-aggregates (**Figure 5.13a1**). In treated cells, there was a progressive decrease in red fluorescence and simultaneous increase in green fluorescence (**Figure 5.13b1-5.13d1**) indicating depolarization of mitochondrial membrane. This result was further substantiated by flow cytometry results (**Figure 5.13e**, **5.13f**). The dot plots of red fluorescence (FL2) versus green fluorescence (FL1) indicated decrease in red fluorescence (~72.3 %) in case of 139 µg mL^{-1} (IC_{50}) of Alg-Chi-Ag NP NCs treated cells, as compared to control cells. The loss of MMP on exposure to Alg-Chi-Ag NP NCs suggested involvement of mitochondrial pathway of apoptosis.

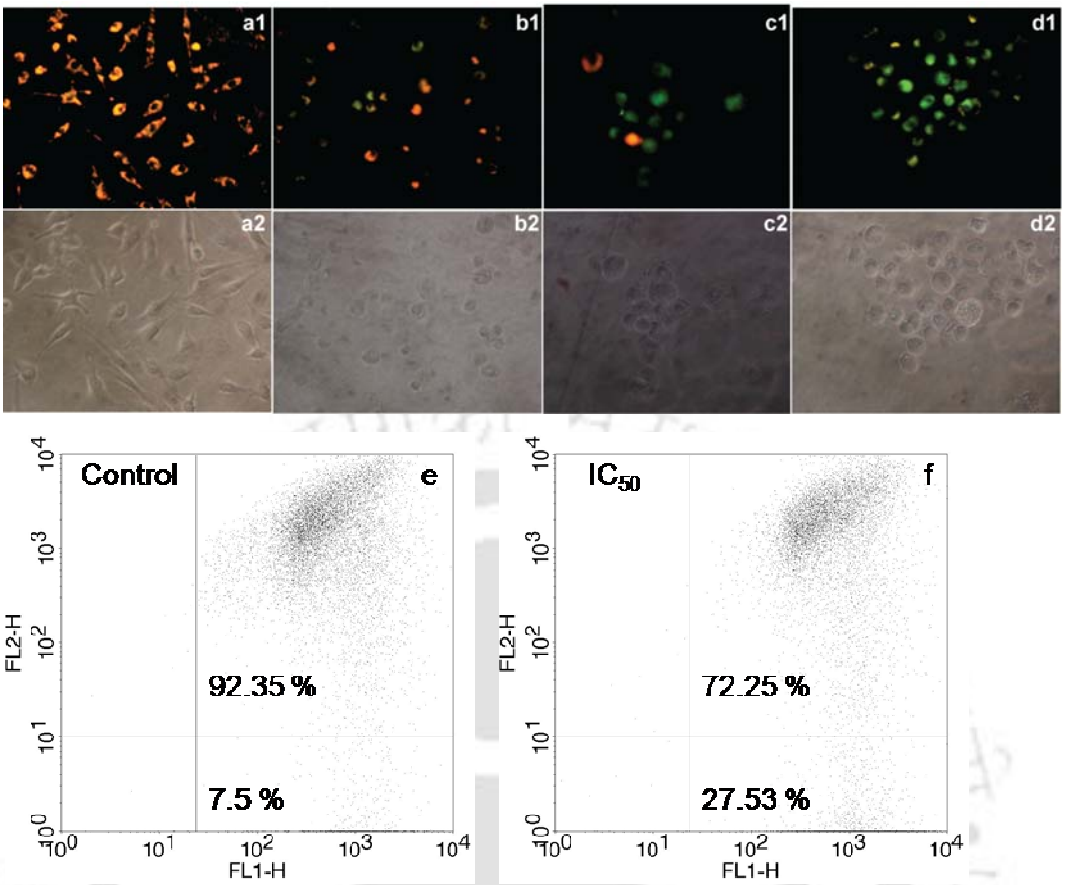

Figure 5.13. Microscopic image of JC 1 staining of **(a1, a2)** untreated, **(b1, b2)** 69.5 µg mL^{-1} (0.5 IC_{50}), **(c1, c2)** 139 µg mL^{-1} (IC_{50}) and **(d1, d2)** 278 µg mL^{-1} (2 IC_{50}) Alg-Chi-Ag NP NCs treated U87MG cells. The images in the lower panel **(a2-d2)** are corresponding bright field images. Flow cytometric analysis of MMP of **(e)** untreated and **(f)** treated with IC_{50} of Alg-Chi-Ag NP NCs.

5.4.11. Cell Cycle analysis

Excess oxidative stress is known to cause DNA damage, which if irreparable leads to apoptosis. To study the effect of Alg-Chi-Ag NP NCs on cell cycle, the cells were labelled with PI and analyzed by flow cytometry. The percentage distribution of cells in each phase of cell cycle for the untreated and treated cells is presented in **Figure 5.14**. Alg-Chi-Ag NPs at low concentration (0.5 IC_{50}) did not cause any notable change in cell cycle as compared to the untreated cells. However at IC_{50} and 2 IC_{50}, there was a marked increase in sub G0/G1 (apoptotic) population i.e. ~17 % and ~33 %, respectively with respect to control (~3 %). This was accompanied by decrease in percentage of cells in G1 phase for both these concentrations. Thus, the cell cycle data implicated possible DNA damage by Ag NPs resulting in apoptosis in treated cells.

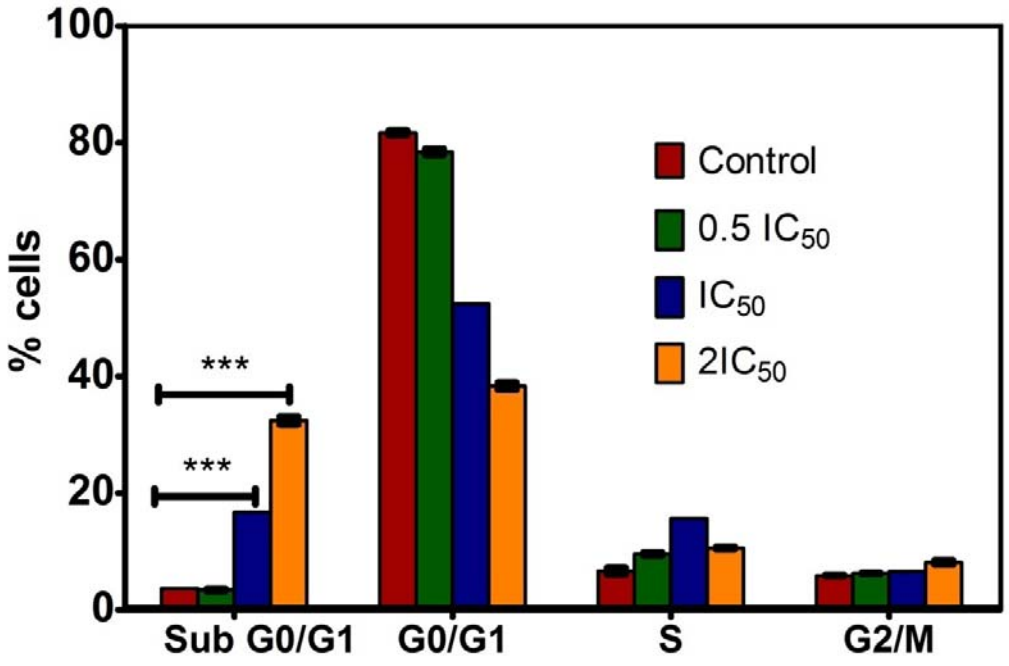

Figure 5.14. Effect of Alg-Chi-Ag NP NCs on cell cycle in U87MG cells evaluated by calculating the percentage of cells in each phase from flow cytometric data. The values are represented as mean ± SEM of three individual experiments. Statistical significance between untreated control and treated sample is denoted by *** ($p < 0.001$).

5.4.12. TUNEL Assay

TUNEL assay was performed to detect fragmented DNA, which is a hallmark of late apoptosis. A group of cysteine proteases, caspases are considered as the central executioners of apoptosis. Caspase-3 mediated activation of an endonuclease, also known as caspase-activated DNase (CAD), breaks the genomic DNA between nucleosomes to generate a series of DNA fragments of length corresponding to multiple integers of approximately 180 base pairs (Hengartner, 2000). In TUNEL assay, bromolated deoxyuridine triphosphates (Br-dUTPs) were added to the 3'-OH termini of broken DNA by deoxynucleotidyl transferase (TdT) enzyme. The incorporated nucleotides were then detected using FITC labelled anti-BrdU mAb in the flow cytometer. The results (**Figure 5.15.**) showed significant ~17 % TUNEL positive cells for IC_{50} Alg-Chi-Ag NP NCs treated cells, indicating presence of higher percentage of fragmented DNA as compared to untreated cells.

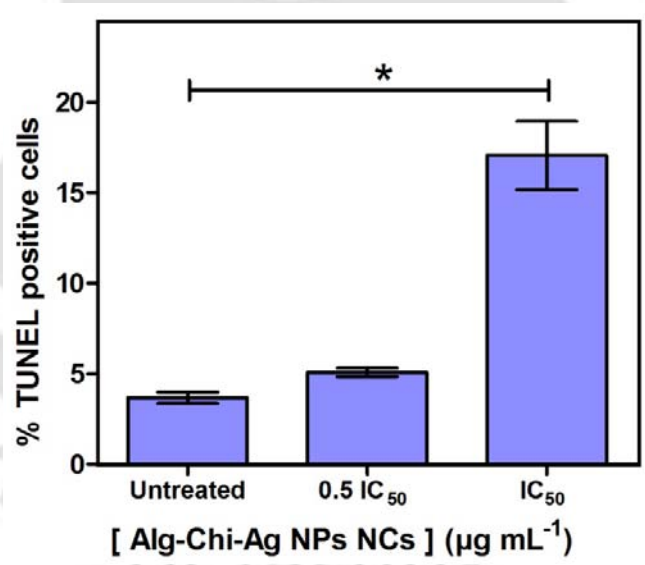

Figure 5.15. TUNEL assay to assess DNA fragmentation. The data were expressed as mean ± SEM of three independent experiments.

5.5. Conclusion

Alginate-chitosan blended NCs for Ag NPs having average size of about 315.1 nm were prepared in a completely 'green' method. The NCs were employed for successful delivery of Ag NPs in human glioblastoma U87MG cells. The Ag NPs confined within the biodegradable NCs were shown to induce apoptosis in cells at a very low concentration (2.4 μg mL^{-1} at IC_{50}) in comparison to previously reported data indicating superior efficacy of the present system. The apoptotic cell death indicated by dual staining and SEM studies was confirmed by TUNEL assay. Exposure to Alg-Chi-Ag NP NCs triggered ROS in cells causing mitochondrial dysfunction and DNA damage ultimately leading to apoptosis. The present study thus implicates possible application of alginate-chitosan blended NCs of Ag NPs in cancer cells for inducing programmed cell death at low concentration of Ag NPs thereby minimizing toxicity.

|Chapter 6|

Reversible Aggregation and Disaggregation of Alginate capped Silver Nanoparticles via Gel Formation

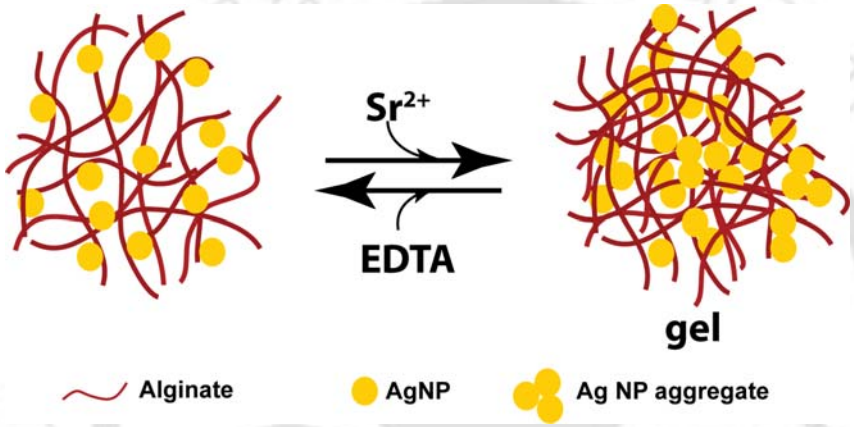

Chapter 6

REVERSIBLE AGGREGATION AND DISAGGREGATION OF ALGINATE CAPPED SILVER NANOPARTICLES VIA GEL FORMATION

6.1. Introduction

An important property of alginate significant for both its biological and industrial applications is that it forms gels in the presence of divalent cations such as Pb^{2+}, Cu^{2+} Cd^{2+}, Ba^{2+}, Ca^{2+}, Co^{2+}, Ni^{2+}, Zn^{2+} and Mn^{2+} with the exception of Mg^{2+} (Smidsrød and Haug, 1972; Smidsrød, 1974). Rees and co-workers have done pioneering work to understand the factors controlling the mechanism of gelation (Grant et al., 1973; Morris et al., 1978; Thom et al., 1982). The most widely accepted model for alginate gel formation is 'egg box' model in which each divalent cation is coordinated with the guluronic acid residues of two alginate chains thereby linking the two chains. Such crosslinking of polymer chains at multiple sites along the alginate backbone leads to an extended gel network.

Previously, studies have been pursued to assemble nanoparticles (NPs) from solution into monolayers and superlattice structures on solid surfaces as well as in solution itself. In this regard, first steps were taken by groups of Mirkin and Alivisatos who by means of hybridization of complementary base sequences of DNA demonstrated assembly of DNA-modified Au NPs into superstructures (Mirkin et al., 1996; Alivisatos et al., 1996; Storhoff and Mirkin, 1999; Storhoff et al., 2000). There are innumerable examples of irreversible aggregation of NPs in literature (Brust et al., 1995; Chen, 2000; Sharma et al., 2004; Mayya et al., 2000; Guan et al., 2009). However, reversible aggregation of NPs is difficult to achieve because of tendency of aggregated NPs to collapse and precipitate into larger insoluble materials although continuous efforts are being made in this direction (Templeton et al., 2000; Otsuka et al., 2001; Guarise et al, 2005; Shim and Gupta, 2007; Liu and Jiang, 2007). It is important to pursue investigations regarding reversible aggregation of functionalized

NPs as that would not only provide controllable aggregates of NPs – with tunable properties – but also may bring in newer understanding of interactions between molecules and NPs. However, there is plenty of opportunity to work in this area.

6.2. Outline of the Research Work

1) Alginate capped Ag NPs were subjected to aggregation as a result of gelation in alginate induced by strontium ions (Sr^{2+}).
2) Reversibility of aggregation of NPs was achieved by addition of ethylenediaminetetraacetic acid (EDTA), a known scavenger of Sr^{2+}.
3) The aggregation behaviour and its reversibility were studied by UV-Vis spectroscopy, transmission electron microscopy (TEM) and changes in hydrodynamic diameter and zeta potential values.

6.3. Experimental Section

6.3.1. Synthesis and characterization of Alginate capped Ag NPs (Alg-Ag NPs)

The synthesis and detailed characterization of Alg-Ag NPs have been described in Experimental Section in Chapter 4. Here 0.05 % (w/v) alginate solution and 10^{-4} M $AgNO_3$ were used.

6.3.2. *Reversible Aggregation and Disaggregation process*

The Alg-Ag NPs were centrifuged, redispersed in MilliQ water and sonicated briefly in an ultrasonic water bath (Allied Scientific Products) to disrupt any possible aggregates prior use for aggregation studies. To 1 mL of redispersed Alg-Ag NPs, 1 mL of strontium nitrate ($Sr\ NO_3$, Merck Limited, Mumbai, India) solution was added at room temperature to obtain different concentrations of Sr^{2+} ions. The samples were briefly shaken well followed by immediate recording of UV-Vis spectra at different time intervals using spectrophotometer (Lambda 25; Perkin-Elmer, Fremont, CA) till saturation was achieved in the spectra. At this point, ethylenediaminetetraacetic acid disodium salt (EDTA, Sisco Research Laboratories Pvt. Ltd., Mumbai, India) solution was added to the sample, the mixture was briefly shaken well and UV-Vis spectra were recorded at different time intervals. UV-Vis spectra of Alg-Ag NPs and Alg-Ag NPs mixed with EDTA were also recorded for control studies.

6.3.3 Transmission electron microscopy measurement

The morphology of NPs and aggregates was evaluated by TEM. For TEM, 5 µL of the sample was drop-cast onto a carbon-coated copper TEM grid which was subsequently air-dried. The drop-coated grid was analyzed by a high resolution transmission electron microscope (JEM 2100; Jeol, Peabody, MA, USA) operating at an accelerating voltage of 200 kV.

6.3.4. DLS measurement

The particle size and zeta potential of the samples were assessed on the Zeta Sizer Nano ZS90 (Malvern Instruments) by dynamic light scattering (DLS) measurements and laser Doppler electrophoresis, respectively. The analysis was performed at a scattering angle of 90º under 25 ºC.

6.4. Results and Discussion

6.4.1. Characterization of Alg-Ag NPs

The UV-Vis spectrum of redispersed Alg-Ag NPs showed peak at ~400 nm (**Figure 6.1a**). This indicated formation of Ag NPs, which have characteristic surface plasmon resonance peak at around 400 nm, depending on the particle sizes. TEM analysis, as is evident from **Figure 6.1b**, indicated that particles were spherical in shape with a narrow size distribution (**Figure 6.1c**). The average size of the NPs as calculated from TEM images was found to be 13.1 ± 2.31 nm

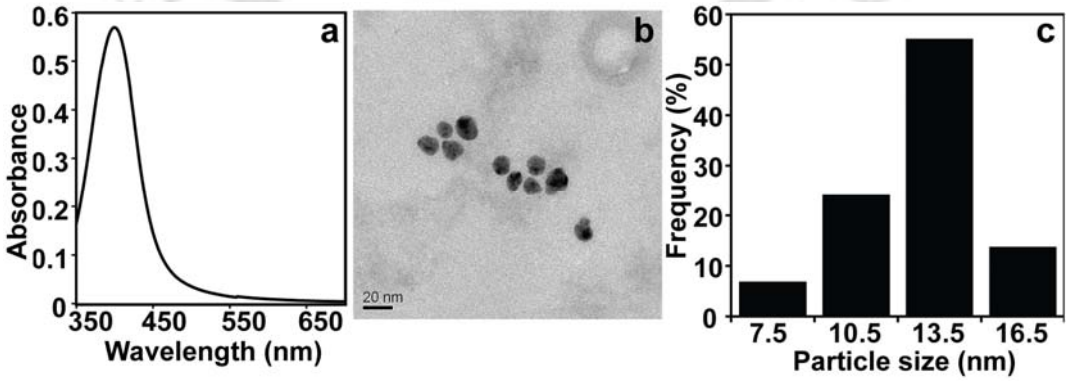

Figure 6.1. (a) UV-Vis spectrum, **(b)** representative TEM image and **(c)** particle size distribution of Alg-Ag NPs.

6.4.2. Reversible Aggregation and Disaggregation of Alg-Ag NPs

An aqueous dispersion of Alg-Ag NPs showed yellow colour, which is characteristic of the presence of Ag NPs. When different amounts of $SrNO_3$ solution were added to Alg-Ag NPs at room temperature, the colour of Alg-Ag NPs changed from yellow to dark yellow to orange within several minutes of Sr^{2+} addition. The intensity of the colour increased with increasing amounts of Sr^{2+}. On addition of EDTA, the colour of the solution was instantly restored to original yellow colour of Ag NPs. The representative cases of above phenomenon described by UV-Vis measurements, TEM studies and changes in hydrodynamic diameter and zeta potential values are discussed in detail below.

6.4.2.1. Case 1: Quantitatively, when 0.2 mM Sr^{2+} was added to 1 mL of Alg-Ag NPs, having an extinction value of 0.533 at 400 nm, the intensity of peak decreased slightly (to a value of 0.519) with broadening of spectrum (**Figure 6.2.**) indicating aggregation of NPs. Time dependent UV-Vis measurements showed that the lowering of intensity and broadening continued with time till 40 min after which there was no change in the spectra, indicating saturation in the observed effect. At this point, 5 mM EDTA solution was added to Alg-Ag NPs-Sr^{2+}. The normalized spectrum obtained after addition of EDTA to Alg-Ag NP- Sr^{2+} complex nearly overlapped well with that of original Alg-Ag NP solution indicating reversibility in aggregation behaviour of NPs (**Figure 6.3a**). The peak slightly blue shifted with respect to that of original Alg-Ag NPs. Similar blue shifting of the peak was also observed for control experiment with Alg-Ag NPs in presence of 5 mM EDTA (**Figure 6.3b**). This could be due to change in the surrounding environment of NPs. As mentioned before in Chapter 1, the surrounding environment of NPs affects the surface plasmon resonance of metal NPs (Kreibig et al., 1995).

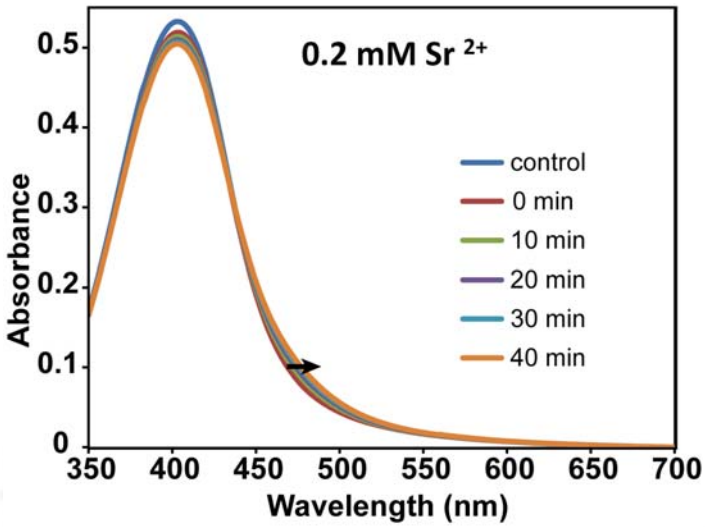

Figure 6.2. UV-Vis spectra of Alg-Ag NPs in presence of 0.2 mM Sr^{2+} at different time intervals. The arrow in the figure shows the increase in broadening of the spectra of Alg-Ag NPs-$Sr^{2+}$with time.

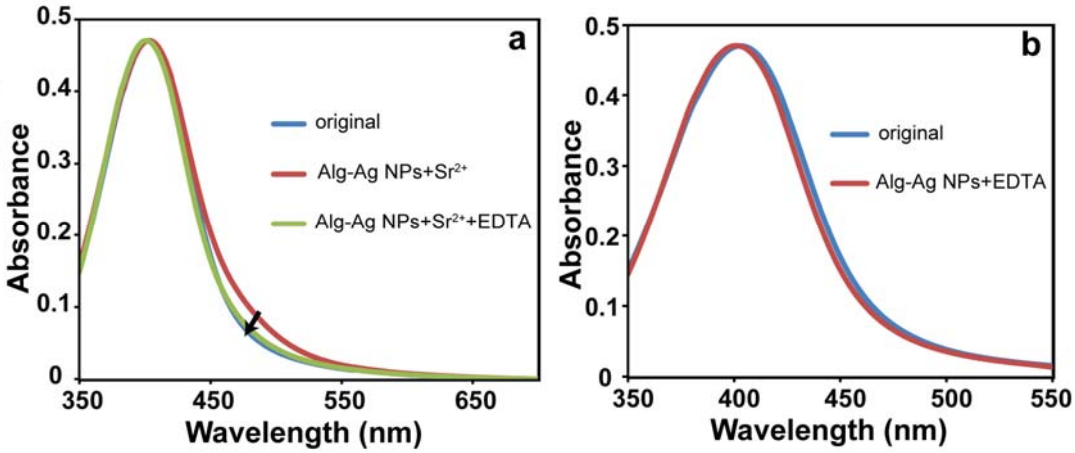

Figure 6.3. (a) Normalized UV-Vis spectra of original Alg-Ag NPs, Alg-Ag NPs-Sr^{2+} (Alg-Ag NPs treated with 0.2 mM Sr^{2+} for 40 min) and Alg-Ag NPs-Sr^{2+} to which 5 mM EDTA was added. The arrow in the figure shows reversal of direction of spectrum of Alg-Ag NP-Sr^{2+} after the addition of EDTA. **(b)** Normalized spectra of Alg-Ag NPs treated with 5 mM EDTA.

The spectroscopic observations correlated well with TEM studies which gave direct evidence of reversibility of aggregation process. The TEM image of Alg-Ag NPs showed well separated NPs (**Figure 6.4A1, 6.4A2**). On addition of 0.2 mM Sr^{2+}, the distance between Alg-Ag NPs decreased to form aggregates with no change in the size

and shape of the NPs (**Figure 6.4B1, 6.4B2**). This TEM sample corresponded to the sample kept for 40 min after addition of Sr^{2+}. On subsequent addition of EDTA, the particles that had come closer to form aggregates dispersed like that of control Alg-Ag NPs (**Figure 6.4C1, 6.4C2**).

The TEM results were further substantiated by DLS and zeta potential measurements. The hydrodynamic diameter of Alg-Ag NPs was 149.6 nm and zeta potential value was -55.7 mV. On addition of 0.2 mM Sr^{2+}, the hydrodynamic diameter decreased to 122.2 nm after 40 min. The zeta potential value also decreased to -23.2 mV. On addition of 5 mM EDTA, the hydrodynamic diameter changed to 69.03 nm and zeta potential value increased to -42.8 mV.

The above results can be explained as follows: In Alg-Ag NPs, the alginate chains were in extended stretched conformation due to repulsion between negatively charged carboxylic groups present in chains. As a result, alginate stabilized Ag NPs also remained separated due to electrostatic repulsion between them. In Alg-Ag NPs-Sr^{2+}, Sr^{2+} formed complex with carboxylic groups of alginate causing charge neutralization which led to folding and retracting of alginate chains, (Chen et al., 2006; 2007a) thereby bringing NPs close to each other causing aggregation. The folding of alginate chains and charge neutralization in Alg-Ag NPs-Sr^{2+} caused reduction in hydrodynamic diameter and zeta potential values, respectively, in comparison to original Alg-Ag NPs. EDTA being a strong chelating agent caused sequestration of alginate bound Sr^{2+} leading to unfolding of alginate chains due to electrostatic repulsion between negatively charged carboxylic acid groups The unfolding of alginate chains caused separation of aggregated Ag NPs.

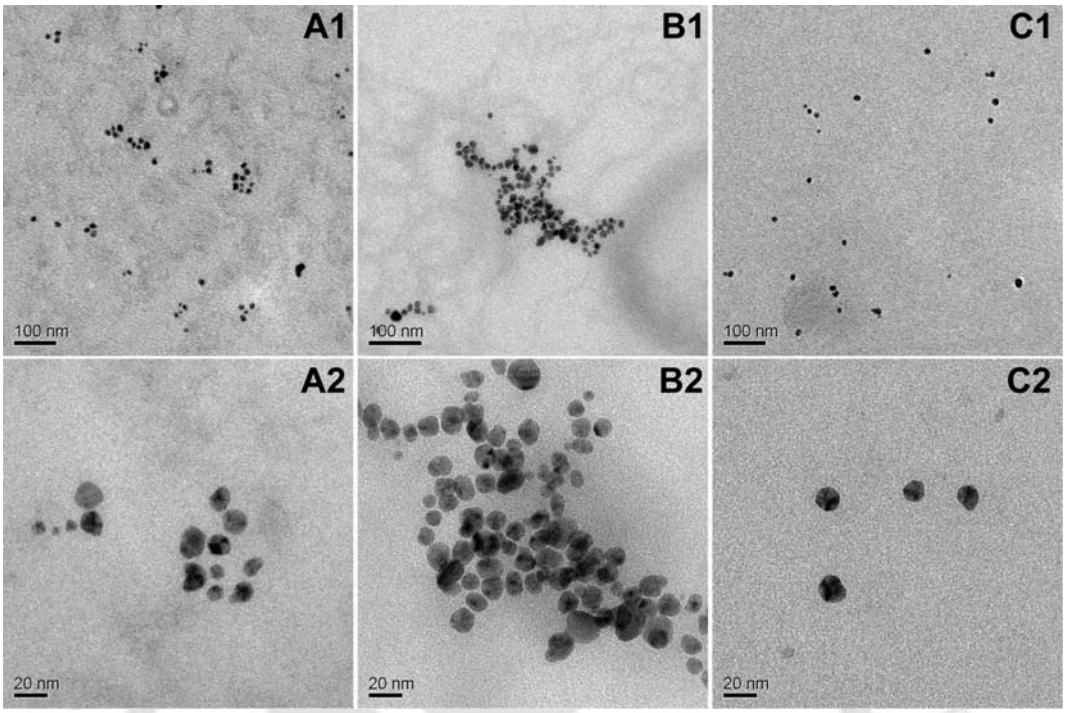

Figure 6.4. Representative TEM images of **(A1, A2)** Alg-Ag NPs, **(B1, B2)** Alg-Ag NPs-Sr^{2+} (Alg-Ag NPs treated with 0.2 mM Sr^{2+} for 40 min) and **(C1, C2)** Alg-Ag NPs-Sr^{2+} treated with 5 mM EDTA solution. Series 1 and 2 are low and high magnification images, respectively.

6.4.2.2. Case 2: At a higher concentration of Sr^{2+} i.e. 0.6 mM, the aggregation was more extensive marked by an appearance of a shoulder in long wavelength region, which continuously red shifted with time as indicated by time dependent UV-Vis measurements shown in **Figure 6.5a.** In this case, saturation occurred after 45 min. At this point when 10 mM EDTA solution was added, the normalized spectrum reversed its direction back but did not overlap with that of original Alg-Ag NPs (as in previous Case 1) even after 40 min incubation with EDTA solution (**Figure 6.5b**). This could be due to presence of small aggregates and fused NPs. The high concentration of Sr^{2+} used caused more gelation of alginate thereby bringing Ag NPs closer causing fusion of NPs.

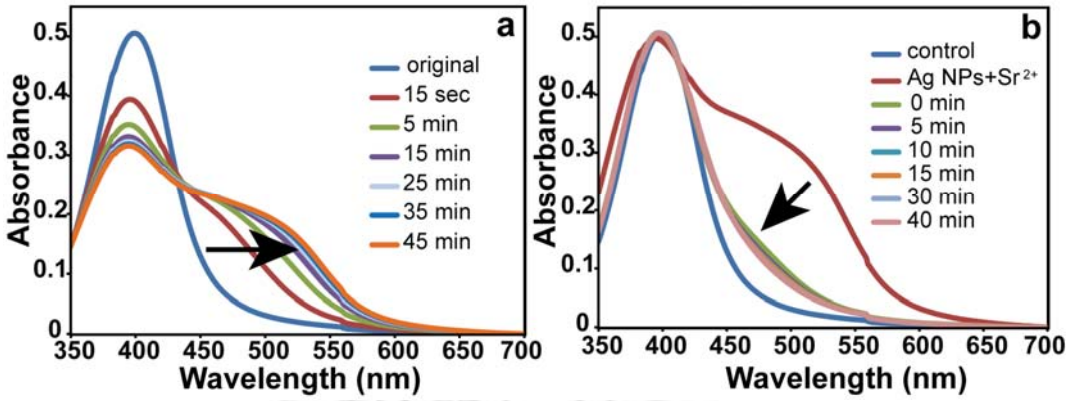

Figure 6.5. UV-Vis spectra of **(a)** Alg-Ag NPs in presence of 0.6 mM Sr^{2+} at different time intervals. The arrow in the figure shows the increase in red shifting of the shoulder of spectra of Alg-Ag NPs-Sr^{2+} with time. **(b)** Normalized UV-Vis spectra of original Alg-Ag NPs, Alg-Ag NPs-Sr^{2+} (Alg-Ag NPs treated with 0.6 mM Sr^{2+} for 45 min) and Alg-Ag NPs-Sr^{2+} to which 10 mM EDTA was added. The arrow in the figure shows reversal of direction of spectra of Alg-Ag NP-Sr^{2+} after the addition of EDTA at different time intervals.

Table 6.1. Time-dependent changes in hydrodynamic diameter after addition of 0.6 mM Sr^{2+} to Alg-Ag NPs.

	Z_{avg} (nm)
Alg-Ag NPs	125.1
Sr^{2+} addition	
5 min	43.97
10 min	50.03
15 min	53.98
20 min	58.38
25 min	60.69
30 min	63.58
35 min	68.48
40 min	71.67
45 min	71.89

The corresponding changes in hydrodynamic diameters and zeta potential values were also measured. **Table 6.1.** presents time-dependent changes in hydrodynamic

diameter values after addition of 0.6 mM Sr^{2+} to Alg-Ag NPs. When 0.6 mM Sr^{2+} was added to Alg-Ag NPs having hydrodynamic diameter 125.1 nm and zeta potential value -54.9 mV, the hydrodynamic diameter and zeta potential changed to 71. 9 nm and -13.7 mV, respectively after 45 min when saturation in change (in the UV-Vis spectrum) occurred. At this point, on addition of 10 mM EDTA solution, the hydrodynamic diameter decreased to 42.5 nm and zeta potential increased to -40.9 mV. The hydrodynamic diameter and zeta potential values for control Alg-Ag NPs treated with 10 mM EDTA for 45 min were 58.8 nm and -41.6 mV, respectively. The values of hydrodynamic diameter and zeta potential after addition of EDTA to Alg-Ag NPs-Sr^{2+} were almost similar to that of control Alg-Ag NPs treated with 10 mM EDTA.

To achieve complete reversibility of aggregation for Alg-Ag NPs treated with high concentration of 0.6 mM Sr^{2+}, the Alg-Ag NPs were incubated with 0.6 mM Sr^{2+} for short time i.e. 10 min. At this point, when 10 mM EDTA was added to Alg-Ag NPs-Sr^{2+}, near complete reversibility of aggregation of NPs was observed as indicated by **Figure 6.6**. As with the previous case, this was also supported by TEM images shown in **Figure 6.7**.

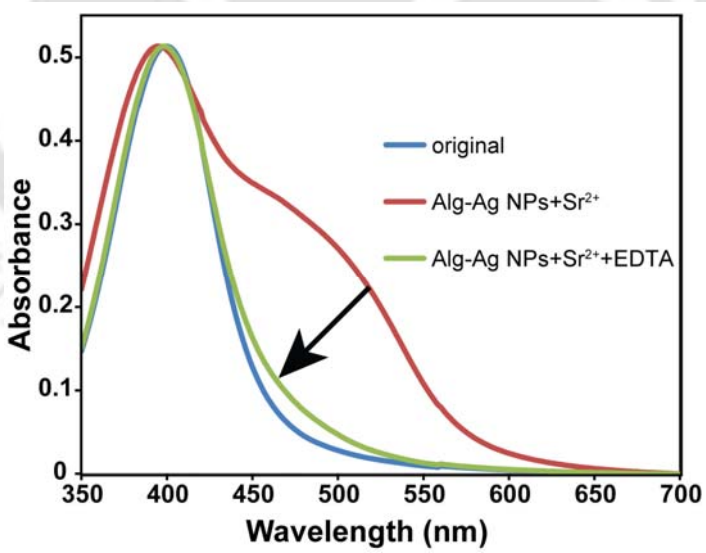

Figure 6.6. Normalized UV-Vis spectra of original Alg-Ag NPs, Alg-Ag NPs-Sr^{2+} (Alg-Ag NPs treated with 0.6 mM Sr^{2+} for 10 min) and Alg-Ag NPs-Sr^{2+} to which 10 mM EDTA was added. The arrow in the figure shows reversal of direction of spectrum of Alg-Ag NP-Sr^{2+} after the addition of EDTA.

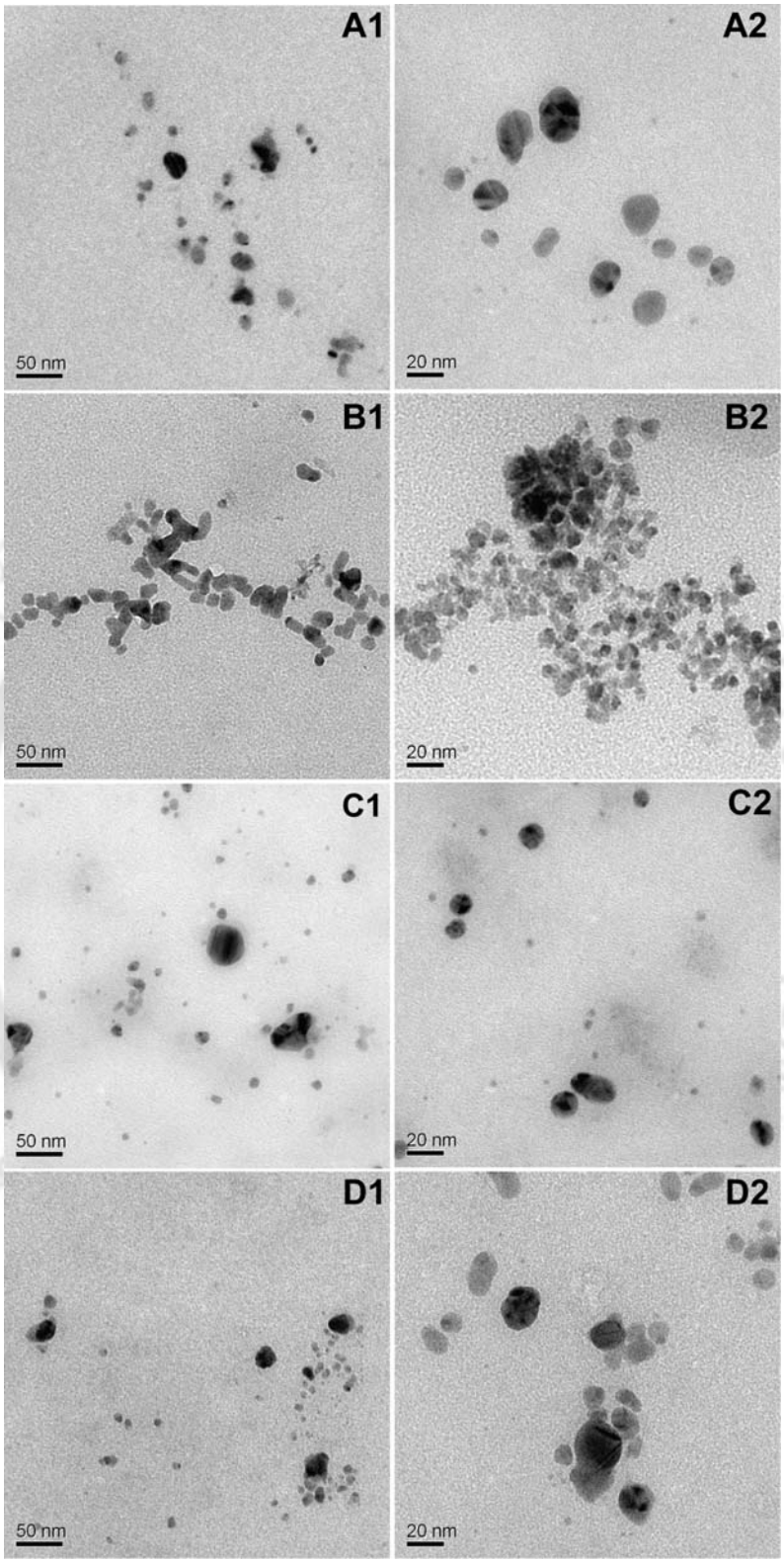

Figure 6.7. Representative TEM images of **(A1, A2)** Alg-Ag NPs, **(B1, B2)** Alg-Ag NPs-Sr^{2+} (Alg-Ag NPs treated with 0.6 mM Sr^{2+} for 10 min), **(C1, C2)** Alg-Ag NPs-Sr^{2+} treated with 10 mM EDTA solution and (**D1, D2**) Alg-Ag NPs treated with 10 mM EDTA. Series 1 and 2 are low and high magnification images, respectively.

6.5. Conclusion

The present study demonstrates a simple approach to obtain reversible aggregation and disaggregation of alginate capped Ag NPs at room temperature. The reversible aggregation behaviour of Alg-Ag NPs was controllable and reproducible. The concept and 'green' methodology developed in the present work can easily be extended to other metal NPs to prepare natural polymer-based biocompatible metal-aggregates at room temperature that can serve as useful surface enhanced Raman spectroscopy (SERS) substrates. Several studies have shown that aggregates of NPs are better substrates for SERS applications than individual NPs due to the enhancement of the electric field between the particles in the aggregates. (Kneipp et al., 1997; Kneipp et al., 1998; Nikoobakht and El-Sayed, 2003; Schwartzberg et al., 2004; Faulds et al., 2004; Sun et al., 2011).

|Chapter 7|

Concluding Remarks and Future Prospects

Chapter 7

CONCLUDING REMARKS AND FUTURE PROSPECTS

The main focus of the present dissertation has been to develop novel nanomaterials in the form of metal nanoparticles (NPs) and their nanocomposites with biofriendly polymers and understand their interaction with biological systems with an aim of pursuing their therapeutic implications.

The research work presented herein began with our interest to understand the effect of gold on the antibacterial property of silver since gold is known to be nontoxic to bacteria. A suitable way to pursue this was to investigate antibacterial property of bimetallic NPs containing both gold and silver. This was further motivated by the unexplored therapeutic potential of bimetallic NPs, which are increasingly being used in the fields of sensing, optoelectronics and catalysis. Our results showed that the antibacterial efficacy of silver was significantly enhanced in the presence of gold even though the size of core-shell NP was large (~30 nm). The core shell NPs killed both Gram positive and Gram negative bacteria at low silver concentrations in comparison to similar sized Ag NP alone. The enhanced antibacterial property of bimetallic gold silver core-shell NPs can be explored further in conjunction with bio-friendly polymers for effective antimicrobial therapy.

Next, we investigated antibacterial efficacy of Ag NPs contained in chitosan nanocarrier (NC), which was previously developed in our laboratory and shown to induce apoptosis in human colon cancer cells. The results demonstrated synergistic effect of both chitosan NPs and Ag NPs leading to elevated antibacterial property of the nanocomposite in comparison to either chitosan NPs or Ag NPs alone at their respective concentrations. With the NC, the antibacterial tests could be easily performed in bacterial medium pH (~7.2), unlike chitosan that precipitates at this pH. The nanocomposite was found to be effective against both Gram positive and Gram negative bacteria. Our findings suggest the possibility of using this nanocomposite as an efficient antibacterial agent in various biomedical and therapeutic applications.

Further, in our pursuit to develop novel methods of 'green' synthesis of Ag NPs for biological applications, we synthesized Ag NPs using a natural biopolymer sodium alginate as both reducing agent and stabilizer. The method developed was completely 'green' and can easily be extended to prepare other biocompatible metal NPs. The synthesized alginate stabilized Ag NPs (Alg-Ag NPs) were demonstrated to be antibacterial against both Gram positive and Gram negative bacteria, and hence were subsequently used for developing antibacterial film for practical applications like food packaging materials, wound dressings and grafts onto various implants. The film was fabricated by blending Alg-Ag NPs with chitosan which formed polyelectrolyte complex that was cast into stable films with improved mechanical properties. The incorporation of Ag NPs in polymer matrix i.e. in the form of film has the dual advantages of both macroscopic and nanoscale components being together. The film can be handled easily and at the same time, the bactericidal property of Ag NPs can be fully exploited. In future, other biocompatible metal NPs can be prepared by our 'green' method which can be subsequently used for fabrication of films for various practical purposes.

The methodology developed in the above study was subsequently used to synthesize biodegradable alginate-chitosan based NC system of Ag NPs (Alg-Chi-Ag NPs NC). The Alg-Chi-Ag NPs NC was shown to induce apoptosis in refractory U87MG cells at very low concentration of Ag NPs, with IC_{50} value of Ag NPs being 2.4 μg mL^{-1}, which is far below than previously reported values. The molecular mechanism of cytotoxicity was also investigated, which revealed involvement of oxidative stress that caused mitochondrial dysfunction and DNA damage leading to apoptosis in treated cells. In future, the present NC can suitably be functionalized with appropriate cancer cell specific markers in order to achieve 'active targeting' towards cancer cells. Further, it can be used as such or after appropriate functionalization, in animal models to test its efficacy of inducing apoptosis *in vivo*. These studies could open up new strategies for cancer treatment. Furthermore, the method developed in the present study can also be used to prepare NC system of other NPs.

Finally, we were successful in achieving reversibility in aggregation behaviour of NPs, which is an intriguing area of research. Our methodology took advantage of gel forming ability of alginate in presence of divalent cations. The Alg-Ag NPs came together on formation of alginate gel and got separated with breaking of gel. This study leaves plenty of scope to achieve reversible aggregation behaviour of other NPs in a

simple and controlled manner. The aggregates generated in the present study can be pursued as substrates for surface enhanced Raman spectroscopy. Further work in this area will contribute to the fundamental understanding of interactions between molecules and NPs.

REFERENCES

Agnihotri, S.A., Mallikarjuna, N.N. & Aminabhavi, T.M. Recent advances on chitosan based micro and nanoparticles in drug delivery. *Journal of Controlled Release* **100**, 5–28 (2004).

Alivisatos, A.P., Johnsson, K.P., Peng, X., Wilson, T.E., Loweth, C.J., Bruchez, M.P., Jr. & Schultz, P.G. Organization of 'nanocrystal molecules' using DNA. *Nature* **382**, 609-611 (1996).

Allemann, E., Leroux, J.C. & Gurny, R. Polymeric nano and microparticles for the oral delivery of peptides and peptidomimetics. *Advanced Drug Delivery Reviews* **34**, 171–189 (1998).

Alsberg, E., Anderson, K.W., Albeiruti, A., Rowley, J.A. & Mooney, D.J. Engineering growing tissues. *Proceedings of the National Academy of Sciences* **99**, 12025–12030 (2002).

Amidi, M., Mastrobattista, E., Jiskoot, W. & Hennink, W.E. Chitosan based delivery systems for protein therapeutics and antigens. *Advanced Drug Delivery Reviews* **62**, 59–82 (2010).

Anal, A.K., Bhopatkar, D., Tokura, S., Tamura, H. & Stevens, W.F. Chitosan-Alginate Multilayer Beads for Gastric Passage and Controlled Intestinal Release of Protein *Drug Development and Industrial Pharmacy* **29**, 713-724 (2003).

Anitha, A., Rani, V.V.D., Krishna, R., Sreeja, V., Selvamurugan, N., Nair, S.V., Tamura, H., & Jayakumar, R. Synthesis, characterization, cytotoxicity and antibacterial studies of chitosan, O-carboxymethyl and N,O-carboxymethyl chitosan nanoparticles. *Carbohydrate Polymers* **78**, 672–677 (2009).

Arora, S., Jain, J., Rajwade, J.M. & Paknikar, K.M. Cellular responses induced by silver nanoparticles: *in vitro* studies. *Toxicology Letters* **179**, 93–100 (2008).

Arosio, D., Manzoni, L., Araldi, E.M.V. & Scolastico, C. Cyclic RGD functionalized gold nanoparticles for tumor targeting. *Bioconjugate Chemistry* **22**, 664–672 (2011).

Artursson, P., Lindmark, T., Davis, S.S. & Illum, L. Effect of chitosan on the permeability of monolayers of intestinal epithelial cells (Caco-2). *Pharmaceutical Research* **11** 1358–1361 (1994).

Asharani, P.V., Wu, Y.L., Gong, Z. & Valiyaveettil, S. Toxicity of silver nanoparticles in zebrafish models. *Nanotechnology* **19**, 255102-255109 (2008),

AshaRani, P.V., Mun, G.L.K., Hande, M.P. & Valiyaveettil, S. Cytotoxicity and genotoxicity of silver nanoparticles in human cells. *ACS Nano* **3**, 279-290 (2009).

Baker, C., Pradhan, A., Pakstis, L., Pochan, D.J. & Shah, S.I. Synthesis and antibacterial properties of silver nanoparticles. *Journal of Nanoscience and Nanotechnology* **5**, 244–249 (2005).

Balakrishnan, B., Mohanty, M., Fernandez, A.C., Mohanan, P.V. & Jayakrishnan, A. Evaluation of the effect of incorporation of dibutyryl cyclic adenosine monophosphate in an in situ forming hydrogel wound dressing based on oxidized alginate and gelatin. *Biomaterials* **27**, 1355–1361 (2006).

Banerjee, M., Mallick, S., Paul, A., Chattopadhyay, A. & Ghosh, S.S. Heightened reactive oxygen species generation in the antimicrobial activity of a three component iodinated chitosan silver nanoparticle composite. *Langmuir* **26**, 5901–5908 (2010).

Banerjee, M., Sharma, S., Chattopadhyay, A. & Ghosh, S.S. Enhanced antibacterial activity of bimetallic gold-silver core-shell nanoparticles at low silver concentration. *Nanoscale* **3**, 5120-5125 (2011).

Baram Pinto, D., Shukla, S., Perkas, N., Gedanken, A. & Sarid, R. Inhibition of Herpes Simplex virus type 1 infection by silver nanoparticles capped with mercaptoethane sulfonate. *Bioconjugate Chemistry* **20**, 1497–1502 (2009).

Basmanav, F.B., Kose, G.T. & Hasirci, V. Sequential growth factor delivery from complexed microspheres for bone tissue engineering. *Biomaterials* **29**, 4195–4204 (2008).

Berger, J., Reist, M., Mayer, J.M., Felt, O., Peppas, N.A. & Gurny, R. Structure and interactions in covalently and ionically cross-linked chitosan hydrogels for biomedical applications. *European Journal of Pharmaceutics and Biopharmaceutics* **57**, 19–34 (2004).

Bhumkar, D.R., Joshi, H.M., Sastry, M. & Pokharkar, V.B. Chitosan reduced gold nanoparticles as novel carriers for transmucosal delivery of insulin. *Pharmaceutical Research* **24**, 1415–1426 (2007).

Borchard, G., Luessen, H.L., Boer, A.G., Verhoef, J.C., Lehr, C.M. & Junginger, H.E. The potential of mucoadhesive polymers in enhancing intestinal peptide drug absorption. III: Effects of chitosan–glutamate and carbomer on epithelial tight junctions in vitro. *Journal of Controlled Release* **39**, 131–138 (1996).

Borselli, C., Storrie, H., Lee, F.B., Shvartsman, D., Cezar, C., Lichtman, J.W., Vandenburgh, H.H. & Mooney, D.J. Functional muscle regeneration with combined delivery of angiogenesis and myogenesis factors. *Proceedings of the National Academy of Sciences* **107**, 3287–3292 (2009).

Bouhadir, K.H., Alsberg, E. & Mooney, D.J. Hydrogels for combination delivery of antineoplastic agents. *Biomaterials* **22**, 2625–2633 (2001).

Božanić, D.K., Branković, S.D., Bibić, N., Luyt, A. S. & Djoković, V. Silver nanoparticles encapsulated in glycogen biopolymer: Morphology, optical and antimicrobial properties. *Carbohydrate Polymers* **83**, 883–890 (2011).

Brust, M., Bethell, D., Schiffrin, D.J.& Kiely, C.J. Novel gold dithiol nano networks with non-metallic electronic properties. *Advanced Materials* **7**, 795-799 (1995).

Calafiore, R. Alginate microcapsules for pancreatic islet cell graft immunoprotection: struggle and progress towards the final cure for type 1 diabetes mellitus. *Expert Opinion on Biological Therapy* **3**, 201–205 (2003).

Cao, Y.W., Jin, R. & Mirkin, C.A. DNA modified core shell Ag/Au nanoparticles. *Journal of the American Chemical Society* **123**, 7961–7962 (2001).

Carlson, C., Hussain, S.M., Schrand, A.M., Braydich-Stolle, L.K., Hess, K.L., Jones, R.L., & Schlager, J.J. Unique cellular interaction of silver nanoparticles: Size dependent generation of reactive oxygen species. *The Journal of Physical Chemistry B* **112**, 13608–13619 (2008).

Caruso, E.B., Petralia, S., Conoci, S., Giuffrida, S. & Sortino, S. Photodelivery of nitric oxide from water soluble platinum nanoparticles. *Journal of the American Chemical Society* **129**, 480–481 (2007).

Castilho, L.R. Animal cell technology: From biopharmaceuticals to gene therapy. New York : Taylor & Francis, (2008).

Castino, R., Pucer, A., Veneroni, R., Morani, F., Peracchio, C., Lah, T.T., & Isidoro, C. Resveratrol reduces the invasive growth and promotes the acquisition of a long-lasting differentiated phenotype in human glioblastoma cells. *Journal of Agricultural and Food Chemistry* **59**, 4264–4272 (2011).

Chaloupka, K., Malam, Y. & Seifalian, A.M. Nanosilver as a new generation of nanoproduct in biomedical applications. *Trends in Biotechnology* **28**, 580–588 (2010).

Chan, A.W. & Neufeld, R.J. Tunable semi-synthetic network alginate for absorptive encapsulation and controlled release of protein therapeutics. *Biomaterials* **31**, 9040–9047 (2010).

Chandran, S.P., Ghatak, J., Satyam, P.V. & Sastry, M. Interfacial deposition of Ag on Au seeds leading to Au core Ag shell in organic media. *Journal of Colloid and Interface Science* **312**, 498–505 (2007).

Chávez de Paz, L.E., Resin, A., Howard, K.A., Sutherland, D.S. & Wejse, P.L. Antimicrobial effect of chitosan nanoparticles on *Streptococcus mutans* biofilms. *Applied and Environmental Microbiology* **77**, 3892–3895 (2011).

Chen, J., Wiley, B., Li, Z.Y., Campbell, D., Saeki, F., Cang, H., Au, L., Lee, J., Li, X. & Xie, Y. Gold nanocages: Engineering their structure for biomedical applications. *Advanced Materials* **17**, 2255-2261 (2005).

Chen, K.L., Mylon, S.E. & Elimelech, M. Aggregation kinetics of alginate coated hematite nanoparticles in monovalent and divalent electrolytes. *Environmental. Science and Technology* **40**, 1516-1523 (2006).

Chen, K.L., Mylon, S.E. & Elimelech, M. Enhanced aggregation of alginate coated iron oxide (hematite) nanoparticles in the presence of calcium, strontium, and barium cations. *Langmuir* **23**, 5920-5928 (2007a).

Chen, L., Tian, Z. & Du, Y. Synthesis and pH sensitivity of carboxymethyl chitosan-based polyampholyte hydrogels for protein carrier matrices. *Biomaterials* **25**, 3725-3732 (2003).

Chen, Y.H., Tsai, C.Y., Huang, P.Y., Chang, M.Y., Cheng, P.C., Chou, C.H., Chen, D.H., Wang, C.R., Shiau, A.L., & Wu, C.L. Methotrexate conjugated to gold nanoparticles inhibits tumor growth in a syngeneic lung tumor model. *Molecular Pharmaceutics* **4**, 713–722 (2007b).

Chou, K.S. & Lai, Y.S. Effect of polyvinyl pyrrolidone molecular weights on the formation of nanosized silver colloids. *Materials Chemistry and Physics* **83**, 82–88 (2004).

Chueh, B., Zheng, Y., Torisawa, Y., Hsiao, A.Y., Ge, C., Hsiong, S., Huebsch, N., Franceschi, R., Mooney, D.J. & Takayama, S. Patterning alginate hydrogels using light-directed release of caged calcium in a microfluidic device. *Biomedical Microdevices* **12**, 145–151 (2009).

Chung, Y.C., Su, Y.P. Chen, C.C. Jia, G., Wang, H.L., Wu, J.C.G. & Lin, J.G. Relationship between antibacterial activity of chitosan and surface characteristics of cell wall. *Acta Pharmacologica Sinica* **25**, 932-936 (2004).

Cioffi, N., Torsi, L., Ditaranto, N., Tantillo, G., Ghibelli, L., Sabbatini, L., Bleve-Zacheo, T., D'Alessio, M., Zambonin, P.G., & Traversa, E. Copper nanoparticle/polymer composites with antifungal and bacteriostatic properties. *Chemistry of Materials* **17**, 5255–5262 (2005).

Cossarizza, A., Baccaranicontri, M., Kalashnikova, G. & Franceschi, C. A new method for the cytofluorometric analysis of mitochondrial membrane potential using the J-aggregate forming lipophilic cation 5,5′,6,6′-Tetrachloro-1,1′,3,3′-tetraethylbenzimidazolcarbocyanine Iodide (JC-1). *Biochemical and Biophysical Research Communications* **197**, 40–45 (1993).

Cui, Y., Ren, B., Yao, J.L., Gu, R.A. & Tian, Z.Q. Synthesis of Ag core Au shell bimetallic nanoparticles for immunoassay based on surface-enhanced Raman spectroscopy. *The Journal of Physical Chemistry B* **110**, 4002–4006 (2006).

Dankovich, T.A. & Gray, D.G. Bactericidal paper impregnated with silver nanoparticles for point-of-use water treatment. *Environmental Science & Technology* **45**, 1992–1998 (2011).

Davies, D.H., Elson, C.M. & Hayes, E.R. In *Chitin and Chitosan*, (Eds Skjak-Braek, G., Anthonsen, T., Sandford, P.) Elsevier Applied Science: London, 1989, 467−472.

Davis, T.A., Volesky, B. & Mucci, A. A review of the biochemistry of heavy metal biosorption by brown algae. *Water Research* **37**, 4311–4330 (2003).

Ding, W., Lian, Q., Samuels, R. & Polk, M. Synthesis and characterization of a novel derivative of chitosan. *Polymer* **44**, 547–556 (2003).

Dodane, V. & Vilivalam, V.D. Pharmaceutical applications of chitosan. *Pharmaceutical Science & Technology Today* **1**, 246–253 (1998).

Dreis, S., Rothweiler, F., Michaelis, M., Cinatljr, J., Kreuter, J. & Langer, K. Preparation, characterisation and maintenance of drug efficacy of doxorubicin-loaded human serum albumin (HSA) nanoparticles. *International Journal of Pharmaceutics* **341**, 207–214 (2007).

Du, W.L., Niu, S.S., Xu, Y.L., Xu, Z.R. & Fan, C.L. Antibacterial activity of chitosan tripolyphosphate nanoparticles loaded with various metal ions. *Carbohydrate Polymers* **75**, 385–389 (2009).

Dubas, S.T., Wacharanad, S. & Potiyaraj, P. Tunning of the antimicrobial activity of surgical sutures coated with silver nanoparticles. *Colloids and Surfaces A: Physicochemical and Engineering Aspects* **380**, 25–28 (2011).

Dvir Ginzberg, M., Gamlieli Bonshtein, I., Agbaria, R. & Cohen, S. Liver tissue engineering within alginate scaffolds: Effects of cell-seeding density on hepatocyte viability, morphology, and function. *Tissue Engineering* **9**, 757–766 (2003).

El Sayed, I.H., Huang, X. & El Sayed, M.A. Selective laser photo thermal therapy of epithelial carcinoma using anti-EGFR antibody conjugated gold nanoparticles. *Cancer Letters* **239**, 129-135 (2006).

Elghanian, R., Storhoff, J.J., Mucic, R.C., Letsinger, R.L. & Mirkin, C.A. Selective colorimetric detection of polynucleotides based on the distance dependent optical properties of gold nanoparticles. *Science* **277**, 1078–1081 (1997).

Esteban Cubillo, A., Pecharromán, C., Aguilar, E., Santarén, J. & Moya, J.S. Antibacterial activity of copper monodispersed nanoparticles into sepiolite. *Journal of Materials Science* **41**, 5208–5212 (2006).

Falentin Daudré, C., Faure, E., Svaldo Lanero, T., Farina, F., Jérôme, C., Van De Weerdt, C., Martial, J., Duwez, A.S., & Detrembleur, C. Antibacterial polyelectrolyte micelles for coating stainless steel. *Langmuir* **28**, 7233–7241 (2012).

Faraday, M. The Bakerian Lecture: Experimental relations of gold (and other metals) to light. *Philosophical Transactions of the Royal Society of London* **147**, 145–181 (1857).

Faulds, K., Littleford, R.E., Graham, D., Dent, G. & Smith, W.E. Comparison of surface-enhanced resonance Raman scattering from unaggregated and aggregated nanoparticles. *Analytical Chemistry* **76**, 592–598 (2004).

Ferrer, D., Torres-Castro, A., Gao, X., Sepúlveda Guzmán, S., Ortiz Méndez, U. & José Yacamán, M. Three layer core/shell structure in Au Pd bimetallic nanoparticles. *Nano Letters* **7**, 1701–1705 (2007).

Ferrer, D.A., Torres, L.A.D., Wu, S. & Yacaman, M. J. Crystalline order of silver gold nanocatalysts with hollow core and alloyed shell. *Catalysis Today* **147**, 211–216 (2009).

Finotelli, P.V., Da Silva, D., Penna, M.S., Rossi, A.M., Farina, M., Andrade, L.R., Takeuchi, A.Y., & Leão, M.H.R. Microcapsules of alginate/chitosan containing magnetic nanoparticles for controlled release of insulin. *Colloids and Surfaces B: Biointerfaces* **81**, 206–211 (2010).

Fischbach, C., Kong, H.J., Hsiong, S.X., Evangelista, M.B., Yuen, W., & Mooney, D.J. Cancer cell angiogenic capability is regulated by 3D culture and integrin engagement. *Proceedings of the National Academy of Sciences* **106**, 399–404 (2009).

Foster, L. J. R. & Butt, J. Chitosan films are not antimicrobial. *Biotechnology Letters* **33**, 417–421 (2010).

Fox, C. L., Jr. Silver sulfadiazine: a new topical therapy for Pseudomonas in burns. Therapy of *pseudomonas* infection in burns. *Archives of Surgery* **96**, 184–188 (1968).

Franco-Molina, M.A., Gamboa, E.M., Rivera, C.A.S., Flores, R.A.G., Benavides, P.Z., Tello, P.C., González, J.A., Hernández, D.F.M., Guerra, R.S.T., & Padilla, C.R. Antitumor activity of colloidal silver on MCF-7 human breast cancer cells. *Journal of Experimental & Clinical Cancer Research* **29**, 148 (2010).

Freeman, R.G., Hommer, M.B., Grabar, K.C., Jackson, M.A. & Natan, M.J. Ag clad Au nanoparticles: Novel aggregation, optical, and surface-enhanced Raman scattering properties. *The Journal of Physical Chemistry* **100**, 718–724 (1996).

Frens G. Controlled nucleation for the regulation of the particle size in monodisperse gold solutions. *Nature Physical Science* **241**, 20-22 (1973).

Fuente, J.M. & Berry, C.C. Tat peptide as an efficient molecule to translocate gold nanoparticles into the cell nucleus. *Bioconjugate Chemistry* **16**, 1176–1180 (2005).

Gao, X. & Huang, L. Potentiation of cationic liposome mediated gene delivery by polycations. *Biochemistry* **35**, 1027–1036 (1996).

Gao, J., Liang, G., Zhang, B., Kuang, Y., Zhang, X., & Xu, B. FePt@CoS_2 yolk shell nanocrystals as a potent agent to kill HeLa cells. *Journal of the American Chemical Society* **129**, 1428–1433 (2007).

George, M. & Abraham, T.E. Polyionic hydrocolloids for the intestinal delivery of protein drugs: Alginate and Chitosan-a review. *Journal of Controlled Release* **114**, 1–14 (2006).

Gogoi, S.K., Gopinath, P., Paul, A., Ramesh, A., Ghosh, S.S., & Chattopadhyay, A. Green fluorescent protein expressing *Escherichia coli* as a model system for investigating the antimicrobial activities of silver nanoparticles. *Langmuir* **22**, 9322–9328 (2006).

Gok, C. & Aytas, S. Biosorption of uranium(VI) from aqueous solution using calcium alginate beads. *Journal of Hazardous Materials* **168**, 369–375 (2009).

Gong, P., Li, H.M., He, X.X., Wang, K.M., Hu, J.B., Tan, W.H., Zhang, S.C. & Yang, X. H. Preparation and antibacterial activity of Fe_3O_4@Ag nanoparticles. *Nanotechnology* **18**, 285604 (2007).

Gopinath, P., Gogoi, S.K., Chattopadhyay, A. & Ghosh, S.S. Implications of silver nanoparticle induced cell apoptosis for *in vitro* gene therapy. *Nanotechnology* **19**, 75104-75114 (2008).

Gopinath, P., Gogoi, S.K., Sanpui, P., Paul, A., Chattopadhyay, A. & Ghosh, S.S. Signaling gene cascade in silver nanoparticle induced apoptosis. *Colloid Surface B: Biointerface* **77**, 240–245 (2010).

Goycoolea, F.M., Lollo, G., Remuñán López, C., Quaglia, F. & Alonso, M. J. Chitosan alginate blended nanoparticles as carriers for the transmucosal delivery of macromolecules. *Biomacromolecules* **10**, 1736–1743 (2009).

Grant, G.T., Morris, E.R., Rees, D.A., Smith, P.J.C. & Thom, D. Biological interaction between polysaccharides and divalent cation: the egg-box model. *FEBS Letters* **32**, 195–198 (1973).

Guan, J., Li, J., Guo, Y. & Yang, W. Cooperative dual stimuli triggered aggregation of Poly-l-Histidine functionalized Au Nanoparticles. *Langmuir* **25**, 2679–2683 (2009).

Guarise, C., Pasquato, L. & Scrimin, P. Reversible aggregation/deaggregation of gold nanoparticles induced by a cleavable dithiol linker. *Langmuir* **21**, 5537-5541 (2005).

Guibal, E., Von Offenberg Sweeney, N., Zikan, M.C., Vincent, T. & Tobin, J.M. Competitive sorption of platinum and palladium on chitosan derivatives. *International Journal of Biological Macromolecules* **28**, 401–408 (2001).

Haes, A. & Duyne, R. A unified view of propagating and localized surface plasmon resonance biosensors. *Analytical and Bioanalytical Chemistry* **379**, 920–930 (2004).

Han, G., Chari, N.S., Verma, A., Hong, R., Martin, C.T. & Rotello, V.M. Controlled recovery of the transcription of nanoparticle bound DNA by intracellular concentrations of glutathione. *Bioconjugate Chemistry* **16**, 1356–1359 (2005).

Han, G., Martin, C.T. & Rotello, V.M. Stability of gold nanoparticle bound DNA toward biological, physical, and chemical agents. *Chemical Biology and Drug Design* **67**, 78–82 (2006a).

Han, G., You, C. C., Kim, B., Turingan, R.S., Forbes, N.S., Martin, C.T. & Rotello, V.M. Light-regulated release of DNA and its delivery to nuclei by means of photolabile gold nanoparticles. *Angewandte Chemie International Edition* **45**, 3165–3169 (2006b).

Hans, M. & Lowman, A. Biodegradable nanoparticles for drug delivery and targeting. *Current Opinion in Solid State and Materials Science* **6**, 319–327 (2002).

He, J., Kunitake, T. & Nakao, A. Facile in situ synthesis of noble metal nanoparticles in porous cellulose fibers. *Chemistry of Materials* **15**, 4401–4406 (2003).

Hegde, M., Roscoe, J., Cala, P. & Gorin, F. Amiloride kills malignant glioma cells independent of its inhibition of the sodium-hydrogen exchanger. *Journal of Pharmacology and Experimental Therapeutics* **310**, 67–74 (2004).

Hejazi, R. & Amiji, M. Chitosan based gastrointestinal delivery systems. *Journal of Controlled Release* **89**, 151–165 (2003).

Helander, I.M., Nurmiaho Lassila, E.L., Ahvenainen, R., Rhoades, J. & Roller, S. Chitosan disrupts the barrier properties of the outer membrane of Gram negative bacteria. *International Journal of Food Microbiology* **71**, 235–244 (2001).

Hengartner, M.O. The biochemistry of apoptosis. *Nature* **407**, 770–776 (2000).

Heras, A. N-methylene phosphonic chitosan: a novel soluble derivative. *Carbohydrate Polymers* **44**, 1–8 (2001).

Hirano, S., Zhang, M. & Nakagawa, M. Release of glycosaminoglycans in physiological saline and water by wet spun chitin acid glycosaminoglycan fibers. *Journal of Biomedical Materials Research* **2001**, *56*, 556–561.

Hodak, J.H., Henglein, A., Giersig, M. & Hartland, G.V. Laser induced inter-diffusion in Au Ag core shell nanoparticles. *The Journal of Physical Chemistry B* **104**, 11708–11718 (2000).

Holappa, J., Hjálmarsdóttir, M., Másson, M., Rúnarsson, Ö., Asplund, T., Soininen, P., Nevalainen, T., & Järvinen, T. Antimicrobial activity of chitosan N-betainates. *Carbohydrate Polymers* **65**, 114–118 (2006).

Hsin, Y.H., Chen, C.F., Huang, S., Shih, T.S., Lai, P.S. & Chueh, P.J. The apoptotic effect of nanosilver is mediated by a ROS and JNK dependent mechanism involving the mitochondrial pathway in NIH3T3 cells. *Toxicology Letters* **179**, 130-139 (2008).

Hu, M., Petrova, H., Chen, J., McLellan, J.M., Siekkinen, A.R., Marquez, M., Li, X., Xia, Y. & Hartland, G.V. Ultrafast laser studies of the photothermal properties of gold nanocages. *Journal of Physical Chemistry B* **110**, 1520-1524 (2006)

Huang, X., Jain, P.K., El Sayed, I.H.& El Sayed, M.A, Determination of the minimum temperature required for selective photothermal destruction of cancer cells using immunotargeted gold nanoparticles. *Photochemistry and Photobiology* **82**, 412-417 (2006).

Huang, Z., Li, Z., Chen, R., Chen, G., Lin, D., Xi, G., Chen, Y., Lin, H., & Lei, J. The application of silver nanoparticle based SERS in diagnosing thyroid tissue. *Journal of Physics: Conference Series* **277**, 012014 (2011).

Huebsch, N., Arany, P.R., Mao, A.S., Shvartsman, D., Ali, O.A., Bencherif, S.A., Rivera Feliciano, J. & Mooney, D.J. Harnessing traction mediated manipulation of the cell/matrix interface to control stem cell fate. *Nature Materials* **9**, 518–526 (2010).

Huff, T.B., Tong, L., Zhao, Y., Hansen, M.N., Cheng, J.X. & Wei, A. Hyperthermic effects of gold nanorods on tumor cells. *Nanomedicine* **2**, 125-132 (2007).

Hussain, S.M., Hess, K.L., Gearhart, J.M., Geiss, K.T. & Schlager, J.J. In vitro toxicity of nanoparticles in BRL 3A rat liver cells. *Toxicology in Vitro* **19**, 975–983 (2005).

Ivleva, N.P., Wagner, M., Horn, H., Niessner, R. & Haisch, C. In situ surface enhanced Raman scattering analysis of biofilm. *Analytical Chemistry* **80**, 8538–8544 (2008).

Jain, J., Arora, S., Rajjwade, J.M., Omray, P., Khandelwal, S. & Paknikar, K.M. Silver nanoparticles in therapeutics: Development of an antimicrobial gel formulation for topical use. *Molecular Pharmaceutics* **6**, 1388–1401 (2009).

Janes, K.A., Fresneau, M.P., Marazuela, A., Fabra, A. & Alonso, M.J. Chitosan nanoparticles as delivery systems for doxorubicin. *Journal of Controlled Release* **73**, 255–267 (2001).

Jang, J. & Kim, Y. Fabrication of monodisperse silica polymer core shell nanoparticles with excellent antimicrobial efficacy. *Chemical Communications* 4016-4018 (2008).

Jayakumar, R., Prabaharan, M., Sudheesh Kumar, P.T., Nair, S.V. & Tamura, H. Biomaterials based on chitin and chitosan in wound dressing applications. *Biotechnology Advances* **29**, 322–337 (2011).

Jia, Z., Shen, D. & Xu, W. Synthesis and antibacterial activities of quaternary ammonium salt of chitosan. *Carbohydrate Research* **333**, 1–6 (2001).

Jiang, H.L., Kim, T.-H., Kim, Y.-K., Park, I.-Y., Cho, M.-H., & Cho, C.-S. Efficient gene delivery using chitosan polyethylenimine hybrid systems. *Biomedical Materials* **3**, 025013 (2008).

Kamata, H. & Hirata, H. Redox regulation of cellular signalling. *Cellular Signalling* **11**, 1–14 (1999).

Kang, Y.O., Choi, S.H., Gopalan, A., Lee, K.P., Kang, H.D., & Song, Y.S. Tuning of morphology of Ag nanoparticles in the Ag/polyaniline nanocomposites prepared by γ-ray irradiation. *Journal of Non-Crystalline Solids* **352**, 463–468 (2006).

Kasibhatla, S. & Tseng, B. Why target apoptosis in cancer treatment? *Molecular Cancer Therapeutics* **2**, 573–580 (2003).

Kelly, K.L., Coronado, E., Zhao, L.L. & Schatz, G.C. The optical properties of metal nanoparticles: The influence of size, shape, and dielectric environment. *The Journal of Physical Chemistry B* **107**, 668–677 (2003).

Khor, E. & Lim, L.Y. Implantable applications of chitin and chitosan. *Biomaterials* **24**, 2339–2349 (2003).

Kim, I.Y., Seo, S.J., Moon, H.S., Yoo, M.K., Park, I.Y., Kim, B.C. & Cho, C.S. Chitosan and its derivatives for tissue engineering applications. *Biotechnology Advances* **26**, 1–21 (2008a).

Kim, J. S., Kuk, E., Yu, K.N., Kim, J.H., Park, S.J., Lee, H.J., Kim, S.H., Park, Y.K., Park, Y.H., Hwang, C.Y., Hwang, Kim, Y.K., Lee, Y.S., Jeong, D.H. & Cho, M.H. Antimicrobial effects of silver nanoparticles. *Nanomedicine: Nanotechnology, Biology and Medicine* **3**, 95–101 (2007a).

Kim, K.J., Sung, W.S., Suh, B.K., Moon, S.K., Choi, J.S., Kim, J.G. & Lee, D.G. Antifungal activity and mode of action of silver nanoparticles on *Candida albicans. BioMetals* **22**, 235–242 (2008b).

Kim, Y.H., Lee, D.K., Cha, H.G., Kim, C.W. & Kang, Y.S. Synthesis and characterization of antibacterial Ag-SiO_2 nanocomposite. *The Journal of Physical Chemistry C* **111**, 3629–3635 (2007b).

Kneipp, J., Kneipp, H., Wittig, B. & Kneipp, K. Following the dynamics of pH in endosomes of live cells with SERS nanosensors. *The Journal of Physical Chemistry C* **114**, 7421–7426 (2010).

Kneipp, K., Kneipp, H., Manoharan, R., Hanlon, E.B., Itzkan, I., Dasari, R.R. & Feld, M.S. Single molecule detection of a cyanine dye in silver colloidal solution using near infrared surface-enhanced Raman scattering. *Applied Spectroscopy*, **52**, 175-178 (1998).

Kneipp, K., Wang, Y., Kneipp, H., Perelman, L., Itzkan, I., Dasari, R. & Feld, M.S. Single molecule detection using surface-enhanced Raman scattering (SERS). *Physical Review Letters* **78**, 1667–1670 (1997).

Köping Höggård, M. Tubulekas, I., Guan, H., Edwards, K., Nilsson, M., Vårum, K.M., & Artursson, P. Chitosan as a nonviral gene delivery system. Structure property

relationships and characteristics compared with polyethylenimine in vitro and after lung administration in vivo. *Gene Therapy* **8**, 1108–1121 (2001).

Kora, A.J., Sashidhar, R.B. & Arunachalam, J. Gum kondagogu (*Cochlospermum gossypium*): A template for the green synthesis and stabilization of silver nanoparticles with antibacterial application. *Carbohydrate Polymers* **82**, 670–679 (2010).

Kreibig, U. & Vollmer, M. Optical Properties of Metal Clusters, Springer: New York, (1995)

Kumar, A., Vemula, P.K., Ajayan, P.M. & John, G. Silver nanoparticle embedded antimicrobial paints based on vegetable oil. *Nature Materials* **7**, 236–241 (2008).

Kumar, M.N.V.R. A review of chitin and chitosan applications. *Reactive and Functional Polymers* **46**, 1–27 (2000).

Kurita, K. Chemistry and application of chitin and chitosan. *Polymer Degradation and Stability* **59**, 117–120 (1998).

Kurita, K., Ikeda, H., Yoshida, Y., Shimojoh, M. & Harata, M. Chemoselective protection of the amino groups of chitosan by controlled phthaloylation: Facile preparation of a precursor useful for chemical modifications. *Biomacromolecules* **3**, 1–4 (2002).

Laflamme, P., Benhamou, N., Bussières, G. & Dessureault, M. Differential effect of chitosan on root rot fungal pathogens in forest nurseries. *Canadian Journal of Botany* **77**, 1460–1468 (2000).

Langer, R. & Tirrell, D.A. Designing materials for biology and medicine. *Nature* **428**, 487–492 (2004).

Lara, H.H., Ayala Nuñez, N.V., Ixtepan Turrent, L. & Rodriguez Padilla, C. Mode of antiviral action of silver nanoparticles against HIV-1. *Journal of Nanobiotechnology* **8**, 1 (2010).

Larsen, M.U., Seward, M., Tripathi, A. & Shapley, N.C. Biocompatible nanoparticles trigger rapid bacteria clustering. *Biotechnology Progress* **25**, 1094–1102 (2009).

Lee, K.Y. & Mooney, D.J. Alginate: Properties and biomedical applications. *Progress in Polymer Science* **37**, 106–126 (2012).

Lee, K.Y., Peters, M.C. & Mooney, D.J. Comparison of vascular endothelial growth factor and basic fibroblast growth factor on angiogenesis in SCID mice. *Journal of Controlled Release* **87**, 49–56 (2003).

Leong, K. & Wen, J. Gene delivery via polymer nanoparticles. *Dekker Encyclopedia of Nanoscience and Nanotechnology*, Second Edition-Six Volume Set (Print Version) 1394–1403 (2008).

Li, H. & Rothberg, L. Colorimetric detection of DNA sequences based on electrostatic interactions with unmodified gold nanoparticles. *Proceedings of the National Academy of Sciences* **101**, 14036–14039 (2004).

Li, X., Xie, H., Lin, J., Xie, W. & Ma, X. Characterization and biodegradation of chitosan–alginate polyelectrolyte complexes. *Polymer Degradation and Stability* **94**, 1–6 (2009).

Li, X.Y., Jin, L.J., McAllister, T.A., Stanford, K., Xu, J.Y., Lu, Y.N., Zhen, Y.H., Sun, Y.X. & Xu, Y.P. Chitosan-alginate microcapsules for oral delivery of egg yolk immunoglobulin (IgY). *Journal of Agricultural and Food Chemistry* **55**, 2911–2917 (2007).

Lin, Y.H., Liang, H.F., Chung, C.K., Chen, M.C. & Sung, H.W. Physically crosslinked alginate/N, O carboxymethyl chitosan hydrogels with calcium for oral delivery of protein drugs. *Biomaterials* **26**, 2105–2113 (2005).

Liu, H., Du, Y., Wang, X. & Sun, L. Chitosan kills bacteria through cell membrane damage. *International Journal of Food Microbiology* **95**, 147–155 (2004).

Liu, W., Wu, Y., Wang, C., Li, H.C., Wang, T., Liao, C.Y., Cui, L., Zhou, Q.F., Yan, B., & Jiang, G.B. Impact of silver nanoparticles on human cells: Effect of particle size. *Nanotoxicology* **4**, 319–330 (2010).

Liu, X.F., Guan, Y.L., Yang, D.Z., Li, Z. &Yao K.D. Antibacterial action of chitosan and carboxymethylated chitosan. *Journal of Applied Polymer Science* **79**, 1324–1335 (2001).

Liu, Y., Chen, S., Zhong, L. & Wu, G. Preparation of high-stable silver nanoparticle dispersion by using sodium alginate as a stabilizer under gamma radiation. *Radiation Physics and Chemistry* **78**, 251–255 (2009).

Liu, Z. & Jiang, M. Reversible aggregation of gold nanoparticles driven by inclusion complexation. *Journal of Materials Chemistry* **17**, 4249–4254 (2007).

Loo, C., Lowery, A., Halas, N.J., West, J.L.& Drezek, R. Immunotargeted nanoshells for integrated cancer imaging and therapy. *Nano Letters* **5**, 709-711 (2005).

Lu, L., Sun, R.W., Chen, R., Hui, C.K., Ho, C.M., Luk, J.M., Lau, G.K. & Che, C.M. Silver nanoparticles inhibit hepatitis B virus replication. *Antiviral Therapy* **13**, 253–262 (2008).

Lu, L., Wang, H., Zhou, Y., Xi, S., Zhang, H., Hu, J. & Zhao, B. Seed mediated growth of large, monodisperse core shell gold silver nanoparticles with Ag-like optical properties. *Chemical Communications* 144–145 (2002).

Lu, Y., Mei, Y., Ballauff, M. & Drechsler, M. Thermosensitive core-shell particles as carrier systems for metallic nanoparticles. *The Journal of Physical Chemistry B* **110** 3930-3937 (2006).

Lu, Z., Yeh, T.K., Tsai, M., Au J.S. & Wientjes, M. G. Paclitaxel loaded gelatin nanoparticles for intravesical bladder cancer therapy. *Clinical Cancer Research* **10**, 7677–7684 (2004).

Ma, H.L., Hung, S.C., Lin, S.Y., Chen, Y.L. & Lo, W.H. Chondrogenesis of human mesenchymal stem cells encapsulated in alginate beads. *Journal of Biomedical Materials Research Part A* **64**, 273–281 (2003).

Madhumathi, K, Sudheesh Kumar, P.T., Abhilash, S., Sreeja, V., Tamura, H., Manzoor, K., Nair, S.V., & Jayakumar, R. Development of novel chitin/nanosilver composite scaffolds for wound dressing applications. *Journal of Materials Science: Materials in Medicine* **21**, 807–813 (2009).

Mahmoudi, M. & Serpooshan, V. Silver coated engineered magnetic nanoparticles are promising for the success in the fight against antibacterial resistance threat. *ACS Nano* **6**, 2656–2664 (2012).

Malcher, M., Volodkin, D., Heurtault, B., André, P., Schaaf, P., Möhwald, H., Voegel, J.-C., Sokolowski, A., Ball, V., Boulmedais, F. & Frisch, B. Embedded silver ions containing liposomes in polyelectrolyte multilayers: Cargos films for antibacterial agents. *Langmuir* **24**, 10209–10215 (2008).

Mallick, S., Sharma, S., Banerjee, M., Ghosh, S.S., Chattopadhyay, A. & Paul, A. Iodine stabilized Cu nanoparticle chitosan composite for antibacterial applications. *ACS Applied Materials & Interfaces* **4**, 1313–1323 (2012).

Mallik, K., Mandal, M., Pradhan, N. & Pal, T. Seed mediated formation of bimetallic nanoparticles by UV irradiation: A photochemical approach for the preparation of 'core−shell' type structures. *Nano Letters* **1**, 319–322 (2001).

Mandal, M., Ranjan, N. R., Kundu, S., Kumar Ghosh, S., Panigrahi, M. & Pal, T. Synthesis of Au core - Ag shell type bimetallic nanoparticles for single molecule detection in solution by SERS method. *Journal of Nanoparticle Research* **6**, 53–61 (2004).

Maneerung, T., Tokura, S. & Rujiravanit, R. Impregnation of silver nanoparticles into bacterial cellulose for antimicrobial wound dressing. *Carbohydrate Polymers* **72**, 43–51 (2008).

Marambio-Jones, C. & Hoek, E.M.V. A review of the antibacterial effects of silver nanomaterials and potential implications for human health and the environment. *Journal of Nanoparticle Research* **12**, 1531–1551 (2010).

Másson, M., Holappa, J., Hjálmarsdóttir, M., Rúnarsson, Ö.V., Nevalainen, T., & Järvinen, T. Antimicrobial activity of piperazine derivatives of chitosan. *Carbohydrate Polymers* **74**, 566–571 (2008).

Mayya, K.S., Patil, V.& Sastry, M. An optical absorption investigation of cross-linking of gold colloidal particles with a small dithiol molecule. *Bulletin of the Chemical Society of Japan* **73**, 1757-1761 (2000).

McIntosh, C.M., Esposito, E.A., Boal, A.K., Simard, J.M., Martin, C.T., & Rotello, V.M. Inhibition of DNA transcription using cationic mixed monolayer protected gold clusters. *Journal of the American Chemical Society* **123**, 7626–7629 (2001).

Meng, X., Tian, F., Yang, J., He, C.N., Xing, N., & Li, F. Chitosan and alginate polyelectrolyte complex membranes and their properties for wound dressing application. *Journal of Materials Science: Materials in Medicine* **21**, 1751–1759 (2010).

Mi, F.L., Her, N.L., Kaun, C.Y., Wong, T. & Shyu, S.S. Chitosan tablets for controlled release of theophylline: effect of polymer drug wet or dry blending and anionic-cationic inter polymer. *Journal of applied polymers* **66**, 2495-2505 (1997).

Mie, G. Beiträge zur Optik trüber medien, speziell kolloidaler metallösungen. *Annalen der Physik (Leipzig)* **25**, 377-445 (1908).

Mirkin, C.A., Letsinger, R.L., Mucic, R.C. & Storhoff, J.J. A DNA based method for rationally assembling nanoparticles into macroscopic materials. *Nature* **382**, 607-609 (1996).

Möbus, K., Siepmann, J. & Bodmeier, R. Zinc–alginate microparticles for controlled pulmonary delivery of proteins prepared by spray drying. *European Journal of Pharmaceutics and Biopharmaceutics* **81**, 121–130 (2012).

Moghimi, S. M., Hunter, A.C. & Murray, J.C. Nanomedicine: current status and future prospects. *The FASEB Journal*. **19**, 311-330.

Mørch, Ý.A., Donati, I. & Strand, B.L. Effect of Ca^{2+}, Ba^{2+} and Sr^{2+} on alginate microbeads. *Biomacromolecules* **7**, 1471–1480 (2006).

Morones, J.R., Elechiguerra, J.L., Camacho, A., Holt, K., Kouri, J.B., Ramirez, J.T.& Yacaman, M.J. The bactericidal effect of silver nanoparticles. *Nanotechnology* **16**, 2346–2353 (2005).

Morris, E.R., Rees, D.A., Thom, D. & Boyd, J. Chiroptical and stoichiometric evidence of a specific, primary dimerisation process in alginate gelation. *Carbohydrate Research* **66**, 145–154 (1978).

Moyer, C.A., Brentano, L., Gravens, D.L., Margraf, H.W. & Monafo, W.W. Treatment of large human burns with 0.5% silver nitrate solution. *Archives of Surgery* **90**, 812–867 (1965).

Müller, R.H., Jacobs, C., & Kayser, O. Nanosuspensions as particulate drug formulations in therapy rationale for development and what we can expect for the future. *Advanced Drug Delivery Reviews*, **47**, 3–19 (2001).

Mulvaney, P., Giersig, M. & Henglein, A. Electrochemistry of multilayer colloids: preparation and absorption spectrum of gold-coated silver particles. *The Journal of Physical Chemistry* **97**, 7061–7064 (1993).

Murray, R.G.E., Steed, P. & Elson, H.E. The location of the mucopeptide in sections of the cell wall of *Escherichia coli* and other Gram negative bacteria. *Canadian Journal of Microbiology* **11**, 547–560 (1965).

Murugadoss, A. & Chattopadhyay, A. A 'green' chitosan–silver nanoparticle composite as a heterogeneous as well as micro-heterogeneous catalyst. *Nanotechnology* **19**, 015603/1-015603/9, (2008).

Muzzarelli, R.A.A. Chitin in nature and technology, Plenum Press New York (1986).

Muzzarelli, R.A.A. Modified chitosans carrying sulfonic acid groups. *Carbohydrate Polymers* **19**, 231–236 (1992).

Muzzarelli, R.A.A. Chitin and chitosan hydrogels. In Handbook of Hydrocolloids, 2nd ed., (Eds Phillips, G. O., Williams, P. A.) Woodhead Publishing Ltd: Cambridge, 849− 888 (2009).

Navarro, E., Navarro, E., Piccapietra, F., Wagner, B., Marconi, F., Kaegi, R., Odzak, N., Sigg, L. & Behra, R. Toxicity of silver nanoparticles to *Chlamydomonas reinhardtii*. *Environmental Science & Technology* **42**, 8959–8964 (2008).

Nickel, U., zu Castell, A., Pöppl, K. & Schneider, S. A silver colloid produced by reduction with hydrazine as support for highly sensitive surface-enhanced Raman spectroscopy. *Langmuir* **16**, 9087–9091 (2000).

Nie, S. & Emory, S.R. Probing single molecules and single nanoparticles by surface-enhanced Raman scattering. *Science* **275**, 1102–1106 (1997).

Niemeyer, C.M. Self assembled nanostructures based on DNA: towards the development of nanobiotechnology. *Current Opinion in Chemical Biology* **4**, 609-618 (2000).

Nikoobakht, B. & El Sayed, M.A. Surface enhanced Raman scattering studies on aggregated gold nanorods. *The Journal of Physical Chemistry A* **107**, 3372-3378 (2003).

Oishi, M., Nakaogami, J., Ishii, T. & Nagasaki, Y. Smart PEGylated gold nanoparticles for the cytoplasmic delivery of siRNA to induce enhanced gene silencing. *Chemistry Letters* **35**, 1046–1047 (2006).

O'Neal, D.P., Hirsch, L.R., Halas, N.J., Payne, J.D. & West, J.L. Photothermal tumor ablation in mice using near infrared absorbing nanoshells. *Cancer Letters* **209**, 171-176. (2004).

Otsuka, H., Akiyama,Y., Nagasaki, Y.& Kataoka, K. Quantitative and reversible lectin induced association of gold nanoparticles modified with α-Lactosyl-ω-mercapto-poly(ethylene glycol). *Journal of the American Chemical Society* **123**, 8226-8230 (2001).

Pal, A., Esumi, K. & Pal, T. Preparation of nanosized gold particles in a biopolymer using UV photoactivation. *Journal of Colloid and Interface Science* **288**, 396–401 (2005).

Pal, S., Tak, Y.K. & Song, J.M. Does the antibacterial activity of silver nanoparticles depend on the shape of the nanoparticle? A study of the Gram-negative bacterium *Escherichia coli*. *Applied and Environmental Microbiology* **73**, 1712–1720 (2007).

Panáček, A., Kvitek, L., Prucek, R., Kolar, M., Vecerova, R., Pizurova, N., Sharma, V. K., Nevecna, T. & Zboril, R. Silver colloid nanoparticles: Synthesis, characterization, and their antibacterial activity. *The Journal of Physical Chemistry B* **110**, 16248–16253 (2006).

Pande, S., Ghosh, S.K., Praharaj, S., Panigrahi, S., Basu, S., Jana, S., Pal, A., Tsukuda, T. & Pal, T. Synthesis of normal and inverted gold-silver core-shell architectures in β-Cyclodextrin and their applications in SERS. *Journal of Physical Chemistry C* **111**, 10806–10813 (2007).

Papineau, A.M., Hoover, D.G., Knorr, D. & Farkas, D.F. Antimicrobial effect of water soluble chitosans with high hydrostatic pressure. *Food Biotechnology* **5**, 45–57 (1991).

Pasparakis, G. & Bouropoulos, N. Swelling studies and *in vitro* release of verapamil from calcium alginate and calcium alginate–chitosan beads. *International Journal of Pharmaceutics* **323**, 34–42 (2006).

Pastoriza-Santos, I. & Liz-Marzán, L. M. Formation and stabilization of silver nanoparticles through reduction by N, N -Dimethylformamide. *Langmuir* **15**, 948–951 (1999).

Pawar, S.N. & Edgar, K.J. Alginate derivatization: A review of chemistry, properties and applications. *Biomaterials* **33**, 3279–3305 (2012).

Peer, D., Karp, J.M., Hong, S., Farokhzad, O.C., Margalit, R. & Langer, R. Nanocarriers as an emerging platform for cancer therapy. *Nature Nanotechnology* **2**, 751–760 (2007).

Piao, M. J., Kang, K.A., Lee, I.K., Kim, H.S., Kim, S., Choi, J.Y., Choi, J., & Hyun, J.W. Silver nanoparticles induce oxidative cell damage in human liver cells through inhibition of reduced glutathione and induction of mitochondria-involved apoptosis. *Toxicology Letters* **201**, 92–100 (2011).

Pillai, O. & Panchagnula, R. Polymers in drug delivery. *Current Opinion in Chemical Biology* **5**, 447–451 (2001).

Potara, M., Jakab, E., Damert, A., Popescu, O., Canpean, V., & Astilean, S. Synergistic antibacterial activity of chitosan–silver nanocomposites on *Staphylococcus aureus*. *Nanotechnology* **22**, 135101 (2011).

Pradhan, N., Pal, A. & Pal, T., Silver nanoparticle catalyzed reduction of aromatic nitro compounds. *Colloids Surfaces A* **196**, 247-257 (2002).

Prang, P., Muller, R., Eljaouhari, A., Heckmann, K., Kunz, W., Weber, T., Faber, C., Vroemen, M., Bogdahn, U. & Weidner, N. The promotion of oriented axonal regrowth in the injured spinal cord by alginate-based anisotropic capillary hydrogels. *Biomaterials* **27**, 3560–3569 (2006).

Qi, L., Xu, Z., Jiang, X., Hu, C. & Zou, X. Preparation and antibacterial activity of chitosan nanoparticles. *Carbohydrate Research* **339**, 2693–2700 (2004).

Rabbany, S.Y., Pastore, J., Yamamoto, M., Miller, T., Rafii, S., Aras, R. & Penn, M. Continuous delivery of stromal cell derived factor-1 from alginate scaffolds accelerates wound healing. *Cell Transplantation* **19**, 399–408 (2010).

Rabea, E.I., Badawy, M. E.T., Stevens, C.V., Smagghe, G. & Steurbaut, W. Chitosan as antimicrobial agent: Applications and mode of action. *Biomacromolecules* **4**, 1457–1465 (2003).

Ramos, V., Rodríguez, N., Díaz, M., Rodríguez, M., Heras, A., & Agulló, E. N-methylene phosphonic chitosan. Effect of preparation methods on its properties. *Carbohydrate Polymers* **52**, 39–46 (2003).

Rana, S., Rawat, J. & Misra, R.D.K. Anti-microbial active composite nanoparticles with magnetic core and photocatalytic shell: TiO_2-$NiFe_2O_4$ biomaterial system. *Acta Biomaterialia* **1**, 691–703 (2005).

Raveendran, P., Fu, J. & Wallen, S. L. Completely ‘green’ synthesis and stabilization of metal nanoparticles. *Journal of the American Chemical Society* **125**, 13940–13941 (2003).

Rello, S., Stockert, J.C., Moreno, V., Gámez, A., Pacheco, M., Juarranz, A., Cañete, M., & Villanueva, A. Morphological criteria to distinguish cell death induced by apoptotic and necrotic treatments. *Apoptosis* **10**, 201–208 (2005).

Ren, W., Fang, Y. & Wang, E. A binary functional substrate for enrichment and ultrasensitive SERS spectroscopic detection of folic acid using graphene oxide/Ag nanoparticle hybrids. *ACS Nano* **5**, 6425–6433 (2011).

Risbud, M., Endres, M., Ringe, J., Bhonde, R. & Sittinger, M. Biocompatible hydrogel supports the growth of respiratory epithelial cells: Possibilities in tracheal tissue engineering. *Journal of Biomedical Materials Research* **56**, 120–127 (2001).

Rivas, L., Sanchez Cortes, S., García Ramos, J.V. & Morcillo, G. Mixed silver/gold colloids: A study of their formation, morphology and surface-enhanced Raman activity. *Langmuir* **16**, 9722–9728 (2000).

Rodríguez González, B., Burrows, A., Watanabe, M., Kiely, C.J. & Liz Marzán, L.M. Multishell bimetallic Au Ag nanoparticles: synthesis, structure and optical properties. *Journal of Materials Chemistry* **15**, 1755 (2005).

Roe, D., Karandikar, B., Bonn Savage, N., Gibbins, B. & Roullet, J.B. Antimicrobial surface functionalization of plastic catheters by silver nanoparticles. *Journal of Antimicrobial Chemotherapy* **61**, 869–876 (2008).

Rogers, J.V., Parkinson, C.V., Choi, Y.W., Speshock, J.L. & Hussain, S.M. A preliminary assessment of silver nanoparticle inhibition of monkeypox virus plaque formation. *Nanoscale Research Letters* **3**, 129–133 (2008).

Roller, S. & Covill, N. The antifungal properties of chitosan in laboratory media and apple juice. *International Journal of Food Microbiology* **47**, 67–77 (1999).

Ronghua, H., Yumin, D. & Jianhong, Y. Preparation and anticoagulant activity of carboxybutyrylated hydroxyethyl chitosan sulfates. *Carbohydrate Polymers* **51**, 431–438 (2003).

Rosemary, M.J., MacLaren, I. & Pradeep, T. Investigations of the antibacterial properties of Ciprofloxacin@SiO_2. *Langmuir* **22**, 10125–10129 (2006).

Rowley, J.A., Madlambayan, G. & Mooney, D.J. Alginate hydrogels as synthetic extracellular matrix materials. *Biomaterials* **20**, 45–53 (1999).

Roy, K., Mao, H.Q., Huang, S.K. & Leong, K.W. Oral gene delivery with chitosan DNA nanoparticles generates immunologic protection in a murine model of peanut allergy. *Nature Medicine* **5**, 387–391 (1999).

Rúnarsson, Ö.V., Holappa, J., Nevalainen, T., Hjálmarsdóttir, M., Järvinen, T., Loftsson, T., Einarsson, J.M., Jónsdóttir, S., Valdimarsdóttir, M. & Másson, M. Antibacterial activity of methylated chitosan and chitooligomer derivatives: Synthesis and structure activity relationships. *European Polymer Journal* **43**, 2660–2671 (2007).

Ruvinov, E., Leor, J. & Cohen, S. The promotion of myocardial repair by the sequential delivery of IGF-1 and HGF from an injectable alginate biomaterial in a model of acute myocardial infarction. *Biomaterials* **32**, 565–578 (2011).

Sahoo, A.K., Sk, M.P., Ghosh, S.S. & Chattopadhyay, A. Plasmid DNA linearization in the antibacterial action of a new fluorescent Ag nanoparticle–paracetamol dimer composite. *Nanoscale* **3**, 4226-4233 (2011).

Sandhu, K.K., McIntosh, C.M., Simard, J.M., Smith, S.W. & Rotello, V.M. Gold nanoparticle mediated transfection of mammalian cells. *Bioconjugate Chemistry* **13**, 3-6 (2002).

Sankalia, M.G., Mashru, R.C., Sankalia, J.M. & Sutariya, V.B. Reversed chitosan-alginate polyelectrolyte complex for stability improvement of alpha-amylase: Optimization and physicochemical characterization. *European Journal of Pharmaceutics and Biopharmaceutics* **65**, 215–232 (2007).

Sanpui, P., Chattopadhyay, A. & Ghosh, S.S. Induction of apoptosis in cancer cells at low silver nanoparticle concentrations using chitosan nanocarrier. *ACS Applied Materials and Interfaces* **3**, 218–228 (2011).

Sanpui, P., Murugadoss, A., Prasad, P., Ghosh, S.S. & Chattopadhyay, A. The antibacterial properties of a novel chitosan–Ag-nanoparticle composite. *International Journal of Food Microbiology* **124**, 142–146 (2008).

Schipper, N.G., Olsson, S., Hoogstraate, J.A., Boer, A.G., Varum, K.M. & Artursson, P. Chitosans as absorption enhancers for poorly absorbable drugs 2: mechanism of absorption enhancement. *Pharmaceutical Research* **14**, 923–929 (1997).

Schwartzberg, A.M., Grant, C.D., Wolcott, A., Talley, C.E., Huser, T.R., Bogomolni, R., & Zhang, J.Z. Unique gold nanoparticle aggregates as a highly active surface-enhanced Raman scattering substrate. *The Journal of Physical Chemistry B* **108**, 19191–19197 (2004).

Selvakannan, P. Swami, A., Srisathiyanarayanan, D., Shirude, P.S., Pasricha, R., Mandale, A.B. & Sastry, M. Synthesis of aqueous Au Core−Ag Shell nanoparticles using tyrosine as a pH-dependent reducing agent and assembling phase transferred silver nanoparticles at the air-water interface. *Langmuir* **20**, 7825–7836 (2004).

Shahverdi, A.R., Fakhimi, A., Shahverdi, H.R. & Minaian, S. Synthesis and effect of silver nanoparticles on the antibacterial activity of different antibiotics against *Staphylococcus aureus* and *Escherichia coli*. *Nanomedicine Nanotechnology Biology and Medicine* **3**, 168–171 (2007).

Shalumon, K.T., Anulekha, K.H., Nair, S.V., Nair, S.V., Chennazhi, K.P. & Jayakumar, R. Sodium alginate/poly(vinyl alcohol)/nano ZnO composite nanofibers for antibacterial wound dressings. *International Journal of Biological Macromolecules* **49**, 247–254 (2011).

Sharma, J., Chaki, N.K., Mandale, A.B., Pasricha, R. & Vijayamohanan, K. Controlled interlinking of Au and Ag nanoclusters using 4-aminothiophenol as molecular interconnects. *Journal of Colloid and Interface Science* **272**, 145-152 (2004).

Shi, Z., Neoh, K.G., Kang, E.T. & Wang, W. Antibacterial and mechanical properties of bone cement impregnated with chitosan nanoparticles. *Biomaterials* **27**, 2440–2449 (2006).

Shim, J. Y., & Gupta, V.K. Reversible aggregation of gold nanoparticles induced by pH dependent conformational transitions of a self-assembled polypeptide. *Journal of Colloid and Interface Science* **316**, 977–983, (2007).

Shrivastava, S., Bera, T., Singh, S.K., Singh, G., Ramachandrarao, P., & Dash, D. Characterization of antiplatelet properties of silver nanoparticles. *ACS Nano* **3**, 1357–1364 (2009).

Sies, H. Glutathione and its role in cellular functions. *Free Radical Biology and Medicine* **27**, 916–921 (1999).

Sinha, V.R., Singla, A.K., Wadhawan, S., Kaushik, R., Kumria, R., Bansal, K. & Dhawan, S. Chitosan microspheres as a potential carrier for drugs. *International Journal of Pharmaceutics* **274**, 1–33 (2004).

Smidsrød, O. & Haug, A. Dependence upon the gel-sol state of the ion-exchange properties of alginates. *Acta Chemica Scandinavica* **26**, 2063-2074,(1972).

Smidsrød, O. Molecular basis for some physical properties of alginates in the gel state. *Faraday Discussions of the Chemical Society* **57**, 263 -274 (1974).

Smitha, B., Sridhar, S. & Khan, A.A. Chitosan-sodium alginate polyion complexes as fuel cell membranes. *European Polymer Journal* **41**, 1859–1866 (2005).

Sondi, I. & Salopek Sondi, B. Silver nanoparticles as antimicrobial agent: a case study on *E. coli* as a model for Gram-negative bacteria. *Journal of Colloid and Interface Science* **275**, 177–182 (2004).

Soppimath, K.S., Aminabhavi, T.M., Kulkarni, A.R. & Rudzinski, W. E. Biodegradable polymeric nanoparticles as drug delivery devices. *Journal of Controlled Release* **70**, 1–20 (2001).

Souza, G.R., Levin, C.S., Hajitou, A., Pasqualini, R., Arap, W. & Miller, J. H. In vivo detection of gold imidazole self-assembly complexes: NIR-SERS Signal Reporters. *Analytical Chemistry* **78**, 6232–6237 (2006).

Srnová Šloufová, I., Lednický, F., Gemperle, A. & Gemperlová, J. Core−Shell (Ag)Au bimetallic nanoparticles: Analysis of transmission electron microscopy images. *Langmuir* **16**, 9928–9935 (2000).

Storhoff, J.J. & Mirkin, C.A. Programmed materials synthesis with DNA. *Chemical Reviews* **99**, 1849-1862 (1999).

Storhoff, J.J., Lazarides, A.A., Mucic, R.C., Mirkin, C.A., Letsinger, R.L.& Schatz, G. C. *Journal of the American Chemical Society* **122**, 4640-4650 (2000).

Stössel, P. & Leuba, J.L. Effect of chitosan, chitin and some aminosugars on growth of various soilborne phytopathogenic fungi. *Journal of Phytopathology* **111**, 82–90 (1984).

Sudarshan, N.R., Hoover, D.G. & Knorr, D. Antibacterial action of chitosan. *Food Biotechnology* **6**, 257–272 (1992).

Sun, L., Zhao, D., Ding, M., Xu, Z., Zhang, Z., Li, B., & Shen, D. Controllable synthesis of silver nanoparticle aggregates for surface-enhanced Raman scattering studies. *The Journal of Physical Chemistry C* **115**, 16295–16304 (2011).

Sun, R.W.Y., Chen, R., Chung, N.P.Y., Ho, C.M., Lin, C.L.S. & Che, C.M. Silver nanoparticles fabricated in Hepes buffer exhibit cytoprotective activities toward HIV-1 infected cells. *Chemical Communications* **40**, 5059-5061 (2005).

Takahashi, H., Niidome, T., Nariai, A., Niidome, Y. & Yamada, S. Photothermal reshaping of gold nanorods prevents further cell death. *Nanotechnology* **17**, 4431-4435 **(**2006).

Tankhiwale, R. & Bajpai, S.K. Graft copolymerization onto cellulose based filter paper and its further development as silver nanoparticles loaded antibacterial food-packaging material. *Colloids and Surfaces B: Biointerfaces* **69**, 164–168 (2009).

Templeton, A.C., Zamborini, F.P., Wuelfing, W.P. & Murray, R.W. Controlled and reversible formation of nanoparticle aggregates and films using Cu^{2+}-Carboxylate Chemistry. *Langmuir* **16**, 6682-6688 (2000).

Thom, D., Grant, G.T., Morris, E.R. & Rees, D.A. Characterisation of cation binding and gelation of polyuronates by circular dichroism. *Carbohydrate Research* **100**, 29–42 (1982).

Thomas, M. Conjugation to gold nanoparticles enhances polyethylenimine's transfer of plasmid DNA into mammalian cells. *Proceedings of the National Academy of Sciences* **100**, 9138–9143 (2003).

Tønnesen, H.H. & Karlsen, J. Alginate in drug delivery systems. *Drug Development and Industrial Pharmacy* **28**, 621–630 (2002).

Toshima, N. & Yonezawa, T. Bimetallic nanoparticles-novel materials for chemical and physical applications. *New Journal of Chemistry* **22**, 1179-1201 (1998)

Turkevich, J., Stevenson, P.C. & Hillier, J. A study of the nucleation and growth processes in the synthesis of colloidal gold. *Discussions of the Faraday Society* **11**, 55-75 (1951).

Ueda, S., Masutani, H., Nakamura, H., Tanaka, T., Ueno, M. & Yodoi, J. Redox control of cell death. *Antioxidants & Redox Signaling* **4**, 405–414 (2002).

Varma, A.J., Deshpande, S.V. & Kennedy, J.F. Metal complexation by chitosan and its derivatives: a review. *Carbohydrate Polymers* **55**, 77–93 (2004).

Verma, A., Simard, J.M., Worrall, J.W.E. & Rotello, V.M. Tunable reactivation of nanoparticle inhibited β-Galactosidase by glutathione at intracellular concentrations. *Journal of the American Chemical Society* **126**, 13987–13991 (2004).

Vitol, E.A., Orynbayeva, Z., Bouchard, M.J., Azizkhan Clifford, J., Friedman, G. & Gogotsi, Y. In situ intracellular spectroscopy with surface enhanced raman spectroscopy (SERS) enabled nanopipettes. *ACS Nano* **3**, 3529–3536 (2009).

Wang, L.S., Khor, E.& Lim, L.Y. Chitosan-alginate-$CaCl_2$ system for membrane coat application. *Journal of Pharmaceutical. Sciences* **90**, 1134-1142 (2001).

Wang, X., Du, Y. & Liu, H. Preparation, characterization and antimicrobial activity of chitosan-Zn complex. *Carbohydrate Polymers* **56**, 21–26 (2004).

Wang, F.Q., Li, P., Zhang, J.P., Wang, A.Q. & Wei, Q. A novel pH-sensitive magnetic alginate–chitosan beads for albendazole delivery. *Drug Development and Industrial Pharmacy* **36**, 867–877 (2010a).

Wang, Y., Lee, K. & Irudayaraj, J. Silver nanosphere SERS probes for sensitive identification of pathogens. *The Journal of Physical Chemistry C* **114**, 16122–16128 (2010b).

Winter, G.D. Formation of the scab and the rate of epithelialization of superficial wounds in the skin of the young domestic pig. *Nature* **193**, 293–294. (1962).

Xing, K., Chen, X.G., Li, Y.Y., Liu, C.S., Liu, C.G., Cha, D.S., & Park, H.J. Antibacterial activity of oleoyl-chitosan nanoparticles: A novel antibacterial dispersion system. *Carbohydrate Polymers* **74**, 114–120 (2008).

Xing, Z.C., Chae, W.P., Baek, J.Y., Choi, M.J., Jung, Y., & Kang, I.K. In vitro assessment of antibacterial activity and cytocompatibility of silver containing PHBV nanofibrous scaffolds for tissue engineering. *Biomacromolecules* **11**, 1248–1253 (2010).

Xu, Y., Zhan, C., Fan, L., Wang, L. & Zheng, H. Preparation of dual cross-linked alginate–chitosan blend gel beads and in vitro controlled release in oral site-specific drug delivery system. *International Journal of Pharmaceutics* **336**, 329–337 (2007).

Yan, X., Khor, E. & Lim, L.Y. PEC films prepared from chitosan–alginate coacervates. *Chemical & Pharmaceutical Bulletin* **48**, 941-946 (2000).

Yan, X.L., Khor, E. & Lim, L.Y. Chitosan-alginate films prepared with chitosans of different molecular weights. *Journal of Biomedical Materials Research* **58**, 358–365 (2001).

Yang, Y., Shi, J., Kawamura, G. & Nogami, M. Preparation of Au-Ag, Ag-Au core-shell bimetallic nanoparticles for surface-enhanced raman scattering. *Scripta Materialia* **58**, 862–865 (2008).

Yoksan, R. & Chirachanchai, S. Silver nanoparticle loaded chitosan starch based films: Fabrication and evaluation of tensile, barrier and antimicrobial properties. *Materials Science and Engineering: C* **30**, 891–897 (2010).

Zhang, X., Hui, Z., Wan, D., Huang, H., Huang, J., Yuan, H.& Yu, J. Alginate microsphere filled with carbon nanotube as drug carrier. *International Journal of Biological Macromolecules* **47**, 389–395 (2010).

PUBLICATIONS AND PRESENTATIONS

Journal Publications

1. Madhuchanda Banerjee, Shilpa Sharma, Arun Chattopadhyay and Siddhartha Sankar Ghosh. *Enhanced antibacterial activity of bimetallic gold-silver core–shell nanoparticles at low silver concentration.* **Nanoscale**, 3, 5120-5125, 2011.

2. Shilpa Sharma, Pallab Sanpui, Arun Chattopadhyay and Siddhartha Sankar Ghosh. *Fabrication of Antibacterial Silver Nanoparticle-Sodium Alginate-Chitosan composite films.* **RSC Advances**, 2, 5837-5843, 2012.

3. Amaresh Kumar Sahoo, Shilpa Sharma, Arun Chattopadhyay and Siddhartha Sankar Ghosh. *Quick and simple estimation of bacteria using a fluorescent paracetamol dimer–Au nanoparticle composite.* **Nanoscale**, 4, 1688-1694, 2012.

4. Sadhucharan Mallick, Shilpa Sharma, Madhuchanda Banerjee, Siddhartha Sankar Ghosh, Arun Chattopadhyay and Anumita Paul. *Iodine - Stabilized Cu Nanoparticle Chitosan Composite for Antibacterial applications.***ACS Applied Materials and Interfaces**, 4, 1313–1323, 2012.

Manuscripts under Preparation

5. Shilpa Sharma, Arun Chattopadhyay and Siddhartha Sankar Ghosh. Enhanced antibacterial activity of Ag NPs immobilized in a chitosan nanocarrier.

6. Shilpa Sharma, Chockalingam S., Arun Chattopadhyay and Siddhartha Sankar Ghosh. Alginate-Chitosan blended nanocarrier impregnated silver nanoparticles induce apoptosis in human glioblastoma cells.

7. Shilpa Sharma, Siddhartha Sankar Ghosh and Arun Chattopadhyay. Reversible aggregation and disaggregation of polymer capped Ag NPs via gel formation.

Conference Presentations

1. Shilpa Sharma, Madhuchanda Banerjee, Pallab Sanpui, Arun Chattopadhyay and Siddhartha Sankar Ghosh. *Metal nanoparticles and nanocomposites as antibacterial agents.* **Young Scientists' Colloquium 2012** August 8, 2012, Materials Research Society of India (MRSI), Kolkata Chapter, India. **(*Oral presentation*)**

2. Sadhucharan Mallick, Shilpa Sharma, Madhuchanda Banerjee, Siddhartha Sankar Ghosh, Arun Chattopadhyay and Anumita Paul. *Synthesis and antibacterial properties of iodine doped CS-Ag NP and CS-Cu NP composites.* **Conference on Photochemistry & Luminescence** March 9-10, 2012, IIT Guwahati, India. (***Poster presentation***)

3. Shilpa Sharma, Madhuchanda Banerjee, Pallab Sanpui, Arun Chattopadhyay and Siddhartha Sankar Ghosh. *Nanomaterials as antibacterial agents.* **Miami 2012 Winter Symposium: Nanotechnology in Biomedicine** February 26-29, 2012, Miami, USA. (***Poster Presentation***)

4. Shilpa Sharma, Madhuchanda Banerjee, Arun Chattopadhyay and Siddhartha Sankar Ghosh. *Bimetallic gold silver core-shell nanoparticles showing antibacterial activity at low silver concentration*. **Indo-US Bilateral workshop on Nanoparticle Assembly: From fundamentals to applications** December 12-14, 2011, IIT Delhi, India. (***Poster Presentation***)

5. Shilpa Sharma, Pallab Sanpui, Arun Chattopadhyay and Siddhartha Sankar Ghosh. *Alginate mediated 'green' synthesis of silver nanoparticles and fabrication of films with antibacterial properties*. **2nd International Conference on Advanced Nanomaterials and Nanotechnology** December 8-10, 2011, IIT Guwahati, India. (***Poster Presentation***)

6. Sadhucharan Mallick, Shilpa Sharma, Madhuchanda Banerjee, Siddhartha Sankar Ghosh, Arun Chattopadhyay and Anumita Paul. *Role of iodine in the antimicrobial activity of silver nanoparticle chitosan as well as copper nanoparticle chitosan composite.* **2nd International Conference on Advanced Nanomaterials and Nanotechnology** December 8-10, 2011, IIT Guwahati, India. (***Poster Presentation***)

7. Madhuchanda Banerjee, Shilpa Sharma, Arun Chattopadhyay and Siddhartha Sankar Ghosh. *Bimetallic Gold-Silver Core-Shell nanoparticle exhibiting high bactericidal properties.* **2nd International Conference on Advanced Nanomaterials and Nanotechnology** December 8-10, 2011, IIT Guwahati, India. (***Poster Presentation***)

PERMISSION

This section contains the copies of original *permissions obtained for reproducing Figures and Tables* in **Chapter 1** from other sources, as listed below:

Figure No.	Page No.	Source
1.1. (a)	4	Kelly, K.L., Coronado, E., Zhao, L.L. & Schatz, G.C.The optical properties of metal nanoparticles: The influence of size, shape, and dielectric environment. *The Journal of Physical Chemistry B* **107**, 668–677 (2003).
1.1. (b, c)	4	Haes, A. & Duyne, R. A unified view of propagating and localized surface plasmon resonance biosensors. *Analytical and Bioanalytical Chemistry* **379**, 920–930 (2004).
1.2.	16	Pawar, S.N. & Edgar, K.J. Alginate derivatization: A review of chemistry, properties and applications. *Biomaterials* **33**, 3279–3305 (2012).
1.3.	19	Jayakumar, R., Prabaharan, M., Sudheesh Kumar, P.T., Nair, S.V. & Tamura, H. Biomaterials based on chitin and chitosan in wound dressing applications. *Biotechnology Advances* **29**, 322–337 (2011).

Table No.	Page No.	Source
1.1.	11	Chaloupka, K., Malam, Y. & Seifalian, A.M. Nanosilver as a new generation of nanoproduct in biomedical applications. *Trends in Biotechnology* **28**, 580–588 (2010).
1.2.	15	Pillai, O. & Panchagnula, R. Polymers in drug delivery. *Current Opinion in Chemical Biology* **5**, 447–451 (2001).

RightsLink®

Home | Account Info | Help

Title:	The Optical Properties of Metal Nanoparticles: The Influence of Size, Shape, and Dielectric Environment
Author:	K. Lance Kelly,Eduardo Coronado,Lin Lin Zhao, and, and George C. Schatz*
Publication:	The Journal of Physical Chemistry B
Publisher:	American Chemical Society
Date:	Jan 1, 2003

Logged in as:
Shilpa Sharma

LOGOUT

PERMISSION/LICENSE IS GRANTED FOR YOUR ORDER AT NO CHARGE

This type of permission/license, instead of the standard Terms & Conditions, is sent to you because no fee is being charged for your order. Please note the following:

- Permission is granted for your request in both print and electronic formats, and translations.
- If figures and/or tables were requested, they may be adapted or used in part.
- Please print this page for your records and send a copy of it to your publisher/graduate school.
- Appropriate credit for the requested material should be given as follows: "Reprinted (adapted) with permission from (COMPLETE REFERENCE CITATION). Copyright (YEAR) American Chemical Society." Insert appropriate information in place of the capitalized words.
- One-time permission is granted only for the use specified in your request. No additional uses are granted (such as derivative works or other editions). For any other uses, please submit a new request.

BACK CLOSE WINDOW

TH-1127_08615302

SPRINGER LICENSE
TERMS AND CONDITIONS

Jul 19, 2012

This is a License Agreement between Shilpa Sharma ("You") and Springer ("Springer") provided by Copyright Clearance Center ("CCC"). The license consists of your order details, the terms and conditions provided by Springer, and the payment terms and conditions.

All payments must be made in full to CCC. For payment instructions, please see information listed at the bottom of this form.

License Number	2952500337372
License date	Jul 19, 2012
Licensed content publisher	Springer
Licensed content publication	Analytical and Bioanalytical Chemistry
Licensed content title	A unified view of propagating and localized surface plasmon resonance biosensors
Licensed content author	Amanda J. Haes
Licensed content date	Aug 1, 2004
Volume number	379
Issue number	7
Type of Use	Thesis/Dissertation
Portion	Figures
Author of this Springer article	No
Order reference number	
Title of your thesis / dissertation	Metal Nanoparticles and Nanocomposites as antibacterial and anticancer agents
Expected completion date	Sep 2012
Estimated size(pages)	175
Total	0.00 USD
Terms and Conditions	

Introduction

The publisher for this copyrighted material is Springer Science + Business Media. By clicking "accept" in connection with completing this licensing transaction, you agree that the following terms and conditions apply to this transaction (along with the Billing and Payment terms and conditions established by Copyright Clearance Center, Inc. ("CCC"), at the time that you opened your Rightslink account and that are available at any time at http://myaccount.copyright.com).

Limited License

With reference to your request to reprint in your thesis material on which Springer Science

and Business Media control the copyright, permission is granted, free of charge, for the use indicated in your enquiry.

Licenses are for one-time use only with a maximum distribution equal to the number that you identified in the licensing process.

This License includes use in an electronic form, provided its password protected or on the university's intranet or repository, including UMI (according to the definition at the Sherpa website: http://www.sherpa.ac.uk/romeo/). For any other electronic use, please contact Springer at (permissions.dordrecht@springer.com or permissions.heidelberg@springer.com).

The material can only be used for the purpose of defending your thesis, and with a maximum of 100 extra copies in paper.

Although Springer holds copyright to the material and is entitled to negotiate on rights, this license is only valid, provided permission is also obtained from the (co) author (address is given with the article/chapter) and provided it concerns original material which does not carry references to other sources (if material in question appears with credit to another source, authorization from that source is required as well).

Permission free of charge on this occasion does not prejudice any rights we might have to charge for reproduction of our copyrighted material in the future.

Altering/Modifying Material: Not Permitted
You may not alter or modify the material in any manner. Abbreviations, additions, deletions and/or any other alterations shall be made only with prior written authorization of the author(s) and/or Springer Science + Business Media. (Please contact Springer at (permissions.dordrecht@springer.com or permissions.heidelberg@springer.com)

Reservation of Rights
Springer Science + Business Media reserves all rights not specifically granted in the combination of (i) the license details provided by you and accepted in the course of this licensing transaction, (ii) these terms and conditions and (iii) CCC's Billing and Payment terms and conditions.

Copyright Notice:Disclaimer
You must include the following copyright and permission notice in connection with any reproduction of the licensed material: "Springer and the original publisher /journal title, volume, year of publication, page, chapter/article title, name(s) of author(s), figure number(s), original copyright notice) is given to the publication in which the material was originally published, by adding; with kind permission from Springer Science and Business Media"

Warranties: None

Example 1: Springer Science + Business Media makes no representations or warranties with respect to the licensed material.

Example 2: Springer Science + Business Media makes no representations or warranties with

respect to the licensed material and adopts on its own behalf the limitations and disclaimers established by CCC on its behalf in its Billing and Payment terms and conditions for this licensing transaction.

Indemnity
You hereby indemnify and agree to hold harmless Springer Science + Business Media and CCC, and their respective officers, directors, employees and agents, from and against any and all claims arising out of your use of the licensed material other than as specifically authorized pursuant to this license.

No Transfer of License
This license is personal to you and may not be sublicensed, assigned, or transferred by you to any other person without Springer Science + Business Media's written permission.

No Amendment Except in Writing
This license may not be amended except in a writing signed by both parties (or, in the case of Springer Science + Business Media, by CCC on Springer Science + Business Media's behalf).

Objection to Contrary Terms
Springer Science + Business Media hereby objects to any terms contained in any purchase order, acknowledgment, check endorsement or other writing prepared by you, which terms are inconsistent with these terms and conditions or CCC's Billing and Payment terms and conditions. These terms and conditions, together with CCC's Billing and Payment terms and conditions (which are incorporated herein), comprise the entire agreement between you and Springer Science + Business Media (and CCC) concerning this licensing transaction. In the event of any conflict between your obligations established by these terms and conditions and those established by CCC's Billing and Payment terms and conditions, these terms and conditions shall control.

Jurisdiction
All disputes that may arise in connection with this present License, or the breach thereof, shall be settled exclusively by arbitration, to be held in The Netherlands, in accordance with Dutch law, and to be conducted under the Rules of the 'Netherlands Arbitrage Instituut' (Netherlands Institute of Arbitration).***OR:***

All disputes that may arise in connection with this present License, or the breach thereof, shall be settled exclusively by arbitration, to be held in the Federal Republic of Germany, in accordance with German law.

Other terms and conditions:

v1.3

If you would like to pay for this license now, please remit this license along with your payment made payable to "COPYRIGHT CLEARANCE CENTER" otherwise you will be invoiced within 48 hours of the license date. Payment should be in the form of a check or money order referencing your account number and this invoice number RLNK500821539.

TH-1127_08615302

Once you receive your invoice for this order, you may pay your invoice by credit card. Please follow instructions provided at that time.

Make Payment To:
Copyright Clearance Center
Dept 001
P.O. Box 843006
Boston, MA 02284-3006

For suggestions or comments regarding this order, contact RightsLink Customer Support: customercare@copyright.com or +1-877-622-5543 (toll free in the US) or +1-978-646-2777.

Gratis licenses (referencing $0 in the Total field) are free. Please retain this printable license for your reference. No payment is required.

TH-1127_08615302

ELSEVIER LICENSE
TERMS AND CONDITIONS

Sep 19, 2012

This is a License Agreement between Shilpa Sharma ("You") and Elsevier ("Elsevier") provided by Copyright Clearance Center ("CCC"). The license consists of your order details, the terms and conditions provided by Elsevier, and the payment terms and conditions.

All payments must be made in full to CCC. For payment instructions, please see information listed at the bottom of this form.

Supplier	Elsevier Limited The Boulevard,Langford Lane Kidlington,Oxford,OX5 1GB,UK
Registered Company Number	1982084
Customer name	Shilpa Sharma
Customer address	IIT Guwahati Guwahati, Guwahati 781039
License number	2955730810969
License date	Jul 25, 2012
Licensed content publisher	Elsevier
Licensed content publication	Biomaterials
Licensed content title	Alginate derivatization: A review of chemistry, properties and applications
Licensed content author	Siddhesh N. Pawar,Kevin J. Edgar
Licensed content date	April 2012
Licensed content volume number	33
Licensed content issue number	11
Number of pages	27
Start Page	3279
End Page	3305
Type of Use	reuse in a thesis/dissertation
Intended publisher of new work	other
Portion	figures/tables/illustrations
Number of figures/tables /illustrations	1
Format	both print and electronic
Are you the author of this Elsevier article?	No
Will you be translating?	No
Order reference number	None
Title of your thesis/dissertation	Metal Nanoparticles and Nanocomposites as antibacterial and anticancer agents
Expected completion date	Sep 2012

Estimated size (number of pages)	175
Elsevier VAT number	GB 494 6272 12
Permissions price	0.00 USD
VAT/Local Sales Tax	0.0 USD / 0.0 GBP
Total	**0.00 USD**

Terms and Conditions

INTRODUCTION

1. The publisher for this copyrighted material is Elsevier. By clicking "accept" in connection with completing this licensing transaction, you agree that the following terms and conditions apply to this transaction (along with the Billing and Payment terms and conditions established by Copyright Clearance Center, Inc. ("CCC"), at the time that you opened your Rightslink account and that are available at any time at http://myaccount.copyright.com).

GENERAL TERMS

2. Elsevier hereby grants you permission to reproduce the aforementioned material subject to the terms and conditions indicated.
3. Acknowledgement: If any part of the material to be used (for example, figures) has appeared in our publication with credit or acknowledgement to another source, permission must also be sought from that source. If such permission is not obtained then that material may not be included in your publication/copies. Suitable acknowledgement to the source must be made, either as a footnote or in a reference list at the end of your publication, as follows:
"Reprinted from Publication title, Vol /edition number, Author(s), Title of article / title of chapter, Pages No., Copyright (Year), with permission from Elsevier [OR APPLICABLE SOCIETY COPYRIGHT OWNER]." Also Lancet special credit - "Reprinted from The Lancet, Vol. number, Author(s), Title of article, Pages No., Copyright (Year), with permission from Elsevier."
4. Reproduction of this material is confined to the purpose and/or media for which permission is hereby given.
5. Altering/Modifying Material: Not Permitted. However figures and illustrations may be altered/adapted minimally to serve your work. Any other abbreviations, additions, deletions and/or any other alterations shall be made only with prior written authorization of Elsevier Ltd. (Please contact Elsevier at permissions@elsevier.com)
6. If the permission fee for the requested use of our material is waived in this instance, please be advised that your future requests for Elsevier materials may attract a fee.
7. Reservation of Rights: Publisher reserves all rights not specifically granted in the combination of (i) the license details provided by you and accepted in the course of this licensing transaction, (ii) these terms and conditions and (iii) CCC's Billing and Payment terms and conditions.
8. License Contingent Upon Payment: While you may exercise the rights licensed immediately upon issuance of the license at the end of the licensing process for the transaction, provided that you have disclosed complete and accurate details of your proposed use, no license is finally effective unless and until full payment is received from you (either by publisher or by CCC) as provided in CCC's Billing and Payment terms and conditions. If full payment is not received on a timely basis, then any license preliminarily granted shall be deemed automatically revoked and shall be void as if never granted. Further, in the event that you breach any of these terms and conditions or any of CCC's Billing and Payment terms and conditions, the license is automatically revoked and shall be void as if never granted. Use of materials as described in a revoked license, as well as any use of the materials beyond the scope of an unrevoked license, may constitute copyright infringement and publisher reserves the right to take any and all action to protect its copyright in the materials.
9. Warranties: Publisher makes no representations or warranties with respect to the licensed material.
10. Indemnity: You hereby indemnify and agree to hold harmless publisher and CCC, and their respective officers, directors, employees and agents, from and against any and all claims arising out of your use of the licensed material other than as specifically authorized pursuant to this license.
11. No Transfer of License: This license is personal to you and may not be sublicensed, assigned, or transferred by you to any other person without publisher's written permission.
12. No Amendment Except in Writing: This license may not be amended except in a writing signed by both parties (or, in the case of publisher, by CCC on publisher's behalf).
13. Objection to Contrary Terms: Publisher hereby objects to any terms contained in any purchase order, acknowledgment, check endorsement or other writing prepared by you, which terms are inconsistent with these terms and conditions or CCC's Billing and Payment terms and conditions. These terms and conditions, together with CCC's Billing and Payment terms and conditions (which are incorporated herein), comprise the entire agreement between you and publisher (and CCC) concerning this licensing transaction. In the event of any conflict between your obligations established by these terms and conditions and those established by CCC's Billing and Payment terms and conditions, these terms and conditions shall control.
14. Revocation: Elsevier or Copyright Clearance Center may deny the permissions described in this License at their sole discretion, for any reason or no reason, with a full refund payable to you. Notice of such denial will be made using the contact information provided by you. Failure to receive such notice will not alter or invalidate the denial. In no event will Elsevier or

TH-1127_08615302

Copyright Clearance Center be responsible or liable for any costs, expenses or damage incurred by you as a result of a denial of your permission request, other than a refund of the amount(s) paid by you to Elsevier and/or Copyright Clearance Center for denied permissions.

LIMITED LICENSE

The following terms and conditions apply only to specific license types:

15. **Translation**: This permission is granted for non-exclusive world **English** rights only unless your license was granted for translation rights. If you licensed translation rights you may only translate this content into the languages you requested. A professional translator must perform all translations and reproduce the content word for word preserving the integrity of the article. If this license is to re-use 1 or 2 figures then permission is granted for non-exclusive world rights in all languages.

16. **Website**: The following terms and conditions apply to electronic reserve and author websites:

Electronic reserve: If licensed material is to be posted to website, the web site is to be password-protected and made available only to bona fide students registered on a relevant course if:

This license was made in connection with a course,

This permission is granted for 1 year only. You may obtain a license for future website posting,

All content posted to the web site must maintain the copyright information line on the bottom of each image,

A hyper-text must be included to the Homepage of the journal from which you are licensing at http://www.sciencedirect.com /science/journal/xxxxx or the Elsevier homepage for books at http://www.elsevier.com , and

Central Storage: This license does not include permission for a scanned version of the material to be stored in a central repository such as that provided by Heron/XanEdu.

17. **Author website** for journals with the following additional clauses:

All content posted to the web site must maintain the copyright information line on the bottom of each image, and the permission granted is limited to the personal version of your paper. You are not allowed to download and post the published electronic version of your article (whether PDF or HTML, proof or final version), nor may you scan the printed edition to create an electronic version. A hyper-text must be included to the Homepage of the journal from which you are licensing at http://www.sciencedirect.com/science/journal/xxxxx . As part of our normal production process, you will receive an e-mail notice when your article appears on Elsevier's online service ScienceDirect (www.sciencedirect.com). That e-mail will include the article's Digital Object Identifier (DOI). This number provides the electronic link to the published article and should be included in the posting of your personal version. We ask that you wait until you receive this e-mail and have the DOI to do any posting.

Central Storage: This license does not include permission for a scanned version of the material to be stored in a central repository such as that provided by Heron/XanEdu.

18. **Author website** for books with the following additional clauses:

Authors are permitted to place a brief summary of their work online only.

A hyper-text must be included to the Elsevier homepage at http://www.elsevier.com . All content posted to the web site must maintain the copyright information line on the bottom of each image. You are not allowed to download and post the published electronic version of your chapter, nor may you scan the printed edition to create an electronic version.

Central Storage: This license does not include permission for a scanned version of the material to be stored in a central repository such as that provided by Heron/XanEdu.

19. **Website** (regular and for author): A hyper-text must be included to the Homepage of the journal from which you are licensing at http://www.sciencedirect.com/science/journal/xxxxx. or for books to the Elsevier homepage at http://www.elsevier.com

20. **Thesis/Dissertation**: If your license is for use in a thesis/dissertation your thesis may be submitted to your institution in either print or electronic form. Should your thesis be published commercially, please reapply for permission. These requirements include permission for the Library and Archives of Canada to supply single copies, on demand, of the complete thesis and include permission for UMI to supply single copies, on demand, of the complete thesis. Should your thesis be published commercially, please reapply for permission.

21. **Other Conditions**:

v1.6

If you would like to pay for this license now, please remit this license along with your payment made payable to "COPYRIGHT CLEARANCE CENTER" otherwise you will be invoiced within 48 hours of the license date. Payment should be in the form of a check or money order referencing your account number and this invoice number RLNK500824963. Once you receive your invoice for this order, you may pay your invoice by credit card. Please follow instructions provided at that time.

Make Payment To:
Copyright Clearance Center
Dept 001
P.O. Box 843006

TH-1127_08615302

Boston, MA 02284-3006

For suggestions or comments regarding this order, contact RightsLink Customer Support: customercare@copyright.com or +1-877-622-5543 (toll free in the US) or +1-978-646-2777.

Gratis licenses (referencing $0 in the Total field) are free. Please retain this printable license for your reference. No payment is required.

TH-1127_08615302

ELSEVIER LICENSE
TERMS AND CONDITIONS

Sep 19, 2012

This is a License Agreement between Shilpa Sharma ("You") and Elsevier ("Elsevier") provided by Copyright Clearance Center ("CCC"). The license consists of your order details, the terms and conditions provided by Elsevier, and the payment terms and conditions.

All payments must be made in full to CCC. For payment instructions, please see information listed at the bottom of this form.

Supplier	Elsevier Limited The Boulevard,Langford Lane Kidlington,Oxford,OX5 1GB,UK
Registered Company Number	1982084
Customer name	Shilpa Sharma
Customer address	IIT Guwahati Guwahati, Guwahati 781039
License number	2958770333409
License date	Jul 30, 2012
Licensed content publisher	Elsevier
Licensed content publication	Biotechnology Advances
Licensed content title	Biomaterials based on chitin and chitosan in wound dressing applications
Licensed content author	R. Jayakumar,M. Prabaharan,P.T. Sudheesh Kumar,S.V. Nair,H. Tamura
Licensed content date	May–June 2011
Licensed content volume number	29
Licensed content issue number	3
Number of pages	16
Start Page	322
End Page	337
Type of Use	reuse in a thesis/dissertation
Intended publisher of new work	other
Portion	figures/tables/illustrations
Number of figures/tables /illustrations	1
Format	both print and electronic
Are you the author of this Elsevier article?	No
Will you be translating?	No
Order reference number	None
Title of your thesis/dissertation	Metal Nanoparticles and Nanocomposites as antibacterial and anticancer agents
Expected completion date	Sep 2012

Estimated size (number of pages)	175
Elsevier VAT number	GB 494 6272 12
Permissions price	0.00 USD
VAT/Local Sales Tax	0.0 USD / 0.0 GBP
Total	**0.00 USD**

Terms and Conditions

INTRODUCTION

1. The publisher for this copyrighted material is Elsevier. By clicking "accept" in connection with completing this licensing transaction, you agree that the following terms and conditions apply to this transaction (along with the Billing and Payment terms and conditions established by Copyright Clearance Center, Inc. ("CCC"), at the time that you opened your Rightslink account and that are available at any time at http://myaccount.copyright.com).

GENERAL TERMS

2. Elsevier hereby grants you permission to reproduce the aforementioned material subject to the terms and conditions indicated.
3. Acknowledgement: If any part of the material to be used (for example, figures) has appeared in our publication with credit or acknowledgement to another source, permission must also be sought from that source. If such permission is not obtained then that material may not be included in your publication/copies. Suitable acknowledgement to the source must be made, either as a footnote or in a reference list at the end of your publication, as follows:
"Reprinted from Publication title, Vol /edition number, Author(s), Title of article / title of chapter, Pages No., Copyright (Year), with permission from Elsevier [OR APPLICABLE SOCIETY COPYRIGHT OWNER]." Also Lancet special credit - "Reprinted from The Lancet, Vol. number, Author(s), Title of article, Pages No., Copyright (Year), with permission from Elsevier."
4. Reproduction of this material is confined to the purpose and/or media for which permission is hereby given.
5. Altering/Modifying Material: Not Permitted. However figures and illustrations may be altered/adapted minimally to serve your work. Any other abbreviations, additions, deletions and/or any other alterations shall be made only with prior written authorization of Elsevier Ltd. (Please contact Elsevier at permissions@elsevier.com)
6. If the permission fee for the requested use of our material is waived in this instance, please be advised that your future requests for Elsevier materials may attract a fee.
7. Reservation of Rights: Publisher reserves all rights not specifically granted in the combination of (i) the license details provided by you and accepted in the course of this licensing transaction, (ii) these terms and conditions and (iii) CCC's Billing and Payment terms and conditions.
8. License Contingent Upon Payment: While you may exercise the rights licensed immediately upon issuance of the license at the end of the licensing process for the transaction, provided that you have disclosed complete and accurate details of your proposed use, no license is finally effective unless and until full payment is received from you (either by publisher or by CCC) as provided in CCC's Billing and Payment terms and conditions. If full payment is not received on a timely basis, then any license preliminarily granted shall be deemed automatically revoked and shall be void as if never granted. Further, in the event that you breach any of these terms and conditions or any of CCC's Billing and Payment terms and conditions, the license is automatically revoked and shall be void as if never granted. Use of materials as described in a revoked license, as well as any use of the materials beyond the scope of an unrevoked license, may constitute copyright infringement and publisher reserves the right to take any and all action to protect its copyright in the materials.
9. Warranties: Publisher makes no representations or warranties with respect to the licensed material.
10. Indemnity: You hereby indemnify and agree to hold harmless publisher and CCC, and their respective officers, directors, employees and agents, from and against any and all claims arising out of your use of the licensed material other than as specifically authorized pursuant to this license.
11. No Transfer of License: This license is personal to you and may not be sublicensed, assigned, or transferred by you to any other person without publisher's written permission.
12. No Amendment Except in Writing: This license may not be amended except in a writing signed by both parties (or, in the case of publisher, by CCC on publisher's behalf).
13. Objection to Contrary Terms: Publisher hereby objects to any terms contained in any purchase order, acknowledgment, check endorsement or other writing prepared by you, which terms are inconsistent with these terms and conditions or CCC's Billing and Payment terms and conditions. These terms and conditions, together with CCC's Billing and Payment terms and conditions (which are incorporated herein), comprise the entire agreement between you and publisher (and CCC) concerning this licensing transaction. In the event of any conflict between your obligations established by these terms and conditions and those established by CCC's Billing and Payment terms and conditions, these terms and conditions shall control.
14. Revocation: Elsevier or Copyright Clearance Center may deny the permissions described in this License at their sole discretion, for any reason or no reason, with a full refund payable to you. Notice of such denial will be made using the contact information provided by you. Failure to receive such notice will not alter or invalidate the denial. In no event will Elsevier or

TH-1127_08615302

Copyright Clearance Center be responsible or liable for any costs, expenses or damage incurred by you as a result of a denial of your permission request, other than a refund of the amount(s) paid by you to Elsevier and/or Copyright Clearance Center for denied permissions.

LIMITED LICENSE

The following terms and conditions apply only to specific license types:

15. **Translation**: This permission is granted for non-exclusive world **English** rights only unless your license was granted for translation rights. If you licensed translation rights you may only translate this content into the languages you requested. A professional translator must perform all translations and reproduce the content word for word preserving the integrity of the article. If this license is to re-use 1 or 2 figures then permission is granted for non-exclusive world rights in all languages.

16. **Website**: The following terms and conditions apply to electronic reserve and author websites:

Electronic reserve: If licensed material is to be posted to website, the web site is to be password-protected and made available only to bona fide students registered on a relevant course if:

This license was made in connection with a course,

This permission is granted for 1 year only. You may obtain a license for future website posting,

All content posted to the web site must maintain the copyright information line on the bottom of each image,

A hyper-text must be included to the Homepage of the journal from which you are licensing at http://www.sciencedirect.com /science/journal/xxxxx or the Elsevier homepage for books at http://www.elsevier.com , and

Central Storage: This license does not include permission for a scanned version of the material to be stored in a central repository such as that provided by Heron/XanEdu.

17. **Author website** for journals with the following additional clauses:

All content posted to the web site must maintain the copyright information line on the bottom of each image, and the permission granted is limited to the personal version of your paper. You are not allowed to download and post the published electronic version of your article (whether PDF or HTML, proof or final version), nor may you scan the printed edition to create an electronic version. A hyper-text must be included to the Homepage of the journal from which you are licensing at http://www.sciencedirect.com/science/journal/xxxxx . As part of our normal production process, you will receive an e-mail notice when your article appears on Elsevier's online service ScienceDirect (www.sciencedirect.com). That e-mail will include the article's Digital Object Identifier (DOI). This number provides the electronic link to the published article and should be included in the posting of your personal version. We ask that you wait until you receive this e-mail and have the DOI to do any posting.

Central Storage: This license does not include permission for a scanned version of the material to be stored in a central repository such as that provided by Heron/XanEdu.

18. **Author website** for books with the following additional clauses:

Authors are permitted to place a brief summary of their work online only.

A hyper-text must be included to the Elsevier homepage at http://www.elsevier.com . All content posted to the web site must maintain the copyright information line on the bottom of each image. You are not allowed to download and post the published electronic version of your chapter, nor may you scan the printed edition to create an electronic version.

Central Storage: This license does not include permission for a scanned version of the material to be stored in a central repository such as that provided by Heron/XanEdu.

19. **Website** (regular and for author): A hyper-text must be included to the Homepage of the journal from which you are licensing at http://www.sciencedirect.com/science/journal/xxxxx. or for books to the Elsevier homepage at http://www.elsevier.com

20. **Thesis/Dissertation**: If your license is for use in a thesis/dissertation your thesis may be submitted to your institution in either print or electronic form. Should your thesis be published commercially, please reapply for permission. These requirements include permission for the Library and Archives of Canada to supply single copies, on demand, of the complete thesis and include permission for UMI to supply single copies, on demand, of the complete thesis. Should your thesis be published commercially, please reapply for permission.

21. **Other Conditions**:

v1.6

If you would like to pay for this license now, please remit this license along with your payment made payable to "COPYRIGHT CLEARANCE CENTER" otherwise you will be invoiced within 48 hours of the license date. Payment should be in the form of a check or money order referencing your account number and this invoice number RLNK500827979. Once you receive your invoice for this order, you may pay your invoice by credit card. Please follow instructions provided at that time.

Make Payment To:
Copyright Clearance Center
Dept 001
P.O. Box 843006

TH-1127_08615302

Boston, MA 02284-3006

For suggestions or comments regarding this order, contact RightsLink Customer Support: customercare@copyright.com or +1-877-622-5543 (toll free in the US) or +1-978-646-2777.

Gratis licenses (referencing $0 in the Total field) are free. Please retain this printable license for your reference. No payment is required.

TH-1127_08615302

ELSEVIER LICENSE
TERMS AND CONDITIONS

Jul 20, 2012

This is a License Agreement between Shilpa Sharma ("You") and Elsevier ("Elsevier") provided by Copyright Clearance Center ("CCC"). The license consists of your order details, the terms and conditions provided by Elsevier, and the payment terms and conditions.

All payments must be made in full to CCC. For payment instructions, please see information listed at the bottom of this form.

Supplier	Elsevier Limited The Boulevard,Langford Lane Kidlington,Oxford,OX5 1GB,UK
Registered Company Number	1982084
Customer name	Shilpa Sharma
Customer address	IIT Guwahati Guwahati, Guwahati 781039
License number	2953061227203
License date	Jul 20, 2012
Licensed content publisher	Elsevier
Licensed content publication	Trends in Biotechnology
Licensed content title	Nanosilver as a new generation of nanoproduct in biomedical applications
Licensed content author	Karla Chaloupka,Yogeshkumar Malam,Alexander M. Seifalian
Licensed content date	November 2010
Licensed content volume number	28
Licensed content issue number	11
Number of pages	9
Start Page	580
End Page	588
Type of Use	reuse in a thesis/dissertation
Portion	figures/tables/illustrations
Number of figures/tables /illustrations	1
Format	both print and electronic
Are you the author of this Elsevier article?	No
Will you be translating?	No
Order reference number	TH-1127_08615302

Title of your thesis/dissertation	Metal Nanoparticles and Nanocomposites as antibacterial and anticancer agents
Expected completion date	Sep 2012
Estimated size (number of pages)	175
Elsevier VAT number	GB 494 6272 12
Permissions price	0.00 USD
VAT/Local Sales Tax	0.0 USD / 0.0 GBP
Total	0.00 USD
Terms and Conditions	

INTRODUCTION

1. The publisher for this copyrighted material is Elsevier. By clicking "accept" in connection with completing this licensing transaction, you agree that the following terms and conditions apply to this transaction (along with the Billing and Payment terms and conditions established by Copyright Clearance Center, Inc. ("CCC"), at the time that you opened your Rightslink account and that are available at any time at http://myaccount.copyright.com).

GENERAL TERMS

2. Elsevier hereby grants you permission to reproduce the aforementioned material subject to the terms and conditions indicated.

3. Acknowledgement: If any part of the material to be used (for example, figures) has appeared in our publication with credit or acknowledgement to another source, permission must also be sought from that source. If such permission is not obtained then that material may not be included in your publication/copies. Suitable acknowledgement to the source must be made, either as a footnote or in a reference list at the end of your publication, as follows:

"Reprinted from Publication title, Vol /edition number, Author(s), Title of article / title of chapter, Pages No., Copyright (Year), with permission from Elsevier [OR APPLICABLE SOCIETY COPYRIGHT OWNER]." Also Lancet special credit - "Reprinted from The Lancet, Vol. number, Author(s), Title of article, Pages No., Copyright (Year), with permission from Elsevier."

4. Reproduction of this material is confined to the purpose and/or media for which permission is hereby given.

5. Altering/Modifying Material: Not Permitted. However figures and illustrations may be altered/adapted minimally to serve your work. Any other abbreviations, additions, deletions and/or any other alterations shall be made only with prior written authorization of Elsevier Ltd. (Please contact Elsevier at permissions@elsevier.com)

6. If the permission fee for the requested use of our material is waived in this instance, please be advised that your future requests for Elsevier materials may attract a fee.

7. Reservation of Rights: Publisher reserves all rights not specifically granted in the combination of (i) the license details provided by you and accepted in the course of this licensing transaction, (ii) these terms and conditions and (iii) CCC's Billing and Payment terms and conditions.

8. License Contingent Upon Payment: While you may exercise the rights licensed immediately upon issuance of the license at the end of the licensing process for the transaction, provided that you have disclosed complete and accurate details of your proposed use, no license is finally effective unless and until full payment is received from you (either by publisher or by CCC) as provided in CCC's Billing and Payment terms and conditions. If full payment is not received on a timely basis, then any license preliminarily granted shall be deemed automatically revoked and shall be void as if never granted. Further, in the event that you breach any of these terms and conditions or any of CCC's Billing and Payment terms and conditions, the license is automatically revoked and shall be void as if never granted. Use of materials as described in a revoked license, as well as any use of the materials beyond the scope of an unrevoked license, may constitute copyright infringement and publisher reserves the right to take any and all action to protect its copyright in the materials.

9. Warranties: Publisher makes no representations or warranties with respect to the licensed material.

10. Indemnity: You hereby indemnify and agree to hold harmless publisher and CCC, and their respective officers, directors, employees and agents, from and against any and all claims arising out of your use of the licensed material other than as specifically authorized pursuant to this license.

11. No Transfer of License: This license is personal to you and may not be sublicensed, assigned, or transferred by you to any other person without publisher's written permission.

12. No Amendment Except in Writing: This license may not be amended except in a writing signed by both parties (or, in the case of publisher, by CCC on publisher's behalf).

13. Objection to Contrary Terms: Publisher hereby objects to any terms contained in any purchase order, acknowledgment, check endorsement or other writing prepared by you, which terms are inconsistent with these terms and conditions or CCC's Billing and Payment terms and conditions. These terms and conditions, together with CCC's Billing and Payment terms and conditions (which are incorporated herein), comprise the entire agreement between you and publisher (and CCC) concerning this licensing transaction. In the event of any conflict between your obligations established by these terms and conditions and those established by CCC's Billing and Payment terms and conditions, these terms and conditions shall control.

14. Revocation: Elsevier or Copyright Clearance Center may deny the permissions described in this License at their sole discretion, for any reason or no reason, with a full refund payable to you. Notice of such denial will be made using the contact information provided by you. Failure to receive such notice will not alter or invalidate the denial. In no event will Elsevier or Copyright Clearance Center be responsible or liable for any costs, expenses or damage

incurred by you as a result of a denial of your permission request, other than a refund of the amount(s) paid by you to Elsevier and/or Copyright Clearance Center for denied permissions.

LIMITED LICENSE

The following terms and conditions apply only to specific license types:

15. **Translation**: This permission is granted for non-exclusive world **English** rights only unless your license was granted for translation rights. If you licensed translation rights you may only translate this content into the languages you requested. A professional translator must perform all translations and reproduce the content word for word preserving the integrity of the article. If this license is to re-use 1 or 2 figures then permission is granted for non-exclusive world rights in all languages.

16. **Website**: The following terms and conditions apply to electronic reserve and author websites:
Electronic reserve: If licensed material is to be posted to website, the web site is to be password-protected and made available only to bona fide students registered on a relevant course if:
This license was made in connection with a course,
This permission is granted for 1 year only. You may obtain a license for future website posting,
All content posted to the web site must maintain the copyright information line on the bottom of each image,
A hyper-text must be included to the Homepage of the journal from which you are licensing at http://www.sciencedirect.com/science/journal/xxxxx or the Elsevier homepage for books at http://www.elsevier.com , and
Central Storage: This license does not include permission for a scanned version of the material to be stored in a central repository such as that provided by Heron/XanEdu.

17. **Author website** for journals with the following additional clauses:

All content posted to the web site must maintain the copyright information line on the bottom of each image, and the permission granted is limited to the personal version of your paper. You are not allowed to download and post the published electronic version of your article (whether PDF or HTML, proof or final version), nor may you scan the printed edition to create an electronic version. A hyper-text must be included to the Homepage of the journal from which you are licensing at http://www.sciencedirect.com/science/journal/xxxxx . As part of our normal production process, you will receive an e-mail notice when your article appears on Elsevier's online service ScienceDirect (www.sciencedirect.com). That e-mail will include the article's Digital Object Identifier (DOI). This number provides the electronic link to the published article and should be included in the posting of your personal version. We ask that you wait until you receive this e-mail and have the DOI to do any posting.

Central Storage: This license does not include permission for a scanned version of the material to be stored in a central repository such as that provided by Heron/XanEdu.

TH-1127_08615302

18. **Author website** for books with the following additional clauses:
Authors are permitted to place a brief summary of their work online only.
A hyper-text must be included to the Elsevier homepage at http://www.elsevier.com . All content posted to the web site must maintain the copyright information line on the bottom of each image. You are not allowed to download and post the published electronic version of your chapter, nor may you scan the printed edition to create an electronic version.

Central Storage: This license does not include permission for a scanned version of the material to be stored in a central repository such as that provided by Heron/XanEdu.

19. **Website** (regular and for author): A hyper-text must be included to the Homepage of the journal from which you are licensing at http://www.sciencedirect.com/science/journal/xxxxx. or for books to the Elsevier homepage at http://www.elsevier.com

20. **Thesis/Dissertation**: If your license is for use in a thesis/dissertation your thesis may be submitted to your institution in either print or electronic form. Should your thesis be published commercially, please reapply for permission. These requirements include permission for the Library and Archives of Canada to supply single copies, on demand, of the complete thesis and include permission for UMI to supply single copies, on demand, of the complete thesis. Should your thesis be published commercially, please reapply for permission.

21. **Other Conditions**:

v1.6

If you would like to pay for this license now, please remit this license along with your payment made payable to "COPYRIGHT CLEARANCE CENTER" otherwise you will be invoiced within 48 hours of the license date. Payment should be in the form of a check or money order referencing your account number and this invoice number RLNK500822364.
Once you receive your invoice for this order, you may pay your invoice by credit card. Please follow instructions provided at that time.

Make Payment To:
Copyright Clearance Center
Dept 001
P.O. Box 843006
Boston, MA 02284-3006

For suggestions or comments regarding this order, contact RightsLink Customer Support: customercare@copyright.com or +1-877-622-5543 (toll free in the US) or +1-978-646-2777.

Gratis licenses (referencing $0 in the Total field) are free. Please retain this printable license for your reference. No payment is required.

TH-1127_08615302

ELSEVIER LICENSE
TERMS AND CONDITIONS

Sep 19, 2012

This is a License Agreement between Shilpa Sharma ("You") and Elsevier ("Elsevier") provided by Copyright Clearance Center ("CCC"). The license consists of your order details, the terms and conditions provided by Elsevier, and the payment terms and conditions.

All payments must be made in full to CCC. For payment instructions, please see information listed at the bottom of this form.

Supplier	Elsevier Limited The Boulevard,Langford Lane Kidlington,Oxford,OX5 1GB,UK
Registered Company Number	1982084
Customer name	Shilpa Sharma
Customer address	IIT Guwahati Guwahati, Guwahati 781039
License number	2956451073804
License date	Jul 26, 2012
Licensed content publisher	Elsevier
Licensed content publication	Current Opinion in Chemical Biology
Licensed content title	Polymers in drug delivery
Licensed content author	Omathanu Pillai,Ramesh Panchagnula
Licensed content date	1 August 2001
Licensed content volume number	5
Licensed content issue number	4
Number of pages	5
Start Page	447
End Page	451
Type of Use	reuse in a thesis/dissertation
Intended publisher of new work	other
Portion	figures/tables/illustrations
Number of figures/tables /illustrations	1
Format	both print and electronic
Are you the author of this Elsevier article?	No
Will you be translating?	No
Order reference number	None
Title of your thesis/dissertation	Metal Nanoparticles and Nanocomposites as antibacterial and anticancer agents
Expected completion date	Sep 2012

Estimated size (number of pages)	175
Elsevier VAT number	GB 494 6272 12
Permissions price	0.00 USD
VAT/Local Sales Tax	0.0 USD / 0.0 GBP
Total	**0.00 USD**
Terms and Conditions	

INTRODUCTION

1. The publisher for this copyrighted material is Elsevier. By clicking "accept" in connection with completing this licensing transaction, you agree that the following terms and conditions apply to this transaction (along with the Billing and Payment terms and conditions established by Copyright Clearance Center, Inc. ("CCC"), at the time that you opened your Rightslink account and that are available at any time at http://myaccount.copyright.com).

GENERAL TERMS

2. Elsevier hereby grants you permission to reproduce the aforementioned material subject to the terms and conditions indicated.
3. Acknowledgement: If any part of the material to be used (for example, figures) has appeared in our publication with credit or acknowledgement to another source, permission must also be sought from that source. If such permission is not obtained then that material may not be included in your publication/copies. Suitable acknowledgement to the source must be made, either as a footnote or in a reference list at the end of your publication, as follows:
"Reprinted from Publication title, Vol /edition number, Author(s), Title of article / title of chapter, Pages No., Copyright (Year), with permission from Elsevier [OR APPLICABLE SOCIETY COPYRIGHT OWNER]." Also Lancet special credit - "Reprinted from The Lancet, Vol. number, Author(s), Title of article, Pages No., Copyright (Year), with permission from Elsevier."
4. Reproduction of this material is confined to the purpose and/or media for which permission is hereby given.
5. Altering/Modifying Material: Not Permitted. However figures and illustrations may be altered/adapted minimally to serve your work. Any other abbreviations, additions, deletions and/or any other alterations shall be made only with prior written authorization of Elsevier Ltd. (Please contact Elsevier at permissions@elsevier.com)
6. If the permission fee for the requested use of our material is waived in this instance, please be advised that your future requests for Elsevier materials may attract a fee.
7. Reservation of Rights: Publisher reserves all rights not specifically granted in the combination of (i) the license details provided by you and accepted in the course of this licensing transaction, (ii) these terms and conditions and (iii) CCC's Billing and Payment terms and conditions.
8. License Contingent Upon Payment: While you may exercise the rights licensed immediately upon issuance of the license at the end of the licensing process for the transaction, provided that you have disclosed complete and accurate details of your proposed use, no license is finally effective unless and until full payment is received from you (either by publisher or by CCC) as provided in CCC's Billing and Payment terms and conditions. If full payment is not received on a timely basis, then any license preliminarily granted shall be deemed automatically revoked and shall be void as if never granted. Further, in the event that you breach any of these terms and conditions or any of CCC's Billing and Payment terms and conditions, the license is automatically revoked and shall be void as if never granted. Use of materials as described in a revoked license, as well as any use of the materials beyond the scope of an unrevoked license, may constitute copyright infringement and publisher reserves the right to take any and all action to protect its copyright in the materials.
9. Warranties: Publisher makes no representations or warranties with respect to the licensed material.
10. Indemnity: You hereby indemnify and agree to hold harmless publisher and CCC, and their respective officers, directors, employees and agents, from and against any and all claims arising out of your use of the licensed material other than as specifically authorized pursuant to this license.
11. No Transfer of License: This license is personal to you and may not be sublicensed, assigned, or transferred by you to any other person without publisher's written permission.
12. No Amendment Except in Writing: This license may not be amended except in a writing signed by both parties (or, in the case of publisher, by CCC on publisher's behalf).
13. Objection to Contrary Terms: Publisher hereby objects to any terms contained in any purchase order, acknowledgment, check endorsement or other writing prepared by you, which terms are inconsistent with these terms and conditions or CCC's Billing and Payment terms and conditions. These terms and conditions, together with CCC's Billing and Payment terms and conditions (which are incorporated herein), comprise the entire agreement between you and publisher (and CCC) concerning this licensing transaction. In the event of any conflict between your obligations established by these terms and conditions and those established by CCC's Billing and Payment terms and conditions, these terms and conditions shall control.
14. Revocation: Elsevier or Copyright Clearance Center may deny the permissions described in this License at their sole discretion, for any reason or no reason, with a full refund payable to you. Notice of such denial will be made using the contact information provided by you. Failure to receive such notice will not alter or invalidate the denial. In no event will Elsevier or

TH-1127_08615302

Copyright Clearance Center be responsible or liable for any costs, expenses or damage incurred by you as a result of a denial of your permission request, other than a refund of the amount(s) paid by you to Elsevier and/or Copyright Clearance Center for denied permissions.

LIMITED LICENSE

The following terms and conditions apply only to specific license types:

15. **Translation**: This permission is granted for non-exclusive world **English** rights only unless your license was granted for translation rights. If you licensed translation rights you may only translate this content into the languages you requested. A professional translator must perform all translations and reproduce the content word for word preserving the integrity of the article. If this license is to re-use 1 or 2 figures then permission is granted for non-exclusive world rights in all languages.

16. **Website**: The following terms and conditions apply to electronic reserve and author websites:

Electronic reserve: If licensed material is to be posted to website, the web site is to be password-protected and made available only to bona fide students registered on a relevant course if:

This license was made in connection with a course,

This permission is granted for 1 year only. You may obtain a license for future website posting,

All content posted to the web site must maintain the copyright information line on the bottom of each image,

A hyper-text must be included to the Homepage of the journal from which you are licensing at http://www.sciencedirect.com /science/journal/xxxxx or the Elsevier homepage for books at http://www.elsevier.com , and

Central Storage: This license does not include permission for a scanned version of the material to be stored in a central repository such as that provided by Heron/XanEdu.

17. **Author website** for journals with the following additional clauses:

All content posted to the web site must maintain the copyright information line on the bottom of each image, and the permission granted is limited to the personal version of your paper. You are not allowed to download and post the published electronic version of your article (whether PDF or HTML, proof or final version), nor may you scan the printed edition to create an electronic version. A hyper-text must be included to the Homepage of the journal from which you are licensing at http://www.sciencedirect.com/science/journal/xxxxx . As part of our normal production process, you will receive an e-mail notice when your article appears on Elsevier's online service ScienceDirect (www.sciencedirect.com). That e-mail will include the article's Digital Object Identifier (DOI). This number provides the electronic link to the published article and should be included in the posting of your personal version. We ask that you wait until you receive this e-mail and have the DOI to do any posting.

Central Storage: This license does not include permission for a scanned version of the material to be stored in a central repository such as that provided by Heron/XanEdu.

18. **Author website** for books with the following additional clauses:

Authors are permitted to place a brief summary of their work online only.

A hyper-text must be included to the Elsevier homepage at http://www.elsevier.com . All content posted to the web site must maintain the copyright information line on the bottom of each image. You are not allowed to download and post the published electronic version of your chapter, nor may you scan the printed edition to create an electronic version.

Central Storage: This license does not include permission for a scanned version of the material to be stored in a central repository such as that provided by Heron/XanEdu.

19. **Website** (regular and for author): A hyper-text must be included to the Homepage of the journal from which you are licensing at http://www.sciencedirect.com/science/journal/xxxxx. or for books to the Elsevier homepage at http://www.elsevier.com

20. **Thesis/Dissertation**: If your license is for use in a thesis/dissertation your thesis may be submitted to your institution in either print or electronic form. Should your thesis be published commercially, please reapply for permission. These requirements include permission for the Library and Archives of Canada to supply single copies, on demand, of the complete thesis and include permission for UMI to supply single copies, on demand, of the complete thesis. Should your thesis be published commercially, please reapply for permission.

21. **Other Conditions**:

v1.6

If you would like to pay for this license now, please remit this license along with your payment made payable to "COPYRIGHT CLEARANCE CENTER" otherwise you will be invoiced within 48 hours of the license date. Payment should be in the form of a check or money order referencing your account number and this invoice number RLNK500825992. Once you receive your invoice for this order, you may pay your invoice by credit card. Please follow instructions provided at that time.

Make Payment To:
Copyright Clearance Center
Dept 001
P.O. Box 843006

TH-1127_08615302

Boston, MA 02284-3006

For suggestions or comments regarding this order, contact RightsLink Customer Support: customercare@copyright.com or +1-877-622-5543 (toll free in the US) or +1-978-646-2777.

Gratis licenses (referencing $0 in the Total field) are free. Please retain this printable license for your reference. No payment is required.
